Instituto Tecnológico de Buenos Aires

Tesis para optar al título de

Doctora en Ingeniería

del Instituto Tecnológico de Buenos Aires

Fenómenos de superficie que afectan el transporte y la remoción de virus y bacterias en medios porosos naturales e ingenieriles: Implicaciones para la calidad del agua

Autora: Ing. Guillermina José Gentile

Directora: Dra. María Marta Fidalgo de Cortalezzi

Co-directora: Dra. María Inés Errea

Buenos Aires, Argentina

Junio 2016

Fenómenos de superficie que afectan el transporte y la remoción de virus y bacterias en medios porosos naturales e ingenieriles: Implicaciones para la calidad del agua

por

Guillermina José Gentile

En cumplimiento parcial de los requisitos para optar al grado de

Doctora en Ingeniería

del

Instituto Tecnológico de Buenos Aires

Buenos Aires, Argentina Junio de 2016

Surface phenomena affecting the transport and removal of viruses and bacteria in natural and engineered porous media: Implications for water quality

by

Guillermina José Gentile

A thesis submitted in partial fulfillment of the requirements for the degree

Doctora en Ingeniería

of the

Instituto Tecnológico de Buenos Aires

Buenos Aires, Argentina June, 2016

Instituto Tecnológico de Buenos Aires

Departamento de Doctorado

Los aquí suscriptos certifican que han asistido a la presentación oral de la tesis Fenómenos de superficie que afectan el transporte y la remoción de virus y bacterias en medios porosos naturales e ingenieriles: Implicaciones para la calidad del agua, cuya autora es Guillermina José Gentile, completando parcialmente los requerimientos exigidos para la obtención del título Doctora en Ingeniería.

Fecha: _____

Directora _____

Dra. María Marta Fidalgo de Cortalezzi

Tribunal de tesis _____

Dra. Viviana Andrea Mbayed

_____

Dr. Julián Andrés Rengifo Herrera

_____

Dr. Jorge Daniel Stripeikis

Instituto Tecnológico de Buenos Aires

Departamento de Doctorado

The undersigned attended the oral presentation of the thesis entitled Surface phenomena affecting the transport and removal of viruses and bacteria in natural and engineered porous media: Implications for water quality by Guillermina José Gentile. It has been submitted in partial fulfillment of the requirements for the degree of Doctora en Ingeniería.

Date: _____

Tutor _____

Dr. María Marta Fidalgo de Cortalezzi

Members of the board _____

Dr. Viviana Andrea Mbayed

_____

Dr. Julián Andrés Rengifo Herrera

_____

Dr. Jorge Daniel Stripeikis

ACKNOWLEDGEMENTS

First of all, I must thank María Marta for her guidance, support, and advice throughout these years. But above all, for her kindness, her generosity and the great opportunity she provided me with.

I would like to thank all the past and present members of the CIMA -Liliana, Mauro, Victoria, Ezequiel, Vergenie, Laura, María Inés, Fernando, Marina, Anna, and also Frank and Carole- for their help in the daily work, but most importantly, for their friendship and the shared moments.

I specially thank Lidia and Susana for their endless motivation.

Thanks to the Chemistry staff for all the laughter together and the continuous support.

Thanks for the support I have always received from the Chemical Engineering Department and the Doctorate Department at ITBA.

A huge THANK YOU to mamá, papá, Meme, Ana, Elena, who give me everything and more in my life.

Thanks to Ernestina, the prettiest, the kindest, the funniest, the smartest. My kindred spirit.

And above all, thanks to Rafael for believing in me and always being there for me. You complete me.

RESUMEN

El objetivo general de la tesis fue profundizar el conocimiento de las interacciones presentes en las interfases entre superficies, microorganismos y nanomateriales en medios acuosos. En particular se estudiaron las interacciones en tres sistemas diferentes: transporte de microorganismos y nanopartículas a través de lechos porosos, eliminación en sistemas acuosos de bacteriófagos modelo por medio de membranas cerámicas nanoestructuradas, y membranas empleadas en ultrafiltración de aguas para la remoción de bacteriófagos como modelo de virus patógenos. Los resultados obtenidos podrán ser de utilidad para elaborar mejoras en los procesos estudiados con fines de asegurar la calidad del agua. Adicionalmente, se analizó la factibilidad de la aplicación de membranas en el proceso de ósmosis retardada por presión (PRO) para generación de energía eléctrica en el país.

El transporte en lecho poroso se efectuó en el laboratorio usando columnas rellenas de arena especialmente acondicionada y caracterizada para este tipo de trabajo. Los microorganismos usados fueron bacterias que crecieron y se purificaron en las condiciones deseadas, variando la fuerza iónica de la matriz acuosa con el fin de repetir condiciones naturales relevantes. Las nanopartículas seleccionadas fueron de dióxido de titanio hidrofílico comercial. La caracterización de microorganismos y del óxido incluyó tamaño y carga superficial. Diversas técnicas fueron empleadas para detectar la presencia de los dos elementos del sistema, tales como espectrofotometría UV y visible y reacción en cadena de la polimerasa en tiempo real. Los resultados arrojaron que el flujo de bacterias a través del lecho es completamente modificado por la aparición de las nanopartículas. Además, el empleo de técnicas de modelado permitió explicar y predecir este comportamiento. Estas diferencias en el transporte pueden significar un aporte en el desarrollo de técnicas para protección de acuíferos o en el manejo de situaciones de emergencia.

En el análisis de las interacciones presentes en la remoción de bacteriófagos mediante nanopartículas cerámicas también se estableció un protocolo de crecimiento y purificación de virus apropiado para el trabajo a realizar. Luego se midieron el tamaño y la carga de superficie en las condiciones de estudio tanto para el virus como para el material cerámico. Los resultados de remoción obtenidos a escala laboratorio pudieron ser modelados mediante las teorías clásicas de estabilidad de coloides y adhesión de partículas nanométricas a superficies dentro de ciertos rangos de operación. Estas predicciones serían sumamente útiles en el desarrollo de

nuevas técnicas de purificación de aguas, especialmente en ambientes rurales, de difícil acceso a fuentes de agua corriente, o en situaciones de emergencia.

En el estudio de las interacciones en procesos de ultrafiltración con membranas se empleó uno de los más pequeños bacteriófagos conocidos y una membrana polimérica comercial. El motivo de esta selección fue el proveer la situación más desafiante que puede encontrarse en escenarios naturales. Primeramente, se desarrolló un protocolo de crecimiento y purificación de los bacteriófagos para luego poder determinar su tamaño y su carga superficial; así como las propiedades de la membrana de ultrafiltración utilizada. Con estas mediciones, se procedió al modelado mediante teorías clásicas de estabilidad de coloides y adhesión de partículas nanométricas a superficies tales como las empleadas en filtración de aguas. Se pudieron encontrar relaciones entre la eficiencia del proceso a escala laboratorio y la composición química de la matriz acuosa, lo que permitiría establecer mejores condiciones de contorno para llevar a cabo eficazmente un proceso de ultrafiltración.

El proceso de ósmosis retardada por presión plantea la obtención de energía eléctrica a través del flujo de agua que se origina entre dos soluciones de diferente concentración salina separadas por una membrana semipermeable. La diferencia de potencial químico puede ser transformada en energía luego de la ósmosis empleando una turbina hidráulica. En el presente trabajo se estudió la posibilidad de emplear este método en un escenario real tal como la desembocadura del Río Negro en la Provincia de Río Negro. Se tuvieron en cuenta caudales, condiciones ambientales y limitaciones tanto del proceso como del lugar elegido. Además, para poder obtener la cantidad de energía neta por unidad de área de membrana se tuvieron en cuenta los consumos ocasionados por las bombas empleadas en la operación. De esta forma, se completó el primer paso de una evaluación que podrá ser profundizada en el futuro.

ABSTRACT

The general objective of the present thesis is to advance in the understanding of the interactions present in the interfaces between surfaces, microorganisms, and nanomaterials in aqueous media. In particular, interactions in three different systems were studied: transport of bacteria and nanoparticles through porous media, removal of bacteriophages in aqueous systems by means of nanostructured ceramic membranes, and removal of bacteriophages as model pathogen viruses by ultrafiltration membranes. The obtained results may be useful to improve the processes studied in order to ensure water quality. In addition, the feasibility of employing membranes in pressure retarded osmosis (PRO) process for power generation in our country was analyzed.

Transport in porous medium was studied in the laboratory using columns packed with quartz sand specially conditioned and characterized. The microorganisms were bacteria that grew and were purified in the desired conditions, varying ionic strength of the aqueous matrix to reproduce relevant natural conditions. The selected nanoparticles were commercially made of hydrophilic titanium dioxide. Characterization of the microorganisms and the oxide included size and surface charge. Various techniques were used to detect the presence of both elements in the system, such as UV-Visible spectrophotometry and real-time polymerase chain reaction. Results showed that the flux of bacteria through the porous bed was completely modified by the presence of the nanoparticles. Furthermore, the use of modeling techniques allowed to explain and predict this behavior. These differences in transport can mean a contribution to the development of techniques for protection of aquifers or in handling emergency situations.

In the analysis of the interactions present in the removal of bacteriophages using ceramic nanoparticles, first, a valid protocol for growing and purification of viruses was stablished taking into account the specific work to be performed. Then, size and surface charge were measured, both for the virus and for the ceramic material. The results of the removal obtained at laboratory scale could be modeled using classic theories of colloid stability and adhesion to surfaces, in certain ranges of operation. These predictions may be very helpful in the development of new techniques for water filtration, especially in rural areas where access to safe water sources is difficult, or in emergency situations.

For the study of the interactions in membrane ultrafiltration, one of the smallest known bacteriophages and a commercial polymeric membrane were employed. The reason of this selection was to face the membrane with the most defying condition that can occur in natural

scenarios. First, a protocol for bacteriophage growing and purification was developed. Then their size and surface charge were obtained, as well as the properties of the ultrafiltration membrane. With these measurements, modeling by classic theories of colloid stability and adhesion of nanometric particles onto surfaces such as those used in water filtration was performed. Relationships between the efficiency of the process at laboratory scale and the chemical composition of the water matrix were found, which could help stablishing better conditions to effectively perform an ultrafiltration process.

Pressure retarded osmosis focuses on power generation using a flux of water that is originated between two solutions of different salt concentration separated by a semipermeable membrane. The difference in chemical potential can be later transformed into power by means of a hydroturbine. In the present work, the feasibility of employing this method in a real scenario -the mouth of the Negro River, Province of Río Negro- was studied. Different flows, environmental conditions, and limitations of both the process and the selected location were considered. Besides, to obtain the net energy per membrane unit, consumption by the operation pumps was taken into account. In this way, the first step for an energetic evaluation was conducted and it can be deepened in a future.

TABLE OF CONTENTS

LIST OF FIGURES

LIST OF TABLES

Chapter I

INTRODUCTION

Today, public health policies address water contamination by the presence of pathogen organisms, such as bacteria and viruses. The quest for better and economical treatment processes is a concrete reality affecting to a large extent those populations lacking access to safe drinking water sources.

Transport and fate of microorganisms in soils and natural waters must be understood as the first step to evaluate and improve quality treatments. Furthermore, the irruption of novel products in the environment, like nanoparticles, change the scenario since interactions with organisms and with the medium may occur. Nano-scale products can be associated to colloids and biological compounds not only due to their similar size, but also because of the importance of surface chemistry in their stability and physicochemical processes developed in natural environments.

Forty years ago, membrane filtration was not economically feasible, but new technologies and new materials have made widespread applications possible. Commercial membranes, made of polymers or ceramics, highlight the need to develop “green” processes, with the objective of achieving membranes with specific properties, such as pore size, membrane structure and surface composition. The interactions present on and near the membrane surface, as well as within its structure play a key role in the attachment and retention processes during filtration.

This work focused on three main topics: the transport of bacteria and nanoparticles in porous media and how they affect each other when both are present, surface-particle and particle-particle interactions developed during virus removal by polymeric and ceramic membranes, and innovative uses of membranes in power generation.

Chapter IV presents the study of bacterium and of nanoparticle transport in saturated porous media and how they influenced one another. First of all, growth and purification of the selected strain was carried out in our laboratory, at different environmental relevant conditions of ionic strength. Characterization of bacteria and nanoparticles included size and zeta potential determinations. The importance of these two parameters in aggregation and interactions with the medium was studied in detail and modeled by DLVO theory of colloidal stability. Sand-

packed columns were used to perform the single particle and combined particle experiments. In the former, effluent concentration was measured by means of UV spectrophotometry. In the combined transport, it was necessary to separate both components before measuring any concentration to avoid interference between the species. Thus, various techniques were selected. Quantitative polymerase chain reaction was useful to determine the bacterial concentration since it was not influenced by the presence of nanoparticles. To determine the concentration of suspended TiO_2, microwave-assisted acidic digestion was first performed to dissolve the oxide as well as eliminating the bacterial cells, followed by the addition of a complexation agent that gave the solution a color whose intensity was correlated to the unknown concentration and detected by visible spectrophotometry. The bacteria eluted the column at all considered ionic strengths, but these results completely changed when the nanoparticles were present, reaching retention levels of up to 99.99%. The electrostatic forces between the two kinds of particles proved to be dominant, alongside with other possible mechanisms such as heteroaggregation and ripening. DLVO modeling was highly useful in the system under study and sand bed removal could be evaluated using classical filtration theories. For the case of combined transport, we defined a pseudo-collision efficiency factor to characterize the system, considering the initial ("clean") collector to be a sand grain with its surface modified due to the existence of some degree of bacterial attachment.

The relevance of the work described in Chapter IV resides in the new insight to combined transport phenomenon, which is closely related to the possibility that pathogenic bacteria reach natural aquatic systems. Consequently, when selecting a method to eliminate pathogens from soils or from waters it is important to know in advance how these microorganisms may reach their final disposal site.

Viruses are harder to eliminate than bacteria from water due to their small size and resistance to physical and chemical treatments. An option to eliminate submicron particles from water, is the use of commercial or specifically designed membranes. Electrostatic interactions play a fundamental role in this process as it was studied in Chapters V and VI.

Chapter V describes the study of electrostatic interactions and attachment that exist between a virus and a ceramic membrane. The first step of the work consisted in growth and purification of bacteriophage P22, that was used as a surrogate for pathogenic viruses of similar size. A nanostructured iron oxide ceramic membrane was employed. Different pHs were considered for size and zeta potential measurements of both viruses and ceramic particles. The attachment and kinetics experiments were performed at ITBA by María Victoria Gallardo and Fernando Miguel Yrazu under the guidance and direction of Dr. María Marta Fidalgo de

Cortalezzi. As a result, DLVO modeling was necessary to provide the experimental results with substantial explanation and further insight. Since the mechanism of removal was determined to be electrostatic in nature, DLVO analysis of the attachment predicted it to be effective in a certain range of pH (up to 6.5).

Chapter VI also describes the study of forces between viruses and ultrafiltration membranes. In this case, a much smaller bacteriophage was used and the membrane was made of polyethersulfone. Bacteriophage PP7 was chosen as a surrogate for poliovirus in water treatment processes, since both are icosahedral and have similar size, and because it offers challenging conditions for membrane testing due to its small size. The virus and the membrane were characterized with respect to size and surface charge under a broad range of relevant conditions of pH and ionic strength. The filtration experiments were performed at INIQUI, Universidad Nacional de Salta by Dr. Mercedes Cecilia Cruz under the guidance and direction of Dr. Verónica Beatriz Rajal. Afterwards, the filtration mechanism and its limitations were analyzed and discussed under DLVO and X-DLVO theories. The ultrafiltration experiments showed partial removal of PP7, which could be explained by the influence of the aqueous matrix in the present interactions between the bacteriophages and the surface: divalent cations diminished the effectiveness as opposed to monovalent cations and species with amphoteric behavior such as bicarbonate. These results highlighted the importance of electrostatic interactions in virus-membrane filtration.

The importance of the works presented in Chapters V and VI lies in the confirmation that electrostatic forces, such as van der Waals attraction and electric double layer repulsion, play a key role in virus removal by filtration methods. In particular, polymeric and custom-made ceramic membranes provided similar underlying nature. It was also proved that the efficiency of the process is affected by the constituents of the aqueous matrix. Improvements to current membrane filtration settings can be of great benefit to obtain water with better quality.

Chapter VII offers a different application for water filtration membranes. In this chapter, the work did not focus on potabilization or improving water quality; instead, the production of electric energy was studied. Pressure retarded osmosis is a process that enables power production from two streams of different osmotic pressure. The objective of the work was to simulate this technology in a real scenario, such as the Negro River mouth, in the south of our country, and predict the net power density taking into account natural water qualities and equipment needed. The simulation was performed using UniSim Design with OLI Electrolyte fluid package. The results showed that energy generation was possible and that the simulation was

very useful as a first step to assess the feasibility of this technology. I would like to thank Paula Llano, who kindly revised the simulation performed in the work.

The work described in Chapter VII can be a start point for future research, allowing the introduction of "blue" energy into the energy matrix.

It is worth to mention that, up to now, the work of this thesis resulted in the following articles:

- "Virus removal by iron oxide ceramic membranes". María M. Fidalgo de Cortalezzi, María V. Gallardo, Fernando Yrazu, Guillermina J. Gentile, Oscar Oppezzo, Ramón Pizarro, Hugo R. Poma, Verónica B. Rajal. Journal of Environmental Chemical Engineering, Volume 2, Issue 3, September 2014, Pages 1831-1840. http://dx.doi.org/10.1016/j.jece.2014.08.006
- "Enhanced Retention of Bacteria by TiO_2 Nanoparticles in Saturated Porous Media". Guillermina J. Gentile, María M. Fidalgo de Cortalezzi. Journal of Contaminant Hydrology, Volume 191, August 2016, Pages 66-75. http://dx.doi.org/10.1016/j.jconhyd.2016.05.004

Furthermore, the following presentations are the result of the present thesis:

- "Simulating Pressure Retarded Osmosis Using UniSim Design". Guillermina Gentile, Paula Llano, María Marta Fidalgo de Cortalezzi. Poster session. II Simpósio de Processos de Separação com Membranas, Rio de Janeiro, Brazil. July 29 - August 02, 2013.
- "Simulating Pressure Retarded Osmosis Using UniSim Design". Guillermina Gentile, Paula Llano, María Marta Fidalgo de Cortalezzi. Poster session. 7th IWA Specialized Membrane Technology Conference and Exhibition for Water and Wastewater Treatment and Reuse, Toronto, Canada. August 26 - 29, 2013.
- "Simulating Pressure Retarded Osmosis Using UniSim Design". Guillermina Gentile, Paula Llano, María Marta Fidalgo de Cortalezzi. Poster session. V Seminario por el Día Mundial del Agua, Buenos Aires, Argentina. March 31, 2015.
- "Remoción de Virus mediante Ultrafiltración: Rol de las Interacciones entre Partículas y entre Partículas y Superficies". Guillermina Gentile, Mercedes Cecilia Cruz, María

Dolores Blanco Fernández, Verónica Beatriz Rajal, María Marta Fidalgo de Cortalezzi. Oral session. VIII Congreso Argentino de Ingeniería Química, Buenos Aires, Argentina. August 02 - 05, 2015.

- "Role of Interparticle and Particle-Surface Interactions on Virus Removal by Ultrafiltration Membranes". Guillermina Gentile. Seminar. Department of Civil and Environmental Engineering, University of Missouri, Columbia, MO, USA. October 30, 2015.
- "Attachment of Bacteriophage P22 to Nano Structured Iron Oxide Ceramics: Implications for Drinking Water Treatment". Guillermina Gentile, María Victoria Gallardo, Fernando Yrazu, Oscar Oppezzo, Ramón Pizarro, Hugo Ramiro Poma, Verónica Beatriz Rajal, María Marta Fidalgo de Cortalezzi. Poster session. 15 AIChE Annual Meeting, Salt Lake City, UT, USA. November 8 - 13, 2015.
- "Role of Interparticle and Particle-Surface Interactions on Virus Removal by Ultrafiltration Membranes". Guillermina Gentile, Mercedes Cecilia Cruz, María Dolores Blanco Fernández, Verónica Beatriz Rajal, María Marta Fidalgo de Cortalezzi. Oral session. 15 AIChE Annual Meeting, Salt Lake City, UT, USA. November 8 - 13, 2015.

Chapter II

BACKGROUND

II.1. Colloids, nanoparticles, engineered nanomaterials

Colloids have been defined as particles with one dimension smaller than 1 μm, although some exceptions may exist. Terms such as particles, colloids, colloidal dispersions, and colloidal suspensions can be considered synonyms. Natural and engineered colloidal particles are commonly found in groundwater, surface water, and soils. Contaminants, such as metals, metal oxides, radionuclides, organic compounds, macromolecules, and microorganisms, are colloids themselves or are associated to them in natural environments (i.e., adsorption onto clays or other organic compounds).[1] By definition, colloids include organic and inorganic substances, as well as biological material such as viruses and some bacteria.[2]

Nanoparticles are defined as materials with at least two dimensions between 1 and 100 nm.[3] They have always been present in the environment, from natural or anthropogenic origins.[2] When in air, they were traditionally referred to as ultrafine particles, while in soil and water they are described as colloids, with a slightly different size range.[4] Widely used and investigated engineered nanoparticles include metals (Au, Ag, Cu, Al, Ni, Co), metallic oxides (TiO_2, ZnO, CuO, CeO_2, Fe_3O_4, Fe_2O_3), carbon, and quantum dots.[5]

Engineered nanomaterials are manufactured products that have at least one dimension smaller than 100 nm and are mainly made of carbon, metal, or metal oxide.[3, 6, 7]

In March of 2015, the Nanotechnology Consumer Products Inventory (CPI) listed 1,814 products containing nanomaterials from 622 companies in 32 countries. There are 39 types of nanomaterial components in the Inventory, divided in groups related to the composition: metal and metal oxides (e.g., Ag, Ti, Zn, Au, Mg, Cu, Pt, Fe, Al_2O_3, TiO_2, ZnO_2, iron oxides), carbonaceous (carbon black, carbon nanotubes, fullerenes, graphene), silicon (Si and SiO_2), and other (e.g., polymers, organics, ceramics).[8] In particular, the annual production of TiO_2 exceeds 5,480,000 million tons, which represents 70% of the total production volume of pigments.[9]

Nanoscale products and materials are increasingly used in optoelectronics, electronics, odontology, medicine, drug delivery, cosmetics, sunscreens, catalysts, fabrics, anticorrosion, coatings, food and beverages, automotive, home and garden supplies.[8, 10]

II.1.1. Properties of nanoparticles and nanomaterials

The main properties to characterize nanomaterials in environmental studies are size, solubility, surface area, surface charge, and surface chemistry.[11] Fate and toxicity of natural and engineered particles is mainly determined by their size and size distribution, in conjunction with surface properties.[12]

Differences arise between natural and engineered nanoparticles, the former are polydispersed and chemically complex in nature, while the latter are monodispersed and have precise chemical composition. However, equivalent principles and toxicity apply to both of them.[13]

Due to their high surface area to volume ratio, the properties of nanoparticles differ from those of their constituent molecules, and from those of the bulk material. Besides, size and properties of engineered nanomaterials prior to use are often different from those stated by the supplier due to variations in the physicochemical properties over time and agglomeration.[14]

Surfactants can modify the surface and interfacial properties, leading to stabilization by conserving the particle charge or by modifying its surface.

II.1.2. Transport and fate of nanomaterials and risks for the environment and health

There is an ongoing interest in evaluating the potential risks associated with the application of engineered nanomaterials on living organisms, but first it is necessary to know the sources and fate of produced nanomaterials in order to evaluate their hazards and impact in the environment and health.[15]

Sources of nanoparticles are various and different, among which we can mention: stationary (coal/oil/gas boilers, incinerators, smelters, cooking, cigarette, residential combustors) and mobile emissions (diesel/gasoline/LPG/CNG vehicles, metals in catalytic

converters/fuel cells), atmospheric conversion, industrial processes, and engineered nanoparticle production.[16]

Colloids, nanoparticles and engineered nanomaterials reach the environment due to unintentional and intentional releases and some of them may contaminate soils and waters and interact with living species.[2, 5] Their transport and fate depend on aggregation phenomenon, which may lead to: aggregates well larger than 1 μm;[2] transfer from soil and water to plants as the first step to enter the food chain;[17] interactions among them and with other molecules and cells in the medium;[18] and transformations due to physical and chemical reactions.[17]

Not only the final disposal is important, but also the physical form in which the nanomaterial is present (aggregated or degraded), the final concentration, and the potential organisms affected.[19, 20]

Understanding how nanomaterials behave in the environment is fundamental to estimate their fate. Important properties are degradation, dispersion stability, solubility, and bioaccumulation. Degradation and surface modifications may cause a change in the way the nanoparticles interact with the medium. Dispersion stability affects the transport and consequently the final fate in soils and waters, and depends on the state of aggregation that can be modified by the presence of natural organic matter, clays, as well as ionic strength and pH. Solubility is particularly important in the case of metals and metal oxides that could leach soluble ions into natural waters. Bioaccumulation of these nanoparticles and nanomaterials by organisms is difficult to assess since the transport along the food chain must be known.[19]

Higher human exposure is expected at working places where the raw nanomaterials are present in large quantities. This contact can happen via inhalation, dermal exposure, or ingestion. Another form of contact is by means of the environment after release during manufacture, downstream uses and incineration, or by consumption and use of the final products.[19]

Toxicity research has mainly focused on the respiratory system, although skin and gastrointestinal tract should also be taken under analysis.[13] Carbon and silica nanomaterials may cause pulmonary diseases, granulomas and fibrosis; carbon, silver, and gold nanomaterials may access organs including the central nervous system; quantum dots, carbon, and TiO_2 nanoparticles may penetrate the skin; carbon, MnO_2, and TiO_2 nanoparticles may enter the brain through nasal epithelium olfactory neurons; TiO_2, Al_2O_3, carbon black, cobalt, and nickel nanoparticles can be more toxic than thought if compared with micron sized particles.[5]

II.2. Bacteria

Bacteria are prokaryotic microorganisms. These cells lack of the nucleus that is present in eukaryotic cells.

In particular, this work will focus on the bacterium *Pseudomonas aeruginosa* for the transport experiments. Electrostatic interactions as well as aggregation and attachment will be studied as the main causes for retention in the porous bed; therefore, the bacteria will be considered as particles with charge on their surface.[21-25]

II.2.1. *Pseudomonas aeruginosa*

Pseudomonas aeruginosa is a Gram-negative, aerobic bacterium, known as an opportunistic human pathogen. It is a coccobacillus, a type of bacterium with a shape intermediate between coccus (spherical bacterium) and bacillus (rod-shaped bacterium); therefore, it can be considered as a very short rod.

Pseudomonas derives from the Greek “pseudo” that means "false” and “monas” that means “single unit". *Aeruginosa* indicates the Latin word meaning “verdigris” or “copper rust” that makes reference to the pigment seen in the cultures.

Bacteria that have a thin cell wall surrounded by a second lipid membrane are referred as Gram-negative.

These bacteria can be isolated from soil, water, plants, animals, and humans.[26] They secrete many pigments: pyocyanin (blue-green), pyoverdine (yellow-green and fluorescent), and pyorubin (red-brown), which can serve as means of identifying the bacteria. Their grape-like odor in vitro is also a way of certifying their identity.

II.3. Viruses

Viruses consist of a nucleocapsid which is formed by the genome (single- or double-stranded RNA or DNA) and the surrounding capsid or coat (repeated subunits of proteins). An envelope (lipid bilayer and glycoproteins) may also be present in some viruses.

The amino acids that are on the outer and the inner surface of the capsid are the only ones that can be in contact with the solution and thus, contribute to the surface charge.[27] Interactions and reactions between viruses and materials are therefore, similar to those shown by proteins. Surface charge and isoelectric point (IEP) depend on the ionization of functional groups on the capsid and envelope.[28]

Methods of stock preparation and purification influence the contact between the viruses and host cell debris, protein residues, or other present materials. This alters the external surface and net charge of the viruses, consequently affecting their behavior in an electrolyte suspension, their interactions with different surfaces, as well as determination of the IEP.[29]

According to the studies of interest, the easiest way of modifying the capsid charge, as with any nanoparticle, is not changing the capsid itself but the pH of the solution, which in turn will influence the charge of the coat protein. Therefore, for relevant environmentally experiments, pH should be adjusted between 5 and 8.[29]

II.3.1. Multiplication process

The multiplication process has four consecutive stages: adsorption of the virus to the host cell, penetration into the cell, multiplication of the virus in the interior of the cell, and release of the progeny.

When the viruses are released, the first growth cycle is completed. Afterwards, the progeny may repeat the process and a second growth cycle will occur. This process will continue at an exponential rate[30] until no bacteria remains.

II.3.2. Bacteriophages

Bacteriophages are viruses that infect bacteria. In particular, this work will focus on two different bacteriophages that have been employed as model substitutes of human pathogen viruses.

Virus attachment to adsorbents and virus filtration depend on electrostatic interactions as well as aggregation and attachment. Therefore, the viruses will be considered as particles with charge on their surface.[1, 31-33] Both bacteriophages, P22 and PP7, were considered as spheres due to their icosahedral shape.[34]

II.3.2.1. Bacteriophage PP7

Bacteriophage PP7 belongs to Leviviridae family, Levivirus genus and infects *Pseudomonas aeruginosa*. It is naked, has icosahedral capsid (T=3), and positive sense single-stranded RNA. The RNA consists of 3,588 nucleotides[35] and represents 39% of the virion weight.[36] The coat protein has a molecular weight of 13,874 and contains 42% of hydrophobic residues.[37] There are 180 copies of the coat protein of 127 amino acids each.[35] A copy of A-protein, required for maturation of the virion and for pilus attachment, is also present.[36]

The first P in its name indicates that it is a phage of *Pseudomonas aeruginosa*, the second P makes reference to the place where it was first isolated: Pangbourne (Berkshire, England).[38] The natural habitat of PP7 is the same as its host bacterium, which include soil, water, sewage, the intestinal canal, and the human skin.[38]

II.3.2.2. Bacteriophage P22

Bacteriophage P22 belongs to Podoviridae family and infects *Salmonella typhimurium*. It has icosahedral capsid (T=7), an 18-nm tail that consists of six tail spikes, and linear double-stranded DNA. The DNA, of 41,754 bp, represents 55% of the virion weight. There are nine structural proteins: 415 copies of the major capsid protein (gp5), 12 copies of the portal protein (gp1), two hub proteins (gp4 and gp10), three pilot/injection proteins (gp7, gp16, gp20), 3 copies of the tail needle protein (gp26), and 18 copies of the tailspike/endorhamnosidase protein (gp9).[36]

II.4. Quality of natural waters

Aquatic chemistry studies the different reactions and processes related to the distribution and circulation of species in natural waters. Water interacts with the atmosphere and earth, due to processes such as dissolution and precipitation, oxidation and reduction, acid-base, and complexation.[39]

Natural aquatic environments are very difficult to reproduce artificially since reactions and processes in nature have different time and spatial scales than those in the laboratory. Therefore, modeling is vital, specially simple and useful models, that although they do not

account for all the complexity of natural waters, they are helpful in understanding the underlying phenomena.[39]

Different parameters are important to evaluate the quality of natural waters: physical (odor, taste, color, suspended solids, temperature), chemical (total dissolved solids, alkalinity, hardness, metals, organic matter, nutrients, fluorides), and biological (species diversity, bacteria, viruses, protozoa).[40]

Water contamination is the result of natural and anthropogenic processes. The former include geological, biological and physicochemical processes in the biosphere, putrefaction of organic matter, and arsenical pyrite dissolution in aquifers. The latter involve industrial emissions, wastewater and sewage, chemicals from agricultural activities, industrial and domestic waste, presence of hydrocarbons, gas leaks from underground storage tanks, and infiltrations from landfills and waste deposits.

In particular, waters can be contaminated by the presence of pathogens. These organisms infect a host, where they grow and multiply.[41] Many of these pathogens (such as bacteria, viruses, protozoa, helminths, fungi, and rickettsiae) infect humans.[42] Transmission of infectious agents include the transport from the reservoir to the host.

Groundwater flow is governed by the Darcy's law:

$$Q = -k\,A\,\frac{\mathrm{d}h}{dL} \qquad \text{(II.1)}$$

where Q: water flux, k: hydraulic conductivity, A: cross-sectional area to flow, Δh: change in hydraulic charge, L: length of the column. And Darcy velocity (v) can be defined as:

$$v = \frac{Q}{A} = -k\frac{dh}{dL} \qquad \text{(II.2)}$$

The hydraulic conductivity is a measure of the ability of the materials for transporting water and depends on the porosity and on the water flux.

In porous media, the cross-sectional area to flow (A) is not the effective cross-sectional area (A_v) since only the free volume (pores) is available to the water flow. Therefore, filtration velocity in porous media (v_s) will be different from Darcy's:

$$Q = v\,A = v_s\,A_v \qquad \text{(II.3)}$$

II.4.1. Mechanisms of transport of contaminants

Basically, contaminants are transported by advection, mechanical dispersion, diffusion, and hydrodynamic dispersion[43] (Fig. II.1).

Advection is responsible for carrying dissolved solids with the water flow. The amount of transported solutes depends on their concentration. If this is the only mechanism present, contaminants will emerge abruptly since the direction and rate of transport coincide with that of the groundwater flow (piston flow that replaces the water in the pores with the contaminated water).

Mechanical dispersion is the process of mixing that takes place in porous media as a result of the movement of fluids through the pore space. The flow of water is divided into various smaller fluxes, altering its direction. Thus, the mass of contaminants is expanded to an increasing volume, but its concentration diminishes. Dispersion is both longitudinal (the dilution occurs along the advancing front) and transversal (the solute front is dispersed perpendicularly to the flow).

Diffusion is characteristic of small solutes, such as colloids, molecules and ions. In this case, the gradient of concentration in the porous media is the driving force. It is a very slow process and can occur when there is no hydraulic gradient driving flow and the pore water is static.

Hydrodynamic dispersion is the result of mechanical dispersion and diffusion acting together. It is typical in groundwater flux, since these two mechanisms cannot be separated.

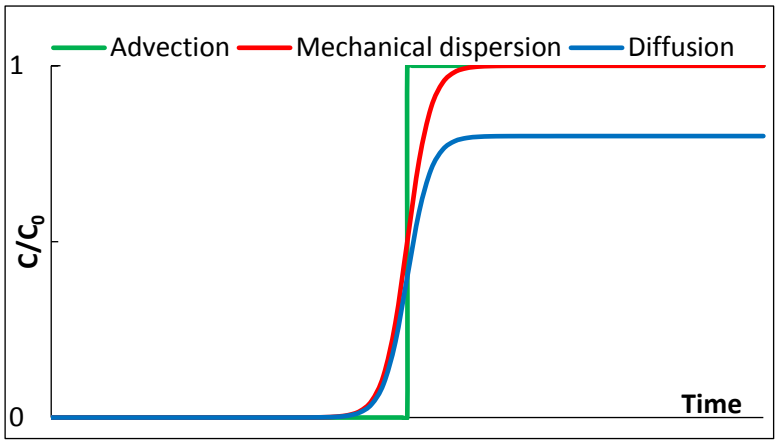

Fig. II.1: Breakthrough curves for the different mechanisms present in groundwater transport of contaminants.

For mass transport, Fick's law relates solute flux to concentration gradient in a liquid:

$$\frac{Q}{A} = -D\,\nabla C \tag{II.4}$$

where D: diffusion coefficient, C: contaminant concentration. When the fluid is at rest, diffusion is the only mechanism that takes place, therefore:

$$\frac{Q}{A} = -D_x\frac{\partial C}{\partial x} - D_y\frac{\partial C}{\partial y} - D_z\frac{\partial C}{\partial z} \tag{II.5}$$

$$\frac{\partial C}{\partial t} = D_x\frac{\partial C^2}{\partial x^2} + D_y\frac{\partial C^2}{\partial y^2} + D_z\frac{\partial C^2}{\partial z^2} \tag{II.6}$$

While, when the fluid is moving:

$$\frac{Q}{A} = v_xC + v_yC + v_zC - D_x\frac{\partial C}{\partial x} - D_y\frac{\partial C}{\partial y} - D_z\frac{\partial C}{\partial z} \tag{II.7}$$

$$\frac{\partial C}{\partial t} = -v_x\frac{\partial C}{\partial x} - v_y\frac{\partial C}{\partial y} - v_z\frac{\partial C}{\partial z} + D_x\frac{\partial C^2}{\partial x^2} + D_y\frac{\partial C^2}{\partial y^2} + D_z\frac{\partial C^2}{\partial z^2} \tag{II.8}$$

II.5. Removal of contaminants in water systems

II.5.1. Adsorption onto porous media

Porous medium is a group of collectors or grains on which particles from an aqueous suspension are deposited.[44] This deposition is a two-step process, first particles should move from the bulk solution to the vicinity of the surface and afterwards they must be adhered to the collector. This last step is closely related to interactions that depend on the nature of both particles and collectors.

Particle transport to the vicinity of the collector or grain is due to three mechanisms: Brownian motion (diffusion), gravitational sedimentation and interception (Fig. II.2). The small colloidal particles (< 1 μm) are subject to chaotic Brownian motion, which is due to collisions between these colloids and molecules of the fluid. For bigger particles (> 1 μm) gravitational settling and interception are the main responsible mechanisms. Gravity leads to the settling of denser particles on the collector. Interception is due to the contact between the particle moved by the flow and the collector due to its finite size.[45]

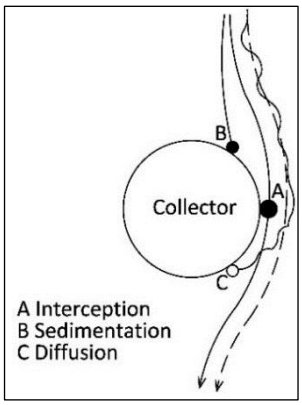

Fig. II.2: Transport mechanisms in water filtration.

The classic filtration model by Yao, et al. was based on additivity of the three mechanisms.[45] It does not account for viscous or hydrodynamic, nor van der Waals forces.[46] However, the inclusion of these interactions can lead to cumbersome work, not always of benefit. Rajagopalan and Tien developed a semi-empirical correlation equation for predicting filtration efficiency.[47, 48] Another correlation equation was given by the work of Tufenkji and

Elimelech for calculating the efficiency of a single collector in physicochemical filtration.[46] In this last correlation equation, the first step (transport) of the deposition is expressed by the number of particles that reach a collector by advective rate entering the projection of the collector; the second step (attachment) is obtained taking into account the portion of particles that effectively attaches to the collector among all the particles that contact it. If these two values are multiplied, the single collector efficiency is obtained.[1, 46, 49]

Physical structure of the media plays a key role in the retention mechanisms. If the material is very porous, it will have more surface area and a greater number of particles will be retained. Rougher materials offer more tortuous paths augmenting the retention. Size exclusion offers a physical constraint, when large colloids cannot enter the smallest pores, and then influences the transport behavior.[50]

Bacteria and viruses are present in the subsurface suspended in the water phase as well as attached to mobile colloids.[50] In particular, bacteria transport is influenced by physical conditions: water velocity and number of present bacteria,[51-54] physiological factors: bacterium size and motility,[55-57] surface properties: hydrophobicity and presence of lipids and polysaccharides.[58-60] Bacterial attachment to solid collectors is highly affected by properties and characteristics of both bacterium and surface as well as the chemistry of the medium.[61-64]

II.5.2. Water treatment processes

Aquatic chemistry is vital since water is fundamental for life. Human activities have influenced the quality of natural waters and restoration of these systems needs the conjunction of physical, inorganic, organic, and interfacial chemistry.[39]

Water for human consumption, must be free of disease causing organisms, toxic minerals and organic substances, should not exhibit turbidity, color, odor or taste, and must have a reasonable temperature.[65] The selection of a water treatment process is closely related to the source of water supply: groundwater, surface water, or reclamation water. Even for each type of source, the treatment will vary with climate, watershed characteristics, geology, saltwater intrusion and human factors such as industrial and wastewater discharges, agricultural runoff, land development, landfills, erosion, etc.[66]

Two general water treatment schemes can be identified, depending on the source of the water supply: surface water or groundwater.

Surface water needs to be treated to remove its particulate content, taste, odor, and microorganisms but it is not usually treated for hardness. The basic treatment consists of a first screening to remove large materials followed by coagulation, flocculation, sedimentation, and filtration. Some facilities may have two stages of coagulation-flocculation-sedimentation, depending on the quality of the incoming water; some source waters of low quality may require additional treatments such as granulated activated carbon (GAC) to furtherly remove organic compounds that produce intense taste and odor. A primary oxidant or disinfectant such as chlorine, ozone, chlorine dioxide or permanganate, is usually added right after the first screening to control bacteria content, algae growth, taste, and odors. Iron and aluminum salts and some polymers that are used as coagulants, lower the pH and thus, lime, soda ash or caustic soda have to be added to adjust the pH to the desired levels. A final disinfectant addition guarantees low microbiological activity in the distribution systems.[67]

The main problem associated with groundwater as a drinking water supply is the hardness, and the content of iron and manganese ions. The treatment includes adding lime for calcium and magnesium removal and soda ash if non-carbonate hardness is present. The excess lime softening treatment consists of the addition of lime and flocculants, causing the precipitation of $CaCO_3$ and $Mg(OH)_2$, which is then removed by settling. The treated water has a high pH and needs to be adjusted with CO_2. If the non-carbonate hardness is high, a treatment with soda ash is required, followed by settling and CO_2 addition to adjust pH. After a filtration and final disinfection stage, water is ready for distribution. Groundwater with low to moderate hardness may not require all of the above mentioned steps, making a much less expensive treatment scheme.[67]

II.5.2.1. Membranes in water treatments

A membrane is a thin layer that separates two phases and allows the flux of matter across itself selectively. In membrane operations, a feed stream will be separated in two smaller streams, on one side the fraction that passes through the membrane (permeate) and on the other, the part that does not (retentate). Porous membranes exhibit high specific surface areas due to their open structure. Non-porous membranes are capable of separations at molecular level; in this case, the transport occurs by a solution-diffusion mechanism, and the separation takes place due to a difference of either solubility or diffusivity between compounds.

According to their morphology, membranes are classified as symmetric or asymmetric: the first ones are homogenous in pore structure along the membrane thickness, while the second ones are formed by several layers with different pore sizes and in some cases, different pore structures. These asymmetric or anisotropic membranes are formed by a thin layer supported onto another layer, which has higher porosity and thickness. Permeate flux and selectivity only depend on the structure of the thin layer. The support layer function is to confer mechanical integrity. The difference between an asymmetric and a mixed membrane is that in the former the material of both layers is the same and in the latter layers are made of different materials.

Membranes can also be divided into two broad categories with respect to their composition: organic and inorganic. Organic membranes are commonly made of cellulose acetate, polysulfone (PSf), polyethersulfone (PES), polyacrylonitrile (PAN), polyetherimide, polycarbonate, polyetheretherketone (PEEK), polypropylene (PP), polytetrafluoroethylene (PTFE), polyamide, polyvinylidene-fluoride (PVDF).[68] Inorganic membranes include carbon, metal, metallic oxide, and ceramic materials.[69]

Membranes can be further classified with respect to their pore size, for microfiltration (0.1 - 10 μm), ultrafiltration (0.005 - 0.1 μm), nanofiltration (0.001 - 0.005 μm) and reverse osmosis (< 0.001 μm),[69] as illustrated in Fig. II.3. In microfiltration and ultrafiltration, porous membranes are used, where the separation mechanism is screening. In nanofiltration, membranes are porous; the separation mechanism is not only screening, but solution/diffusion and exclusion as well. On the other hand, dense membranes are employed in nanofiltration and reverse osmosis; since they do not have pores, diffusion happens in the free volume among macromolecules chains that constitute the membrane.

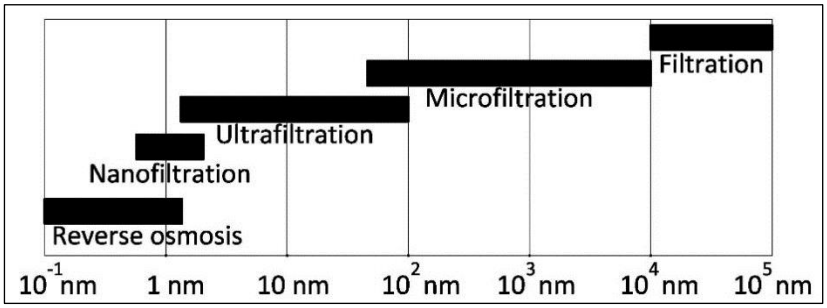

Fig. II.3: Porous size of membranes for water filtration.

Table II.1 presents some examples of retained species employing membrane processes.[69]

Table II.1: Retained species in microfiltration (MF), ultrafiltration (UF), nanofiltration (NF), and reverse osmosis (RO).

Species	Molar weight (Da)	Size (nm)	Applicable process			
			MF	UF	NF	RO
Yeast and fungi		10^3 - 10^4	X			
Bacteria		300 - 10^4	X	X		
Colloids		100 - 10^3	X	X		
Viruses		30 - 300	X	X		
Proteins	10^4 - 10^6	2 - 10		X		
Polysaccharides	10^3 - 10^6	2 - 10		X	X	
Enzymes	10^3 - 10^6	2 - 5		X	X	
Simple sugars	200 - 500	0.8 - 1			X	X
Organic compounds	100 - 500	0.4 - 0.8			X	X
Inorganic ions	10 - 100	0.2 - 0.4				X

UF membranes have a pore size range similar to the size of enteric viruses, resulting in a good mechanical barrier.[70]

Viruses are removed by membranes due to three mechanisms: size exclusion, adsorption (hydrophobic and attraction of different charges) and electrostatic repulsion (when the virus and membrane have similar surface charge, giving rise to repulsive forces that in turn will prevent the virus from passing through the membrane pores).[71-73] The predominant mechanism will be size exclusion (physical straining) when the hydrodynamic diameter of the virus is larger than the pores.[71] On the contrary, when the pores are larger than the viruses, adsorption and electrostatic repulsion will be predominant and the surface properties and charge of both viruses and membranes in the water system will become relevant for the filtration process.

The separation can be driven by pressure (Fig. II.4), concentration, or temperature difference.

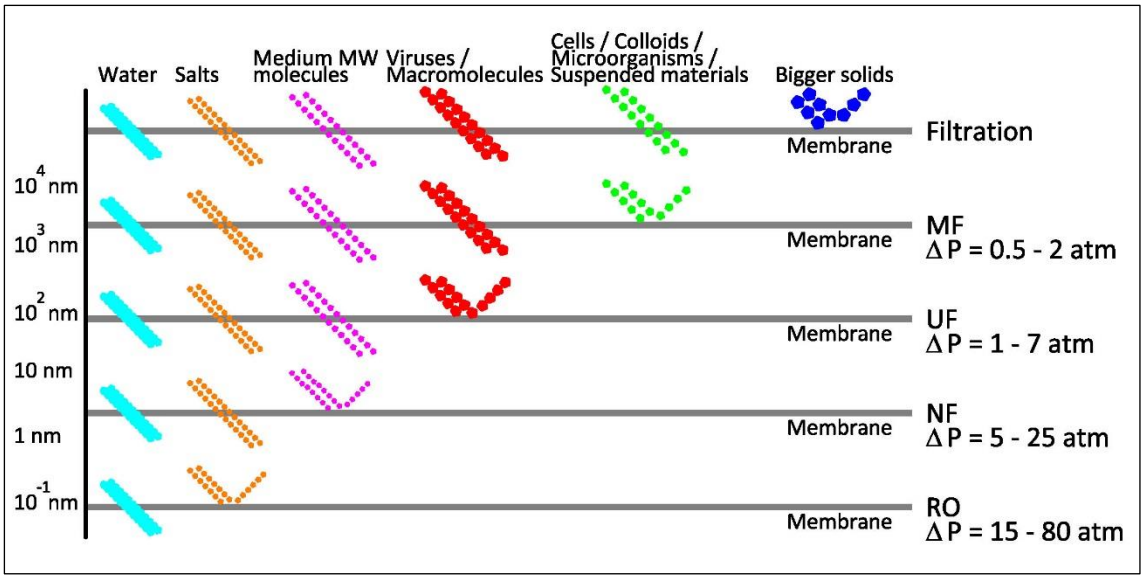

Fig. II.4: Pressure driven filtration processes.

II.6. Osmosis

When two aqueous solutions of different salt concentration are separated by a semipermeable membrane, a gradient of concentration will establish through this membrane. This will originate a water flux from the most diluted solution (of high chemical potential) to the most concentrated one (of low chemical potential).

If the diluted solution is pure water, its salt concentration will be null and osmotic pressure can be defined as the hydrostatic pressure (or water column) that is necessary to apply to the salt solution in order to stop the flux, and can be expressed as:

$$\pi = \Phi\ I\ M\ R_g\ T \qquad \text{(II.9)}$$

where π: osmotic pressure (kPa), Φ: osmotic reflection coefficient, I: number of ions per dissociated molecule, M: molarity, R_g: gas constant (kPa dm^3 K^{-1} mol^{-1}), T: temperature (K). When various salts are present in a solution, Eq. II.9 can be generalized to Eq. II.10:

$$\pi = \sum_{i=1}^{n} \Phi_i\ I_i\ M_i\ R_g\ T \qquad \text{(II.10)}$$

where Φ_i, I_i, M_i correspond to each salt.

Therefore, osmosis is the passage of fluid through a semipermeable membrane where the driving force is a difference in the osmotic pressure on both sides of this membrane. The objective of osmosis is to achieve the most stable thermodynamic state, which leads to equate both osmotic pressures.

Three different types of osmosis are established upon osmotic pressures of the solutions and applied hydrostatic pressures, as follows in Table II.2 and in Fig. II.5:

Table II.2: Types of osmosis processes.

Osmosis	ΔP	Water flux
Forward osmosis (FO)	= 0	From diluted solution to concentrated solution.
Pressure retarded osmosis (PRO)	$< \Delta\pi$	
Reverse osmosis (RO)	$> \Delta\pi$	From concentrated solution to diluted solution.

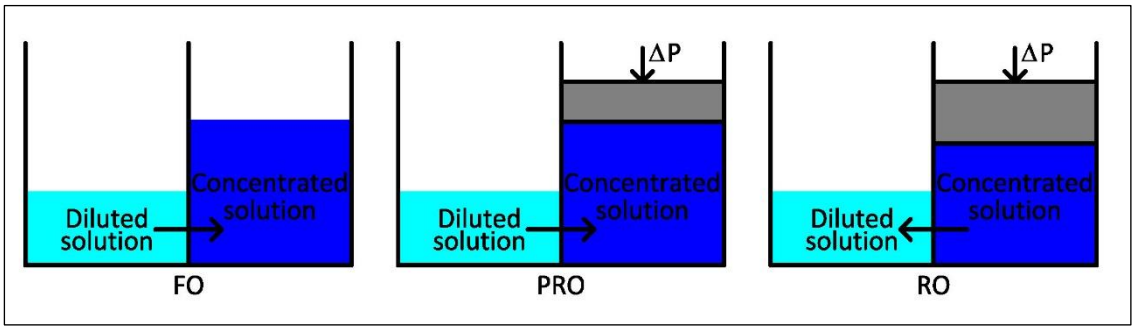

Fig. II.5: Types of osmosis processes.

The difference of applied hydrostatic pressures to the concentrated and to the diluted solutions (ΔP) in relation to the difference of osmotic pressures between the two solutions ($\Delta\pi$) will determine whether the water flux will be forward or reverse.

In the case of forward osmosis, a net difference of hydrostatic pressures will not exist. If osmosis is retarded by the applied pressure, flux will be forward but slower. In reverse osmosis, water flux will be from the concentrated to the diluted solution, as opposed to the two previous situations.

The location of the membrane is different for each case in order to obtain better results. Integrity of the membrane and resistance to the mass transfer and applied pressure are desirable. Therefore, the denser part of the membrane will face the diluted solution in forward osmosis and it will face the concentrated solution in pressure retarded osmosis and reverse osmosis.[74]

Flux across the membrane can be obtained from:[74, 75]

$$J_w = A\,(\Delta\pi - \Delta P) \qquad \text{(II.11)}$$

where J_w: water flux (m s^{-1}), A: water permeability coefficient (m s^{-1} kPa^{-1}), $\Delta\pi$: osmotic pressure difference (kPa), ΔP: hydrostatic pressure difference (kPa). The sign of J_w will indicate the water flux sense, according to the process.

II.6.1. The water-energy nexus: Energy production by pressure retarded osmosis

Membrane processes have grown significantly in different applications due to a number of technological advances that rendered them more efficient, economical, and easy to use.[76] Among these advances, we can cite the development of new materials or modification of existing ones, improved manufacturing processes that lead to membranes with better selectivity, permeability and resistance to chemical or biological attacks, and reformulation processes both at the pre-treatment stage as in the design of the membrane modules specifically.

In addition to the separation unit itself, there is a growing interest in the re-engineering of the membrane treatment system from an economic standpoint, aiming for minimization of consumed energy and not only quality and quantity of water obtained. This is of particular relevance since energy is the controlling cost in membrane systems.[77]

There is an interrelationship between water and energy. While water is required for power generation, obtaining drinking water also needs energy. Both resources are limited and limit the availability of the other. Therefore, water treatment projects should take into account and are influenced by energy consumption, and vice versa. Thus, it is not surprising to find that

the same processes and materials used in water treatment, e.g., membranes, find application in the energy field.

Membranes were first used in field of power generation with fuel cells, as fundamental part of the MEA (membrane-electrode-assembly) in PEMFC (proton exchange membrane fuel cells).[78] Another process for power generation involving membranes is pressure retarded osmosis (PRO), where the integration between water and energy is even more evident. In a PRO system, the difference of chemical potential that exists between a current with high salt content and one with low content is utilized for electricity generation.[74] The PRO concept emerged in the 1970s from a theoretical thermodynamic study but its practical realization was not feasible in its origins.[74, 79] More recently, and motivated by the quest for renewable energy sources, research projects have been reinitiated; and the first PRO plant was built in Norway.[80] However, the obtained efficiencies are far from the theoretic maximum, with limitations due to membrane materials, natural waters pre-treatment, fouling, and global use of energy available in the system.[81, 82]

Two water flows, the feed solution (FS) at low pressure and the draw solution (DS) pressurized and saltier enter a membrane module. The DS receives water from the FS through the semipermeable membrane due to its higher osmotic pressure. After the osmosis takes place, the concentrated solution will be diluted. If this diluted draw solution (DDS) is depressurized through a hydroturbine, electricity can be obtained. However, not all the now less concentrated stream will be used for power generation, since part of it will be recycled to pressurize the feed.[83, 84] A scheme of a typical plant is shown in Fig. II.6.

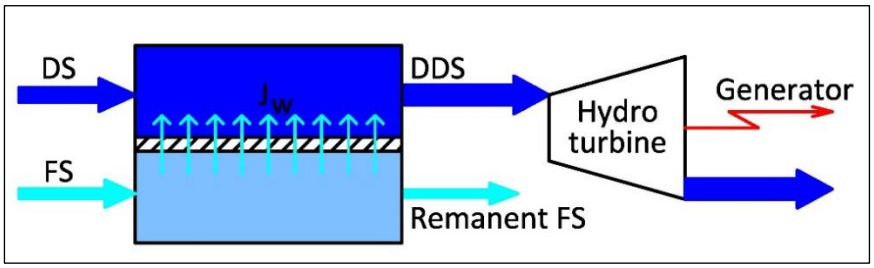

Fig. II.6: Pressure retarded osmosis scheme.

The diluted solution can be river water and the concentrated solution seawater or synthetic solutions that may or may not emulate those typical concentrations.[74, 85-90] Both solutions, natural or synthetic, will feed the unit where the membrane is placed. Pretreatment of the inlets can be required, according to water qualities to protect the membrane integrity.

Power can be obtained as:[74, 75]

$$W = J_w \, \Delta P \quad \text{(II.12)}$$

where W: power density (W m^{-2}). The maximum amount of power that can be theoretically obtained is related to ΔP:

$$W_{max} = A \frac{\Delta \pi^2}{4} \quad \text{(II.13)}$$

when: $\Delta P = \frac{\Delta \pi}{2}$ (II.14)

Typical operation pressures are from 11 to 15 bar for seawater and atmospheric for river water.[80, 91]

For the case of river water and seawater, the PRO plant can be installed at or below sea level. In the former case, river water is taken at the river mouth and seawater is pumped to the plant through underground tubing, afterwards the river flow can be maintained by discharging the seawater that emerges from the membrane module. In the latter case, the plant may be installed 100 to 130 m below sea level.[80]

II.6.1.1. Membranes for pressure retarded osmosis

Semipermeable membranes usually used in osmosis are asymmetric and possess a thin dense layer upon a porous support.[74, 80, 92] The dense layer is placed facing the solution whose pressure is higher; therefore, the membrane is capable of bearing the transmembrane pressure difference.

Most membranes used in PRO are made of cellulose triacetate (CTA) which forms a hydrophilic surface. Polyamide thin film composite (TFC) membranes are also employed, where the active layer of polyamide is formed by interfacial polymerization on a support layer of polysulfone made by phase separation on a thin layer of polyester.[80, 92, 93] Disadvantage of CTA

membranes is their low resistance to the action of microorganisms and diffusion of salts in the opposite direction to the water flow, from the concentrated towards the dilute solution. The configuration presents symmetric channels at both sides so the concentrated and the diluted solutions flow tangentially to the membrane. The membrane should allow an elevate water flux and simultaneously a high salt rejection.

Membrane optimization is expected to improve obtained power per unit area of membrane. In order to achieve this goal, membranes with thinner, less tortuous and more porous supports should be developed.[74] Furthermore, the configuration of the module where the membrane is placed should allow an optimal mixture to minimize fouling. Previous studies demonstrated that a PRO plant needs to produce 4 - 6 W m^{-2} to be profitable and at least five years of membrane lifespan.[74, 75, 80, 86, 94]

A drawback in processes conducted by difference in osmotic pressure is diffusion of salts in the opposite direction to the water flow.[95] Salts pass across the membrane from the concentrated to the diluted solution due to a concentration gradient. Therefore, the effective transmembrane osmotic pressure difference is lesser than the difference of osmotic pressures in both bulk solutions. The salt permeability coefficient for a specific membrane is expressed as:[74]

$$B = \frac{A\,(1-R)(\Delta P-\Delta\pi)}{R} \qquad \text{(II.15)}$$

$$\text{with: } R = 1 - \frac{C_P}{C_F} \qquad \text{(II.16)}$$

where B: salt permeability coefficient (m s^{-1}), R: salt rejection, C_P: salt concentration in the permeate, C_F: salt concentration in the feed.

Another phenomenon that reduces the difference in osmotic pressure is concentration polarization that consists in accumulation or diminishment of solute near the interface. Both types of concentration polarization will be present simultaneously. There will be a diminishment in the amount of solute per volume unit in the concentrated solution since it will be diluted as long as water will flow across the membrane. In this way, external concentration polarization (ECP) will arise by dilution in the dense layer. Besides, there will be an increase in salt

concentration within the porous support and internal concentration polarization (ICP) will be present. Fig. II.7 shows these two phenomena.

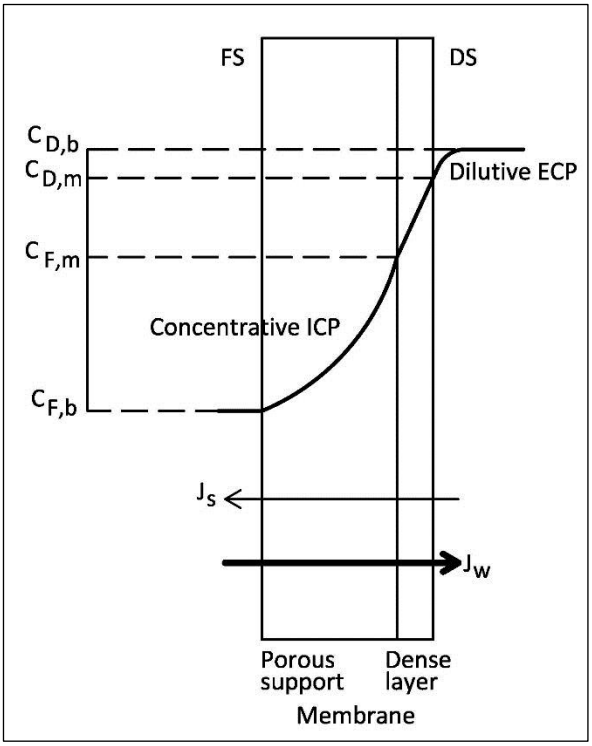

Fig. II.7: Phenomena that reduces the difference in osmotic pressure: ECP and ICP.

Influence of both phenomena should be taken into account to evaluate the water flow through the membrane, as described by the following expression:[74, 94, 96, 97]

$$J_w = A\left[\pi_{D,b} e^{-\frac{J_w}{k}} \frac{1-\frac{\pi_{F,b}}{\pi_{D,b}} e^{J_w K} e^{\frac{J_w}{k}}}{1+\frac{B}{J_w}(e^{J_w K}-1)} - \Delta P\right] \quad \text{(II.17)}$$

where k: mass transfer coefficient (m s^{-1}), K: solute resistivity to diffusion in the porous support (s m^{-1}), $\pi_{D,b}$: osmotic pressure in the bulk concentrated solution (kPa), $\pi_{F,b}$: osmotic pressure in the bulk diluted solution (kPa).

In ideal conditions, the water flux (J_w) will decrease until cancelled when $\Delta P = \Delta\pi$ and the power density (W) will increase up to a maximum value when $\Delta P = 0.5\ \Delta\pi$ and then it will diminish until cancelled when $\Delta P = \Delta\pi$. However, in real operation conditions, diffusion of salts opposed to water flux (represented by B) and concentration polarization (represented by k and

K) cause the osmotic pressure difference across the membrane to be lower than the osmotic pressure difference within both solutions, and therefore, the obtained J_w and W are lower than the expected values. Internal concentration polarization is increased by the passage of salt opposed to J_w and it is more important than the external concentration polarization.[74, 98] As water permeates, the concentrated solution will be diluted and the contrary will occur to the other solution. In this way, the driving force will be shrinking, reducing J_w and W.

II.6.1.2. Biofouling

Another important factor that decreases the process efficiency is the fouling produced during operation. Feed water usually has colloids and microorganisms (bacteria, fungi, microalgae) that can adsorb to the membrane and form a fouling cake.

Microorganisms reach the membrane by diffusion, sedimentation, or gravity. Accumulation is produced by aggregation (adhesion, adsorption) and by growing (cell multiplication). Adhesion of microorganisms will be first produced on the membrane and then to the previously deposited ones. Afterwards, these microorganisms will grow and reproduce, at the expense of the nutrients from the water that continuously feeds the system. Treatment of large quantities of water in a short time requires more contact between the liquid and the membrane surface, thus, increasing the possibility of contact between the microorganisms and the membrane.

Biofouling can be detected directly by microscopic observation or by biochemical/microbiological characterization of materials collected on the membrane. Indirect recognition can be made by evaluating efficiency variations (decrease in flow, increase in transmembrane pressure, more transport of solutes) or by determining a higher content of bacteria in the retentive than in the feed.

Some effects of biofouling are:

- Reduction in permeate: it gradually decreases and can be restored after cleaning.
- Reduction in solute rejection: it results from the increase of concentration polarization within the biolayer and the degradation of the membrane.

- Increase on mineral scales: it is due to the increase in concentration polarization and besides, nucleation points are generated enabling the growing of precipitates.
- Increase in transmembrane pressure: it is due to the blockage of spaces from the feed channel and to the increase in fluid friction when the biolayer is formed on the surface.
- Contamination in the permeate: caused by release of cells and biomass.
- Biodegradation of the membrane: caused by enzymatic hydrolysis of the polymers that constitute the membrane or by change in pH associated to the microcolonies. Both effects are favored by high temperatures and access to nutrients.
- Biological deterioration of the module: the components of the system can also be affected and damaged by the presence of the biolayer or its consequences.
- Reduction in the membrane lifespan: as a combination of the above mentioned effects, in addition to excessive cleaning and inadequate quantities of biocides.

Biofouling is favored by low feed water velocity, high temperature and operation pressures, high quantities of nutrients and organic matter, feed channels of small dimensions, and polymers that constitute the membrane that have strong affinity to bacteria.

Biofilms consist of extracellular polymeric substances, dead and viable cells, and ionic debris from dragged or precipitated inorganic matter. These structures are not always homogeneous, but sometimes an extensive network of channels filled with fluid.

One way to avoid this type of fouling is avoiding bacterial adhesion to the membrane using inhibitors, which should not interact adversely with the material of the membrane. Once the biofilm has been formed, cleaning will be necessary to remove it. The cleaning frequency is determined in order to avoid new biofilm growth and stabilization. In addition, older biofilms are more difficult to remove.

Chapter III

MATERIALS AND METHODS

III.1. Nanoparticles

For the transport experiments, Aeroxide TiO_2 P25 nanoparticles (Evonik Degussa Corporation, NJ, USA) were used. P25 is hydrophilic fumed TiO_2, mixture of rutile and anatase, with an average primary particle size of 21 nm, as reported by the manufacturer. The suspensions were prepared adding first the weighed nanoparticles to a considerable amount of water, then the required amount of salt (NaCl) and finally the remaining quantity of water to reach the needed concentrations of both salt and TiO_2. This procedure ensured that NaCl was diluted in order to avoid, as much as possible, aggregation of the nanoparticles while the suspension was prepared.

For the study of P22 removal by ceramic membranes, iron oxide nanoparticles were synthesized in the laboratory following a previously published procedure.[99] Briefly, lepidocrocite was obtained by oxidation of $FeCl_2$ (PPE, Argentina) under controlled pH. Secondly, the prepared lepidocrocite was reacted with anhydrous acetic acid (Anedra, Argentina) to yield ferroxane nanoparticles by the attack of the acid on the hydrogen bonds of the mineral structure. Finally, the ferroxane particles were sintered at 450°C and converted to iron oxide ceramic (hematite).

III.2. Bacteria

Bacteria *Pseudomonas aeruginosa* (ATCC 15692-B2) were used for the transport experiments. This selection was based on the minimal nutritional requirements and the tolerance of a wide variety of physical conditions.[26]

To multiply the bacteria, a portion of the original stock was spiked into 10 mL of autoclaved 8 g/L nutrient broth (Britania, Argentina) and incubated for 24 hours at 37°C on an orbital shaker at 120 rpm, the suspension was then centrifuged at 5,800 xg for 15 minutes and the supernatant discarded.

Purification consisted of pellet resuspension in 10 mL of the desired background solution (water, 1 mM, 10 mM, or 100 mM NaCl) followed by centrifugation at 5,800 xg for 15 minutes. To achieve higher purity, this procedure was performed three successive times. The final stock suspension was kept at 4°C overnight prior to use.[23]

Titration was made by counting CFU (colony-forming unit) in Petri dishes with nutrient agar, which was prepared mixing 8 g/L of nutrient broth, 8 g/L of NaCl (Anedra, Argentina) and 15 g/L of agar-agar technical for microbiology (Merck, Germany). A plate containing only melted soft agar served as negative control for bacteria. The plates were incubated at 37°C for 24 hours.

III.3. Bacteriophages

Two different bacteriophages were selected based on previous filtration and attachment experiments that were the basis of the present work. Bacteriophage P22 was used in the study of virus removal by ceramic membranes derived from ferroxane nanoparticles and bacteriophage PP7 was used in the study of virus ultrafiltration with commercial polyethersulfone membranes.

III.3.1. Bacteriophage P22

To replicate P22, first the host bacteria *Salmonella typhimurium* strain DA1468 were multiplied by adding 100 μL of the original stock to 50 mL of L broth: 10 g/L tryptone (Britania, Argentina), 5 g/L yeast extract (Britania, Argentina), 5 g/L NaCl (Anedra, Argentina) in an Erlenmeyer flask and incubated for 48 hours at 37°C. Afterwards, the Erlenmeyer was connected to an air pump until turbidity was observed. At that moment, 300 μL of the original stock of P22 were added and the aeration was continued placing the Erlenmeyer in a 40°C water bath. The lysis was produced when the culture clarified. Under the same conditions, 0.2 mL of chloroform were added to destroy any bacteria that could be still present. After 15 minutes, the culture was centrifuged to remove the viruses from bacterial debris at 5,000 rpm for 5 minutes. The supernatant, containing the viruses, was separated and 0.2 mL of chloroform were added to ensure proper conservation at 4°C.

After replication, to purify the P22 bacteriophage, the suspension was centrifuged at 15,000 rpm for 60 minutes. Then, the supernatant was filtered through a 0.22 μm PVDF

membrane (Millipore GVW P02500). This suspension was dialyzed through a 100 kDa MWCO membrane (SpectraPor Biotech CE, Spectrum Laboratories, USA) twice: first, against Milli-Q water, and second, against 15 mM NaCl solution for 20 hours each. The final suspension was filtered again and kept at 4°C.

Finally, the concentration of each P22 suspension was determined, after the last filtration, by means of successive dilutions for PFU (plaque-forming unit) counting.[30] The host bacteria need to grow in an optimal environment (temperature, pH, appropriate nutrients, salt concentration) for lysis to happen.[30] In this particular case, soft L agar was prepared with 10 g/L tryptone, 5 g/L yeast extract, 5 g/L NaCl, and 7.5 g/L of agar-agar technical for microbiology (Britania, Argentina). L agar for Petri dishes was prepared with 10 g/L tryptone, 5 g/L yeast extract, 5 g/L NaCl, and 15 g/L of agar-agar technical for microbiology. Each dilution of the bacteriophage mixed with concentrated host bacteria in soft agar was spread on the surface of the agar plate. Also, a plate containing only melted soft L agar served as negative control for bacteria and a plate only seeded with bacteria served as negative control for bacteriophage. The plates were incubated at 37°C for 24 hours. The bacteria grew as a film and circular plaques (clear zones) indicated the lysis produced by the bacteriophage.

III.3.2. Bacteriophage PP7

To replicate PP7, first the host bacteria *Pseudomonas aeruginosa* (ATCC 15692-B2) were spiked into 10 mL of autoclaved 8 g/L nutrient broth (Britania, Argentina) and incubated for 24 hours at 37°C on an orbital shaker at 120 rpm. 1 mL of original stock of PP7 was then added and incubated under the same conditions. Afterwards, the virus suspension was centrifuged at 1,000 xg for 15 minutes and the supernatant filtered through a 0.22 μm PVDF membrane.

To purify the PP7 bacteriophage, the suspension was dialyzed through a 100 kDa MWCO membrane twice: first, against Milli-Q water, and second, against the appropriate solution (fifteen in total: NaCl, $NaNO_3$, $NaHCO_3$, $CaCl_2$, $MgCl_2$ of 1 mM, 10 mM, 100 mM ionic strength) for 20 hours each. The final suspension was again filtered and kept at 4°C.

Finally, the concentration of each PP7 suspension was determined, after the last filtration, by means of successive dilutions for PFU (plaque-forming unit) counting.[30] The soft nutrient agar for bacteriophage titration was prepared mixing 8 g/L of nutrient broth and 7.5 g/L of agar-agar technical for microbiology (Merck, Germany). The nutrient agar for Petri dishes was

prepared mixing 8 g/L of nutrient broth, 8 g/L of NaCl and 15 g/L of agar-agar technical for microbiology. A plate containing only melted soft agar served as negative control for bacteria. A plate only seeded with bacteria served as negative control for bacteriophage. The plates were incubated at 37°C for 24 hours.

III.4. Bacteriophages as model viruses

Bacteriophages have been used as surrogates for pathogens in medical and environmental studies.[73, 100-111] In particular, they can serve as model organisms for mammalian viruses due to the fact that they are innocuous for humans, can grow to high titers, are easy and rapid to enumerate, and do not need specialized testing facilities.[112] Furthermore, they are suited when population numbers, environmental characteristics, spatial structures, etc., are needed to be changed.[103]

An ideal model organism should present similar ecology and resistance to treatment processes as the pathogens, and simple laboratory methodology.[113]

Water is the vector for some viral illnesses such as hepatitis and gastroenteritis, but these are difficult to detect in aqueous systems. Therefore, the search for substitutes easier to detect and enumerate and that grow in the same medium and under the same conditions is relevant. There are several procedures for detecting phages in water, ranging from traditional plate counting to more complex techniques such as qPCR or electron microscopic examination.[104, 113, 114]

Bacteriophages can also be used to trace water movements. Advantages are related to their good survival and high numbers of the cultures, the easiness of detection and enumeration, and their harmlessness to the environment. Drawbacks are adsorption to soils, inactivation by treatment and natural environmental processes and the presence of other organisms.[110, 113]

Many surrogates and mammalian viruses have been used to test membranes employed in water filtration.[102, 115-117] In the present work, two bacteriophages, P22 and PP7, were employed in filtration experiments. Basically, they were selected due to their similar size with small mammalian viruses.[118] Besides, PP7 share structure and morphology with enteroviruses such as polio viruses; both have an icosahedral capsid with a diameter of about 25 nm and a single-strand RNA genome.[100] PP7 is also a standard used by membrane manufacturers to challenge membranes.[109, 112, 119]

Filtration can remove viruses from natural waters by size exclusion and by electrostatic interactions. Size exclusion is the result of spatial constraint and it is not affected by process conditions. On the other hand, filtration conditions and characteristics of the affluent affect electrostatic interactions.[112] When the predominant mechanism is size exclusion, any surrogate of similar size and shape can be a good option to replace pathogenic viruses. On the contrary, when taking into account interactions originated by surface charges on the viruses and the adsorbent, further analysis should be made to imitate natural pathogens. Another important consideration is that aggregation of the model virus under the test conditions should be minimal in order to present the most challenging condition.

III.5. Size determinations by dynamic light scattering (DLS)

Dynamic light scattering is based on the fact that fine particles are in constant random Brownian motion, they diffuse at a speed related to their size: small particles diffuse faster. The speed of Brownian motion is dependent on the temperature, making its control essential for accurate size measurement.

To measure the diffusion speed, the sample is illuminated with a laser and the produced speckle pattern is observed. The scattering intensity at a specific angle will fluctuate with time, and is detected using a sensitive avalanche photodiode detector (APD). The intensity changes are analyzed with a digital autocorrelator which generates a correlation function; giving the size and the size distribution.[120]

In the present work, particle size was measured with a Zetasizer Nano ZS (Malvern, UK). In this way diameters of bacterium *Pseudomonas aeruginosa*, bacteriophages P22 and PP7, and nanoparticles of TiO_2 were obtained. Hydrodynamic diameter obtained by DLS is an equivalent diameter that accounts for interactions with the solvent in which the particles are suspended. Therefore, the calculated diameter indicates the apparent size taking into consideration attraction and association to water molecules and electrolytes.

III.6. Zeta potential

The charge acquired by a particle in a medium arises from the surface charge and from the concentration and type of ions in the solution. This charge is responsible for stability and can be

modified by altering the pH, the ionic strength, and the type of ions in the solution. It also affects its behavior such as aggregation, interaction with membranes and other surfaces, ligand binding affinity, filtration, etc. Consequently, knowledge of this charge is of benefit to control these interactions as well as to predict stability.

Surfaces in contact with an electrolyte solution have charge in the same way as dispersed particles and colloids.

The charge on a particle surface is balanced by oppositely charged ions (counterions) in the adjacent solution, forming a layer of counterions, and thus, an electrical double layer will start to develop (Fig. III.1).

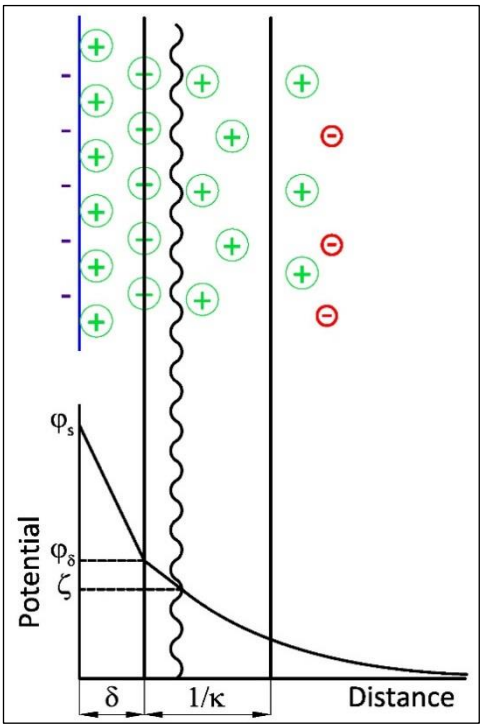

Fig. III.1: Developing of electrical double layer and variation of potential close to a charged particle.

In practice, measurement of the surface charge is not feasible, but zeta potential can be measured instead. Electrokinetic phenomena is the result of the relative movement between a charged interface and the adjacent electrolyte solution, so that part of the double layer charge moves with the liquid. The plane of shear separates the fixed from the mobile parts of the electrical double layer. The electrical potential at the shear plane is the zeta potential (ζ). The shear plane lies outside but close to the Stem plane (of a δ thickness from the surface), so that

essentially all of the diffuse layer charge is mobile and the counterions in the Stem layer are fixed.

Thus, zeta potential is useful to predict colloid stability. If all the particles have very negative or very positive zeta potentials, the system will tend to be stable and no flocculation will occur. In general, values of zeta potential higher than 30 mV or lower than -30 mV are considered to give stability.[120]

Zeta potentials of bacterium *Pseudomonas aeruginosa*, TiO_2, bacteriophages P22 and PP7, ferroxane, and polyethersulfone were measured using a Zetasizer Nano ZS (Malvern, UK) and employing Dispersion Technology Software (DTS) (Malvern, UK). First, electrophoretic mobilities were determined by laser Doppler electrophoresis, measuring the speed of the particles in the medium when an electric field was applied. This speed depends on strength of the electric field or voltage gradient, the dielectric constant and the viscosity of the medium, and the zeta potential. Then, knowing the viscosity and dielectric constant of the medium, zeta potentials were calculated using the Henry equation and the Smoluchowski approximation:[120]

$$U_E = \frac{\varepsilon \zeta}{\eta} \qquad \text{(III.1)}$$

where U_E: electrophoretic mobility, ε: dielectric constant, ζ: zeta potential, η: viscosity.

To measure the zeta potential of the polyethersulfone membrane an accessory for the Zetasizer was needed. It enabled a small piece (5x4 mm) of the flat membrane to be mounted between two electrodes. Tracer particles were dispersed in the solution of interest and their zeta potential was measured at different distances from the surface. The vertical position of the membrane was varied with respect to the detection optics by moving the accessory. The presence of the flat surface modifies the pattern of electroosmosis between the electrodes when a field is applied, and thus, zeta potential of the tracer particles varies in function of the distance to the membrane. Afterwards, the surface zeta potential is obtained through calculation.[120-122] Two different tracer particles were used arbitrarily, polystyrene latex standard in aqueous buffer at pH 9 (DTS1235, Malvern, UK) or milk substitute.[121]

III.7. UV-Vis spectrophotometry

The spectrometric methods are based on the interaction of electromagnetic radiation, or other particles, with an analyte to identify or determine its concentration.

The molecules absorb radiation at specific wavelengths. The spectrum is a graphical representation of the fraction of light that the sample absorbs or transmits in function of the wavelength.

Absorption spectrophotometry is based on the principle that when light impacts on the sample, part of it (UV and/or Visible) will be absorbed and the transmitted portion will therefore be smaller and can be measured by the detector (Fig. III.2).[123]

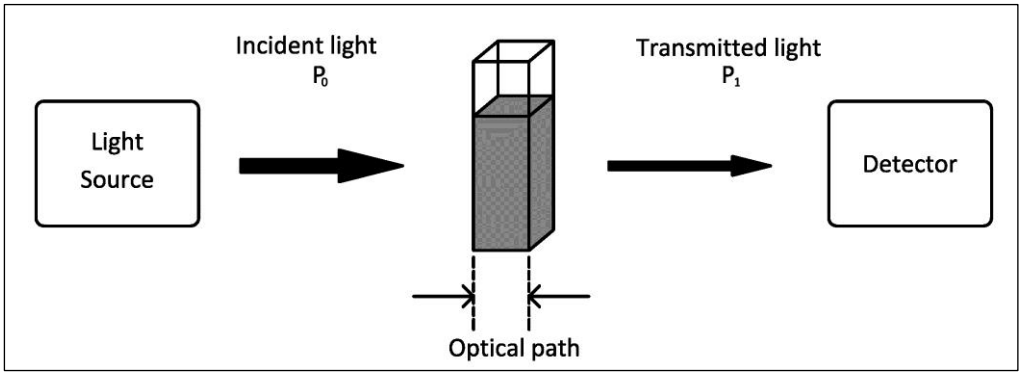

Fig. III.2: Absorption spectrophotometry.

Transmittance is defined as the ratio between the transmitted and the incident power:

$$T = \frac{P_1}{P_0} \quad \text{(III.2)}$$

Transmittance depends on the optical path; when the optical path increases, the absorbed light will be greater, making the transmittance to diminish. Absorbance is the logarithmic ratio between the incident and the transmitted power:

$$A = -logT \quad \text{(III.3)}$$

Therefore, T=1 or A=0 means total transmission and T=0 or A=∞ indicates total absorbance.

When incident light is monochromatic, the Beer-Lambert law indicates that:

$$A_\lambda = \varepsilon_\lambda \, b \, C \qquad \text{(III.4)}$$

where λ: wavelength of incident light, ε_λ: coefficient of absorption (depends on the solvent and on the resolution of the instrument), b: optical path, C: concentration of the absorbing species. Absorbance depends linearly on these three factors, making it an advantage over transmittance.

A spectrophotometer is composed by a source of light, dispersion elements (filters and monochromators) and detectors (Fig. III.3).[123]

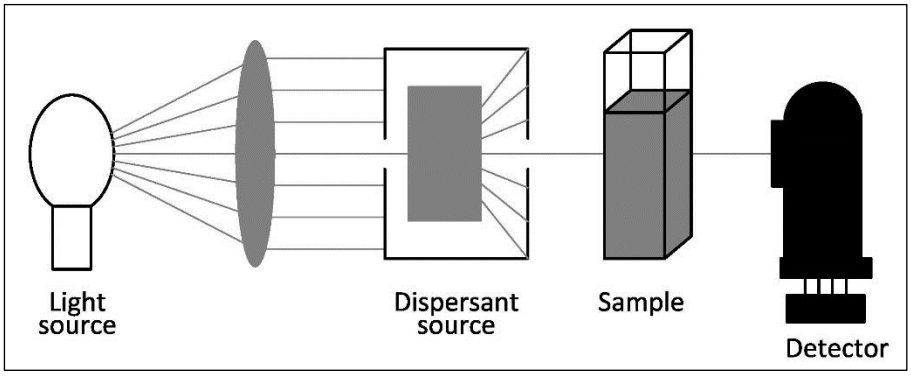

Fig. III.3: Components of a UV-Vis spectrophotometer.

The radiation source must have sufficient radiant energy in the entire wavelength region where it is used and the intensity must be constant during the measuring period. The detectors must have linear response and enough sensitivity in the spectral range of interest. Interference filters use the optical interference to obtain radiation of low bandwidth. Monochromators are used since incident light should be monochromatic to achieve exact measurements and the wavelength should allow the analyte's maximum absorption.

Dual-beam instruments allow the absorbance measurement of the sample and the reference at the same time (Fig. III.4) and the absorbance is obtained by subtracting the absorbance of the reference to that of the sample.[123]

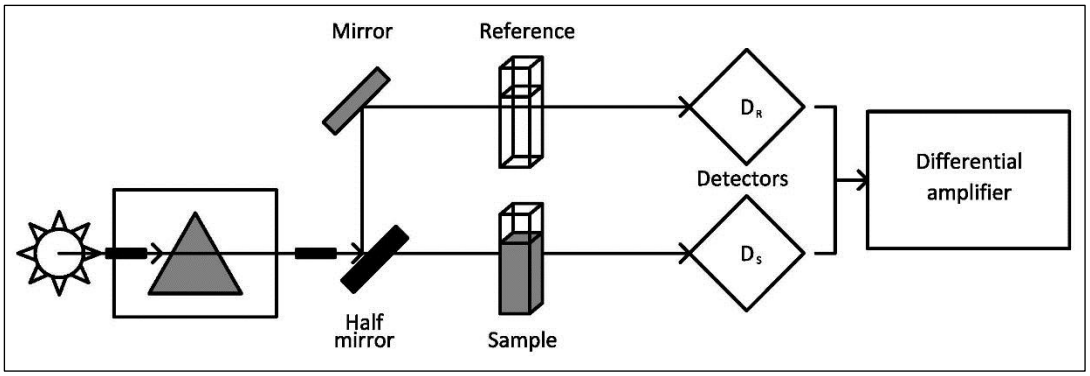

Fig. III.4: Double-beam spectrophotometer with spatial separation of the beams.

This technique was used to quantify the concentration of the particles eluting the column, with an UV-Vis spectrophotometer (Shimadzu UV 1650 PC). It was employed for the single transport experiments as well as to detect Ti without the interference of the bacteria in the combined transport experiments. Optimal wavelength was determined from the peak of the individual adsorption spectrum of a concentrated sample of each species. 325 nm was found for TiO_2, 262 nm for *Pseudomonas aeruginosa*, and 410 nm for digested Ti. The detection limit of absorbance is 0.005.

III.8. Microwave-assisted digestion previous to colorimetric detection

Conversion of solid samples or suspended material to solutions is often needed as a previous step in analytical procedures. Sample digestion include adding concentrated acids, followed by temperature increase to accelerate oxidation of organic compounds and enhance rupture of chemical bonds.[124] Technology based on microwave-assisted heating offers better results as well as shorter times. As shown in Fig. III.5, microwaves have a wavelength between 10^{-3} and 1 m.

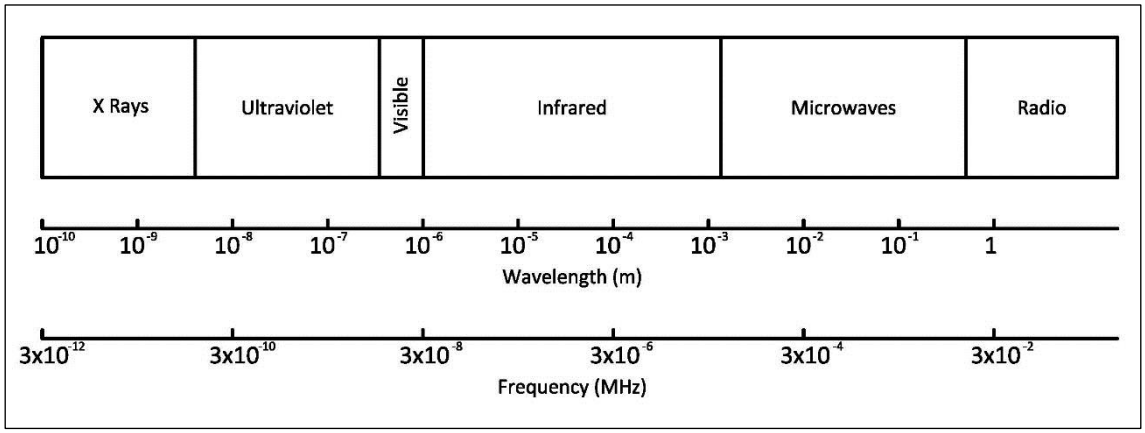

Fig. III.5: Electromagnetic spectrum.

Absorbent matter absorbs the energy from the microwaves and increase their temperature, due to dipolar rotation (e.g., organic solvents) and ionic conduction (e.g., salts, acids). The energy associated to the microwaves is not enough to break chemical bonds. Fig. III.6 shows a schematic representation of a sample treated by microwave heating.[125]

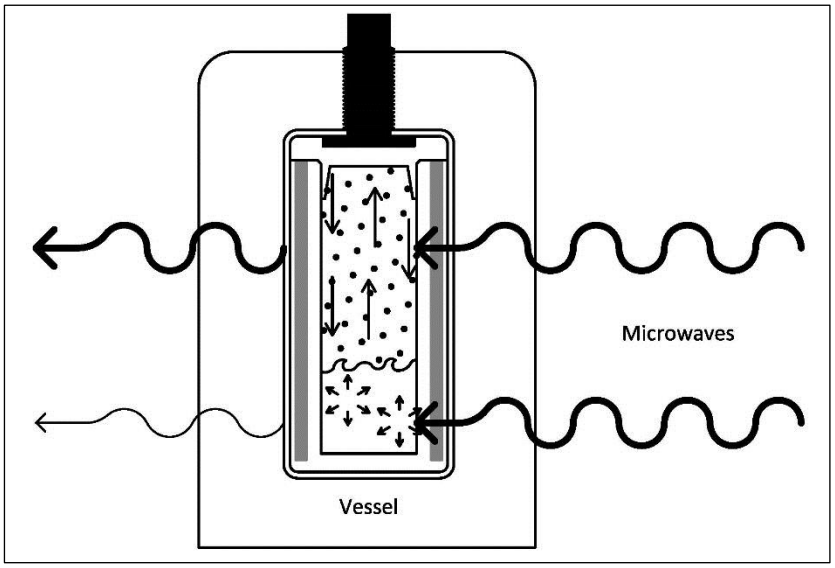

Fig. III.6: Microwave heating.

This process needs continuous temperature control as well as pressure control since all the organic matter is decomposed producing CO_2 and H_2O vapors.

In the cotransport experiments, it was important to measure the concentration of TiO_2 exiting the column without any interference of the present bacteria. The selected method was

spectrophotometry at 410 nm. Microwave-assisted digestion was used for pre-treatment of the samples, which included removal of all organic matter.

3 mL of each sample was mixed with 3 mL of H_2SO_4 (18 M) and 0.23 g of $(NH_4)_2SO_4$ (digestion catalyst). To allow gases from this first reaction escape the vessel, the samples were left for some minutes uncapped under the laboratory hood. This was followed by digestion in a MARS 5 microwave reaction system (CEM, NC, USA), and then centrifugation at 3,000 rpm for 15 min to remove the decanted organic matter. To detect and measure the concentration of the digested Ti, 1 ml of H_2O_2 (30%) was added; in this way a peroxy bond is formed with the Ti giving an orange coloration whose intensity is related to the concentration of Ti. To have the same volume in all the samples, water was added up to 10 mL. Finally, each sample absorbance was measured at 410 nm with a spectrophotometer (Shimadzu UV 1650 PC). A blank sample was prepared by repeating the above procedure without the TiO_2.[126]

III.9. Quantitative polymerase chain reaction (qPCR)

Polymerase chain reaction is an in vitro technique that allows amplification of a specific region of the DNA, which is between two regions of known sequence. qPCR allows amplifying and quantifying in a continuous and simultaneous way. The objective of PCR is to "see" a microorganism or a gene through its genetic material (target), free from the influence of other molecules. If it is required, a second objective is to quantify the target.[127]

In general, the target is present in a matrix (sample) along with other nucleic acids, organic molecules, and inorganic substances. The first step is to extract the nucleic acid of interest and sometimes purification is needed. Then, amplification and detection are performed. If the genetic material is RNA, retrotranscription is needed during amplification.

To extract the nucleic acids, different methods may be applied to release them, protect and stabilize from degradation. Afterwards, inhibitors of amplification are eliminated, and the sample and target are concentrated to a small volume. Finally, the target is collocated in a compatible medium where it is amplified and detected.

Reagents for polymerase chain reaction are DNA polymerase, primers, nucleotides, PCR buffer, Mg^{2+}, and the target.

PCR consists of a series of repeated temperature changes, called cycles. The first step of the cycle is denaturation and consists in heating the reaction to 94°C for less than 1 minute. It

causes melting of the DNA template by disrupting the hydrogen bonds between complementary bases, yielding single-stranded DNA molecules. The second step is annealing; the reaction temperature is lowered to the melting temperature (52 - 60°C) allowing annealing of the primers to the single-stranded DNA template. This temperature must be low enough to allow for hybridization of the primer to the strand, but high enough for the hybridization to be specific. The third step is elongation; the temperature is usually 72°C allowing the DNA polymerase to synthesize a new DNA strand complementary to the DNA template strand. The extension time depends both on the DNA polymerase used and on the length of the DNA fragment to amplify. At each extension step, the amount of DNA target is doubled, leading to exponential amplification of the specific DNA fragment.[127]

For the cotransport experiments, qPCR was the selected technique to determine the number of bacteria exiting the column. Two main reasons were decisive: first, the bacteria eluting from the column are a combination of culturable, nonculturable, and nonviable cells,[23] then qPCR exhibits an advantage over classic determination by plaque counting; second, interference produced by TiO_2 was discarded since the technique only detects the bacterial DNA. qPCR was performed using CFX96 (Bio-Rad, USA) and PowerWater DNA isolation kit (Mo Bio Laboratories Inc., CA, USA) to extract the DNA of the bacteria. A portion of the gene encoding 16S rRNA of *P. aeruginosa* chromosome was amplified. Quantification was made by absolute PCR using SyBr-Green (Bio-Rad, USA). Agarose gel electrophoresis was performed to corroborate the reaction products and the quality of the standard. Additionally, it was determined that the presence of TiO_2 nanoparticles did not generate inhibition of the polymerase chain reaction, through a control test using a standard corresponding to a DNA fragment of *Arabidopsis thaliana*.

For the virus removal using ceramic membranes, qPCR was one of the methods applied to determine the concentration of P22 phage in the samples. qPCR was performed extracting DNA from P22 suspensions using the Pure Link Viral RNA/DNA Mini Kit (Invitrogen, Carlsbad, CA). The DNA was detected using a GeneAmp 5700 Sequence Detection System (Applied Biosystems). PCR mixtures contained DNA sample, 2X PCR master mix (TaqMan Universal Master Mix II, no UNG; Applied Biosystems, Indianapolis, IN), forward and reverse primers, and TaqMan probe. Amplification was initiated using the hot start method at 95°C for 10 minutes, 40 cycles of 95°C for 15 seconds, and 60°C for 1 minute.

III.10. X-ray powder diffraction (XRD)

X-ray powder diffraction is used to obtain information about the structure, composition and state of polycrystalline materials. The X-ray pattern of a crystalline substance can be thought of as a "fingerprint"; each crystalline material has a unique diffraction pattern, and therefore, X-ray diffraction constitutes an identification method. The equipment consists of a high voltage source, an X-ray tube, a goniometer and a detector. The tube contains a tungsten filament and a metal anode. When an electric current passes through the filament, electrons are emitted and accelerated by the applied voltage. The electrons hit the anode and produce X-rays. The emission of X-rays takes a very low portion of the energy produced, more than 99% is converted to heat and must be eliminated by refrigeration with water. The tube is under vacuum (10^{-6} mm Hg) and has beryllium windows through which the X-rays exit. The analysis of minerals requires a monochromatic X-radiation, which is generally achieved by a filter or a monochromator at the exit of the tube.

When a beam of monochromatic X-radiation is directed at a crystalline material, reflection or diffraction of the X-rays is observed at various angles with respect to the incident beam. The relationship between the wavelength of the X-ray beam (λ), the angle of diffraction (2θ), and the distance between each set of atomic planes of the crystal lattice (d), is given by the Bragg's law:

$$n\lambda = 2dSin\theta \qquad \text{(III.5)}$$

where n represents the order of diffraction. From this equation we can calculate the interplanar distances of a crystalline material.

The Joint Committee on Powder Diffraction Standards (JCPDS) has published the powder diffraction patterns of many compounds. An unknown compound can be identified by comparing its pattern with those in the powder diffraction file.

In the present work, this technique was employed to confirm that the sand was 100% quartz and to know some characteristics such as Krumbein's roundness and Rittenhouse sphericity; using a diffractometer PW 1730/10, Cu anode, 40 kV, 20 mA.

III.11. DLVO theory

DLVO theory, developed independently by Derjaguin and Landau (1941) and by Verwey and Overbeek (1948), explains colloid stability as well as attachment between colloids and surfaces, such as collectors and membranes. This theory is based on the van der Waals attraction and the electrical double layer repulsion.

The van der Waals interaction is the result of short-term magnetic forces that form between identical or different particles which may have the same, different or no net charge, due to transition dipoles. This interaction depends on geometry of the particles and on properties of these particles and the medium in which they interact, given by the Hamaker constant (A). For aqueous suspensions, Hamaker constants are between $3x10^{-21}$ and $1x10^{-19}$ J; dense minerals have high values, while low-density materials, especially biological, have low values.[1] Hamaker constants for organic colloids are smaller than $1x10^{-20}$ J.[39] The electrical double layer arises when a particle with electrical charge on its surface is surrounded by counterions that are present in an electrolyte solution. These counterions tend to be localized close to the particles, but at the same time they tend to diffuse throughout the solution. The surface charge with the counterions form the electrical double layer. When two particles with similar charge approach, the electrical double layers overlap giving origin to repulsion.

Theories trying to explain the double layer interaction have been developed, but lack of information of the systems renders them of little practical use. The surface potential, for instance, is a key parameter but it cannot be determined and the zeta potential should be used instead. Another point is the lack of information on the dynamics of the double layer interaction; thus, calculations should be made upon constant-charge approximation (CCA) or constant-potential approximation (CPA).

CCA is expected when the particles have a fixed surface charge density. The total diffuse layer charge remains constant and when the surfaces approach each other, this charge is compressed into a smaller volume making the charge density between the particles increase and therefore, the repulsion augments.[128]

On the contrary, CPA arises when the surface chemical equilibrium is maintained during the approach of the two particles, which is not feasible as the encounter happens in a short time. The expressions developed by Hogg, Healy, and Fuerstenau using CPA[129] are in agreement with exact results[130] for low surface potentials.

The linear superposition approximation (LSA) may be an intermediate solution since it points out the existence of a region between the surfaces where the potential is small enough and follows the Poisson-Boltzmann equation making it possible to sum the contributions from each surface. This compromise is only valid when the separation distance is longer than the size of the particles.

The electrical double layer and the van der Waals interaction potential energies are considered additive, giving the total interaction. Therefore, the net potential energy, as function of the separation between the surfaces, depends on the strength of both attraction and repulsion.

The analysis of the total interaction (Fig. III.7) shows that three key-points may be found, according to the interacting particles and the conditions of the medium. First, a pronounced energy well can be encountered at very small distances (primary minimum) where particles are highly unstable and aggregate. At larger separations, where the values of zeta potentials and the ionic strength of solution make the repulsion between the two particles more important than the attraction, a potential energy barrier (maximum) arises and prevents particles from aggregating. If this energy barrier does not exist or disappears, contact between the particles is enhanced and a shallow well (secondary minimum) may exist, where particles rapidly aggregate at longer distances. This profile is the result of the particle size, zeta potential, ionic strength, ions in the solution, and Hamaker constant. The primary minimum cannot be considered to be infinite and a separation between the two surfaces should always be imposed, taken into account that particles are separated by water and hydrated ions.

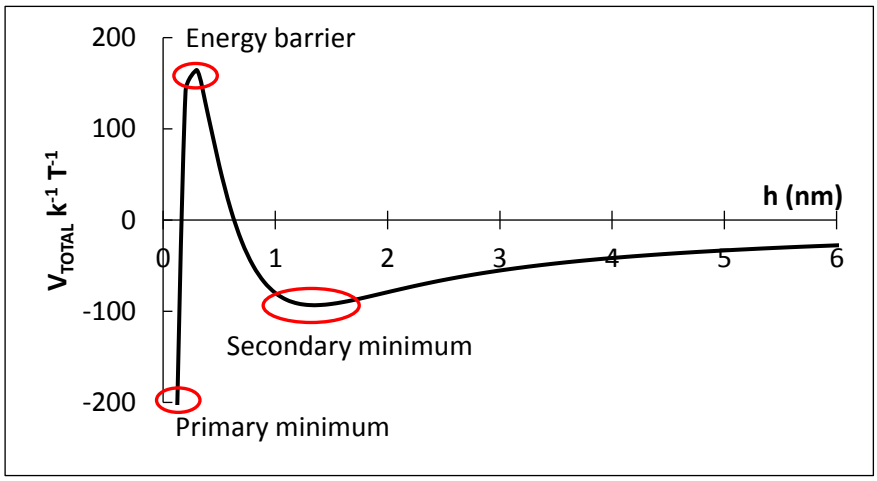

Fig. III.7: Generic total interaction potential energy vs. separation distance between the two surfaces.

The interaction energies may be obtained from different expressions available in the literature, which are simpler to use than solving the Poisson-Boltzmann equation for the system.

In the present work, several equations were used according to the geometry and size of the interacting bodies.

Interactions between a sphere and a plate were calculated as follows:[1, 128, 131]

$$V_{vdWr} = -\frac{A\,a}{6\,h}\left[1 - \frac{5.32\,h}{\lambda}\,ln\left(1 + \frac{\lambda}{5.32\,h}\right)\right] \quad \text{(III.6)}$$

$$V_{vdW} = -\frac{A}{6}\left(\frac{a}{h} + \frac{a}{h+2a} + ln\frac{h}{h+2a}\right) \quad \text{(III.7)}$$

$$V_{EDL} = \frac{128\,\pi\,an_{\infty}}{\kappa^2}\,k\,T\,\gamma_1\,\gamma_2\,e^{-\kappa h} \quad \text{(III.8)}$$

$$V_{EDL} = \frac{2\pi a n_{\infty} kT}{\kappa^2}(\Phi_1^2 + \Phi_2^2)\left[\frac{2\Phi_1^2\Phi_2^2}{\Phi_1^2+\Phi_2^2}\,ln\frac{1+e^{-\kappa h}}{1-e^{-\kappa h}} + ln\left(1 - e^{-2\kappa h}\right)\right] \quad \text{(III.9)}$$

where V_{vdWr}: retarded van der Waals interaction potential energy (J), V_{vdW}: unretarded van der Waals interaction potential energy (J), V_{EDL}: electrical double layer interaction potential energy (J), A: Hamaker constant (J), a: radius of the sphere (m), h: separation (m), λ: characteristic wavelength of the interaction (assumed to be 100 nm), n_{∞}: bulk number of ions (ions m^{-3}), κ: Debye-Hückel reciprocal length (m^{-1}), k: Boltzmann constant (J K^{-1}), T: temperature (K), γ_i: reduced surface potential, Φ: electrical potential (V).

Interactions between two spheres were calculated as follows:[1, 128, 131]

$$V_{vdWr} = -\frac{A\,a_1\,a_2}{6\,(a_1+a_2)\,h}\left[1 - \frac{5.32\,h}{\lambda}\,ln\left(1 + \frac{\lambda}{5.32\,h}\right)\right] \quad \text{(III.10)}$$

$$V_{vdW} = -\frac{A}{6}\left(\frac{2a_1a_2}{h^2+2a_1h+2a_2h} + \frac{2a_1a_2}{h^2+2a_1h+2a_2h+4a_1a_2} + ln\frac{h^2+2a_1h+2a_2h}{h^2+2a_1h+2a_2h+4a_1a_2}\right) \quad \text{(III.11)}$$

$$V_{EDL} = \frac{128\,\pi\,a_1\,a_2\,n_\infty}{(a_1+a_2)\,\kappa^2}\;k\,T\,\gamma_1\,\gamma_2\,e^{-\kappa h} \quad \text{(III.12)}$$

$$V_{EDL} = \frac{2\pi a_1 a_2 n_\infty kT}{(a_1+a_2)\kappa^2}(\Phi_1^2+\Phi_2^2)\left[\frac{2\Phi_1^2\Phi_2^2}{\Phi_1^2+\Phi_2^2}\,ln\frac{1+e^{-\kappa h}}{1-e^{-\kappa h}} + ln\left(1-e^{-2\kappa h}\right)\right] \quad \text{(III.13)}$$

with the aid of:[1]

$$\gamma_i = Tanh\;\frac{z\,e\,\varphi_i}{4\,k\,T} \quad \text{(III.14)}$$

$$\Phi = \frac{ze\varphi}{kT} \quad \text{(III.15)}$$

$$\kappa = 2.32\times10^9\sqrt{\sum C_j\,z_j^2} \quad \text{(III.16)}$$

where z: valence of symmetrical (z-z) electrolyte, e: electron charge (C), φ: electrical surface potential (V) which cannot be experimentally determined and was then replaced by ζ: zeta potential (V), C_j: ion concentration (mol dm^{-3}), z_j: valence of ion j including sign of charge.

Finally, as DLVO theory considers the total interaction potential energy as the sum of both van der Waals and electrical double layer potential energies:

$$V_{TOTAL} = V_{vdW} + V_{EDL} \quad \text{(III.17)}$$

Eqs. III.6 and III.10 are valid if $h \ll a$. Eqs. III.8 and III.12 are valid if $h \ll a$ and $\kappa a > 5$, and were developed using linear superposition approximation (LSA) and Derjaguin integration method (DIM). Eqs. III.9 and III.13 are valid if $\Phi < 50\,mV$,[128] $h \ll a$ and $\kappa a \gg 1$, and were obtained with constant-potential approximation (CPA), linear Poisson-Boltzmann equation solution (LPB) and Derjaguin integration method (DIM). Eq. III.16 was calculated for aqueous solutions at 25°C.

Eqs. III.6, III.8, III.10, and III.12 were particularly used for studying the aggregation of bacterium and TiO_2 and the attachment of these particles between them and onto quartz sand.

Eqs. III.7, III.8, III.11, and III.12 were employed for P22 and Eqs. III.7, III.9, III.11, and III.13 for PP7. Different expressions for V_{EDL} were used for the different bacteriophages P22 and PP7 due to the difference in their sizes.

DLVO theory presents some limitations. It does not consider the effects of other interacting forces such as Born short-range repulsion, hydration forces, Lewis acid-base free interaction, etc. The surfaces are not perfectly even and smooth. The interacting bodies are assumed to have perfect, defined geometry comparable to a sphere or an infinite plate. Hamaker constants are considered to depend only on properties of the material but, in some cases, counterions can react with the particles changing the measured or calculated constants.[132] Furthermore, in the case of biological materials such as viruses and bacteria, a new limitation arises: they are soft particles, not hard in their surface and allow the interchange of water and electrolytes from the interior to the medium and vice versa;[133] thus, the electrical double layer is not limited to the outside but develops within the surface charge layer; in this way the zeta potential importance and meaning may be questioned.[134, 135]

Despite these drawbacks, the results obtained from the calculations are very useful to estimate the height of the energy barrier which is the main responsible for repulsive forces, as well as the depth of the secondary minimum which can increase attraction at longer distances causing aggregation or deposition.[136]

Besides, the higher electrolyte concentration, the more decrease in the height of the energy barrier that enhances collisions leading to aggregation and deposition. This maximum disappears if the electrolyte concentration reaches the critical coagulation concentration (ccc) value. According to DLVO theory two regimes occur: below the ccc, the thickness of the electrical double layer decreases with increasing salt concentration; but above the ccc the double layer is completely suppressed and rapid aggregation takes place independently of the salt concentration.[132]

III.12. Extended DLVO theory (X-DLVO)

Non-DLVO interacting forces like Born repulsion, hydration forces and Lewis acid-base forces may also exist and explain the discrepancies between experimental and theoretical analysis.

Born repulsion arises from the interpenetration of electron orbitals of the atoms at very short distances and can be obtained as:[137]

$$V_B = \frac{A_{132}\sigma_B^6}{7560}\left[\frac{8a+h}{(2a+h)^7} + \frac{6a-h}{h^7}\right] \quad \text{(III.18)}$$

where V_B: Born interaction potential energy (J), σ_B: collision parameter (m).

Lewis acid-base interaction arises from migration of electrons between the surfaces, adsorbed species and the solvent; and can be calculated as follows for two spheres:[31]

$$V_{AB} = 2\pi \frac{a_1 a_2}{a_1+a_2}\lambda_{AB}\Phi_{AB\ (h=h0)}e^{\frac{h0-h}{\lambda_{AB}}} \quad \text{(III.19)}$$

$$\Phi_{AB\ (h=h0)} = -\frac{K_{132}}{2\pi h_0 \lambda_{AB}} \quad \text{(III.20)}$$

$$\log K = -3.5(Cos\theta_1 + Cos\theta_2) - 18 \quad \text{(III.21)}$$

where V_{AB}: Lewis acid-base interaction potential energy (J), λ_{AB}: decay (Debye) length of water (m), $\Phi_{AB\ (h=h0)}$: Lewis acid-base free interaction potential energy between surfaces at contact (J m^{-2}), K: hydrophobic constant (J) θ: contact angle of surface (°). And for a sphere and a plate:[31]

$$V_{AB} = 2\pi a \lambda_{AB}\Phi_{AB\ (h=h0)}e^{\frac{h0-h}{\lambda_{AB}}} \quad \text{(III.22)}$$

Structural or hydration forces are a consequence of hydrophilic surfaces that will add repulsion to the interacting particles. Charged surfaces may be hydrated in a solution, and this water will hinder the approximation of different particles. Then, the extra hydration repulsion is originated when particles need to eliminate the water to be in contact, and diminishes exponentially with distance and depends on the type and concentration of electrolytes present:[132]

$$V_H = \pi a N_A C_h C_e \lambda_{AB}^2 e^{-\frac{h}{\lambda_{AB}}} \quad \text{(III.23)}$$

where V_H: hydration interaction potential energy (J), N_A: Avogadro number, C_h: hydration constant (J), C_e: salt concentration (mol m^{-3}). These hydration forces act at shorter distance than the attractive hydrophobic forces.

To sum up, the total interaction potential energy is therefore obtained as the sum of DLVO and X-DLVO interactions:

$$V_{TOTAL} = V_{EDL} + V_{vdW} + V_B + V_{AB} + V_H \quad \text{(III.24)}$$

III.13. Transport in porous media. Deep-bed filtration

The filtration process through granular beds consists of two successive steps: transport of the particles to the vicinity of the collector (or a previously attached particle) and attachment. Transport is the result of diffusion, gravity, and interception, resulting in a general equation for variation of particle concentration:[45]

$$\frac{\partial C}{\partial t} + v \cdot \nabla C = D_{bm} \nabla^2 C + \left(1 - \frac{\rho}{\rho_p}\right) \frac{mg}{3\pi\mu d_p} \frac{\partial C}{\partial z} \quad \text{(III.25)}$$

where the first term on the left is the variation of particle concentration with time, the second term on the left represents the effects of advection on the concentration, the first term on the right indicates the effects of diffusion and the second the effects of gravity. Interception is included in the boundary conditions when integrating. Since Eq. III.25 cannot be solved analytically, other parameters of the system, such as the collector efficiency, is of great utility.

The efficiency of a single collector is a key parameter to evaluate the performance of a filtration process:[45]

$$\frac{dC}{dL} = -\frac{3}{2} \frac{1-f}{d_c} \alpha_c \eta_0 C \quad \text{(III.26)}$$

where C: suspended particle concentration, L: bed length (m), f: porosity, d_c: average diameter of the collector (m), α_c: clean-bed collision efficiency factor, η_0: single-collector efficiency.

The collision efficiency factor is defined as the ratio between the number of successful collisions and the total number of collisions, and depends on the chemistry of the medium. The single-collector efficiency is the ratio between the rate at which the particles hit the collector and the rate at which the particles flow toward he collector, and depends on filtration velocity, size of the collector, temperature, size, and density of the particles to be filtered. Deposition within the pores produces alterations in the flow path and in the media characteristics; therefore, models are only valid for clean collectors.[45]

Expressions to calculate the initial collector efficiency under favorable conditions were obtained by Rajagopalan and Tien.[47, 48] Later Tufenkji and Elimelech incorporated the influence of hydrodynamic and van der Waals forces on the particles being deposited under Brownian motion, obtaining a new correlation equation for filtration in saturated porous media:[46]

$$\eta_D = 2.4A_S^{\frac{1}{3}}N_R^{-0.081}N_{Pe}^{-0.715}N_{vdW}^{0.052} \quad \text{(III.27)}$$

$$\eta_G = 0.22N_R^{-0.24}N_G^{1.11}N_{vdW}^{0.053} \quad \text{(III.28)}$$

$$\eta_I = 0.55A_S N_R^{1.675}N_A^{0.125} \quad \text{(III.29)}$$

where η_D: single-collector efficiency that accounts for transport by diffusion, η_G: single-collector efficiency that accounts for transport by gravitational settling, η_I: single-collector efficiency that accounts for transport by interception, A_s: porosity-dependent parameter, N_R: aspect ratio, N_{Pe}: Peclet number (ratio of convective to diffusive transport), N_{vdW}: van der Waals number (ratio of van der Waals energy to the particle's thermal energy), N_G: gravity number (ratio of Stokes particle settling velocity to approach velocity of the fluid), N_A: attraction number (influence of van der Waals attraction and fluid velocity on particle deposition due to interception).

The needed parameters for calculations are:[46]

$$A_S = \frac{2(1-\gamma^5)}{2-3\gamma+3\gamma^5-2\gamma^6} \quad \text{(III.30)}$$

$$\gamma = \sqrt[3]{1-f} \quad \text{(III.31)}$$

$$N_R = \frac{d_p}{d_c} \quad \text{(III.32)}$$

$$N_{Pe} = \frac{U d_c}{D_\infty} \quad \text{(III.33)}$$

$$D_\infty = \frac{kT}{6\pi\mu a_p} \quad \text{(III.34)}$$

$$N_{vdW} = \frac{A}{kT} \quad \text{(III.35)}$$

$$N_G = \frac{2ga_p^2(\rho_p - \rho_f)}{9\mu U} \quad \text{(III.36)}$$

$$N_A = \frac{A}{12\pi\mu U a_p^2} \quad \text{(III.37)}$$

where f: porosity, d_p: particle diameter (m), d_c: collector diameter (m), U: Darcy velocity (m s^{-1}), D_∞: diffusion coefficient in an infinite medium (m^2 s^{-1}), k: Boltzmann constant (J K^{-1}), T: temperature (K), μ: fluid viscosity (N s m^{-2}), a_p: particle radius (m), A: Hamaker constant (J), g: gravitational acceleration (m s^{-2}), ρ_p: particle density (kg m^{-3}).

Finally, all the mechanisms are considered to be additive:[45]

$$\eta_0 = \eta_D + \eta_G + \eta_I \quad \text{(III.38)}$$

All the parameters can be obtained from column experiments and then using Eq. III.38 the single-collector efficiency is calculated. Afterwards, the clean-bed collision efficiency factor is determined with Eq. III.26.

For colloidal transport in saturated porous media, the rate of filtration is represented by k_d, the deposition rate coefficient (s^{-1}):[46]

$$k_d = \frac{3}{2}\frac{1-f}{f\,d_c}\,U\,\alpha_c\eta_0 \qquad \text{(III.39)}$$

A limitation of clean bed filtration theory is that it does not consider the concentration of the suspended particles.[50] However, for the present work this drawback was not taken as an impediment since comparative analysis was mainly performed.

Chapter IV

ENHANCED RETENTION OF BACTERIA BY TIO_2 NANOPARTICLES IN SATURATED POROUS MEDIA

Nomenclature

a_b: radius of bacterium (m)

a_T: radius of the primary aggregate of TiO_2 (m)

A: Hamaker constant (J)

A_{bwb}: Hamaker constant of bacterium in water (J)

A_{bwq}: combined Hamaker constant of bacterium and quartz sand in water (J)

A_{Twb}: combined Hamaker constant of TiO_2 and bacterium in water (J)

A_{Twq}: combined Hamaker constant of TiO_2 and quartz sand in water (J)

A_{TwT}: Hamaker constant of TiO_2 in water (J)

C: suspended particle concentration in classical filtration theory

C_j: ion concentration (mol dm^{-3})

d_c: average diameter of the collector (m)

e: electron charge (C)

f: porosity

h: separation between surfaces (m)

k: Boltzmann constant (J K^{-1})

k_d: particle deposition rate coefficient (s^{-1})

L: bed length (m)

n_∞: bulk number of ions (ions m^{-3})

T: temperature (K)

U: Darcy velocity (m s^{-1})

V_{EDL}: electrical double layer interaction potential energy (J)

V_{TOTAL}: total interaction potential energy (J)

V_{vdWr}: retarded van der Waals interaction potential energy (J)

z: valence of symmetrical (z-z) electrolyte

z_j: valence of ion j including sign of charge

α_c: clean-bed collision efficiency factor

γ: reduced surface potential

γ_b: bacterium reduced surface potential

γ_q: quartz sand reduced surface potential

γ_T: TiO_2 reduced surface potential

ζ: zeta potential (V)

η_0: single-collector efficiency

κ: Debye-Hückel reciprocal length (m^{-1})

λ: characteristic wavelength of the interaction (m)

φ: electrical surface potential (V)

IV.1. INTRODUCTION

Groundwater contamination by pathogenic organisms is an important concern that should be addressed, especially in contexts of overgrowing populations with limited access to safe drinking water. Urban population growth and higher demands on agricultural yield to feed an increasing number of people would eventually lead to detrimental effects on groundwater quality.[138, 139] The World Health Organization (WHO) identified inadequate drinking water, sanitation and hygiene as responsible for 842,000 diarrheal disease deaths per year.[140]

The transport and retention of microorganisms and colloids in porous media plays a key role in several natural processes and it is intimately related to sand filtration systems in water treatments.[46, 141-144] Knowledge on bacteria transport through saturated porous media is

fundamental to design bioremediation schemes and to evaluate the transport of pollutants associated to this kind of organisms.[21, 145]

Industrial manufacturing of nanomaterials has continually increased since the last decades of the 20th Century and is expected to follow this trend as they are used in pigments, absorbents, sunscreens, wastewater treatment compounds, and catalysts.[15, 17] The release of these materials to natural soils and waters, to some degree, is therefore unavoidable, and understanding their environmental impact have become even more relevant.[16, 136, 146, 147] Particularly, TiO_2 nanoparticles present a risk due to their widespread use.[15, 17, 146] At present, production of TiO_2 is around 88,000 ton/year.[17] Nanoparticles properties derive not only from their chemical structure, but also from their high surface area, small size, surface chemistry, and electrical properties. These conditions may be altered when dispersed in natural environments.[2, 146, 148-150] As much as their fate and transport in porous media is affected by the conditions in waters, other species will also be affected by their presence. Nanomaterials have shown a strong tendency to adsorb on biological surfaces.[25, 151-153] Therefore, we can expect the combined transport of nanomaterials and microorganisms (bacteria, viruses, etc.) to be altered by this interplay.

Transport of microorganisms and transport of nanoparticles have been investigated using columns packed with glass beads, quartz sand, and natural soils.[21] Studies so far concentrated on microorganism transport by itself, or nanomaterial mobility under the presence of bacteria-modified porous media given by previous growth of biofilm or EPS-coated collectors, and showed that mobility of nanoparticles can be modified by the presence of bacteria. On the other hand, we can also expect the transport of microorganisms to be affected by the nanomaterials in saturated porous media (sand aquifers).

The objective of the present work is to develop an improved understanding of bacteria transport in saturated porous media and to establish the effects of nanoparticles in the water flux, by investigating the interactions and simultaneous breakthrough for both species. To the best of our knowledge, this approach is the first of its kind and will provide a new understanding of microorganisms' retention in soils and waters. We experimentally investigated the transport of *Pseudomonas aeruginosa* and P25 TiO_2 nanoparticles in saturated sand columns. Prior to the transport experiments, the bacteria and nanomaterials were characterized with respect to size and surface charge. DLVO theory of colloidal stability, classical filtration theory, and correlation equations were applied for data analysis.[45-48, 154, 155]

IV.2. MATERIALS AND METHODS

The initial stock of bacteria *Pseudomonas aeruginosa* (ATCC 15692-B2) was kindly provided by the Cátedra de Virología, Facultad de Farmacia y Bioquímica, Universidad de Buenos Aires. Aeroxide TiO_2 P25 nanoparticles were supplied by Evonik Degussa Corporation, NJ, USA. P25 is hydrophilic fumed TiO_2, mixture of rutile and anatase, with an average primary particle size of 21 nm, as reported by the manufacturer. Type I water (resistivity 18 MΩ.cm) and reagent grade NaCl (Anedra, Argentina) were used in all experiments. Nutrient broth (Britania, Argentina) for *P. aeruginosa* was prepared mixing 8 g in 1 L of water. Nutrient agar for Petri dishes was prepared mixing 8 g of nutrient broth, 8 g of NaCl and 15 g of agar-agar technical for microbiology (Merck, Germany) in 1 L of water. Solutions and materials were sterilized by autoclaving at 121°C for 20 minutes. The column and the tubings were sterilized by soaking them in bleach solution and then rinsing with autoclaved nanopure water.[147]

Multiplication and purification of bacteria were conducted as follows. First, the bacteria were incubated in nutrient broth for 24 hours at 37°C placed on an orbital shaker at 120 rpm. The suspension was then centrifuged at 5,800 xg for 15 minutes and the supernatant discarded. The pellet was resuspended in 10 mL of the desired solvent (water, 1 mM, 10 mM, or 100 mM NaCl) and centrifuged at 5,800 xg for 15 minutes. This procedure was repeated twice. The final stock suspension was kept at 4°C overnight prior to use.[23]

TiO_2 and bacteria particles were characterized with respect to size and zeta potential, at all ionic strengths, using a Zetasizer Nano ZS (Malvern, UK) at 21°C. Size was determined by dynamic light scattering (DLS) using number-weighted distribution. Large particles scatter more light than small particles because the intensity of scattering of a particle is proportional to the sixth power of its diameter (Rayleigh's approximation).[120] Therefore, a large particle will produce a significant larger response than a small particle in the intensity-weighted distribution. However, as aggregation processes depend on particle number, when considering changes due to particle-particle and particle-collector attachment, number-weight distributions were considered more relevant than intensity-weight. Electrophoretic mobility of the particles was first measured by laser Doppler velocimetry and phase analysis light scattering, and then converted to zeta potential using the Smoluchowski equation as described elsewhere.[156]

Ottawa No. 12 Flint silica sand (U.S. Silica Company, Berkeley Springs, WV) was used as model bed sediment in the laboratory column experiments. Prior to column packing, the sand was washed with constant agitation according to the following sequence: deionized water, HCl

solution (pH 3), deionized water, NaOH solution (pH 10), $NaHCO_3$ solution, deionized water.[157] It was dried at 105°C, and autoclaved at 121°C for 20 minutes. Sand composition was analyzed by X-ray diffraction (XRD) (diffractometer PW 1730/10, Cu anode, 40 kV, 20 mA) confirming it was 100% quartz and determining Krumbein's roundness 0.7 and Rittenhouse sphericity 0.87. Sieve analysis indicated d_{50} of 529 μm by mass.[158]

IV.2.1. Column experiments

Column experiments were performed using a chromatography glass column with adjustable end pieces (Omnifit, Cambridge, UK) and internal diameter of 25 mm. The column was packed with silica sand under agitation and with a considerable height of water to avoid layering and bubbles of air[23] and then Type I water was circulated until the electrical conductivity was close to zero. The length of the sand bed was 5 cm for all experiments. The effective porosity was determined from a tracer (NaCl) breakthrough curve and modeled with the aid of the software CXTFIX21 (U.S. Salinity Laboratory Agricultural Research Service, U.S. Department of Agriculture, Riverside, California) as described elsewhere.[159] Afterwards, solution of desired ionic strength was pumped for 20 minutes to stabilize the sand prior injection of nanoparticles or microorganisms.

IV.2.2. Transport and breakthrough curves

Flow rate was constant and set at 2.8 mL/min. For the single particle transport study, 5 pore volumes (PV) of the suspension with TiO_2 or *Pseudomonas aeruginosa* at the desired ionic strength were pumped, followed by 3 PV of background solution. For the combined transport of both bacteria and TiO_2, 4 PV of *P. aeruginosa* suspension with the desired ionic strength were pumped, followed by 3 PV of *P. aeruginosa* and TiO_2 suspension with the same ionic strength and then 3 PV of the *P. aeruginosa* suspension. In both cases, effluent samples were collected every 0.3 PV.

Breakthrough curves were obtained from a variety of incoming concentrations and ionic strength levels, presented in Table IV.1, representative of natural waters.[152] The feed concentration of bacteria in the suspensions was between $4x10^4$ and $8x10^6$ CFU/mL, while TiO_2 concentration varied between 30 and 100 ppm. Each experiment was repeated at least six times

for TiO_2, four times for bacteria and three times for combined TiO_2 and *P. aeruginosa* transport, at each ionic strength. The working pH was between 5.2 and 5.8; it was measured and monitored but not adjusted since no significant change was evidenced during the experiments.

During the transport experiments bacteria were not expected to multiply since they were not in the optimum conditions (absence of nutrients, temperature below 37°C) and the time of each run did not exceed 45 minutes. Furthermore, bacteria were harvested at the end of the logarithmic phase, minimizing the potential for cell numbers to increase.[50]

Table IV.1: Experimental conditions.

<table>
<tr><th></th><th>Ionic strength (mM NaCl)</th><th>Particle concentration</th><th>Detection method</th></tr>
<tr><td>Transport of TiO_2</td><td>0; 1; 10; 100</td><td>30; 50; 100 ppm</td><td>UV spec. (λ=325 nm)</td></tr>
<tr><td>Transport of P. aeruginosa</td><td>0; 1; 10; 100</td><td>5 mL stock bacteria + 95 mL solution</td><td>UV spec. (λ=262 nm)</td></tr>
<tr><td rowspan="5">Combined transport of TiO_2 and P. aeruginosa</td><td rowspan="5">0; 1; 10; 100</td><td>5 mL stock bacteria + 95 mL solution</td><td>UV spec. (λ=262 nm)</td></tr>
<tr><td colspan="2">followed by</td></tr>
<tr><td>5 mL stock bacteria + 95 mL solution with TiO_2 (50 ppm)</td><td rowspan="2">qPCR</td></tr>
<tr><td colspan="2">or</td></tr>
<tr><td>5 mL stock bacteria + 95 mL solution with TiO_2 (100 ppm)</td><td>Digestion + Vis. spec. (λ=410 nm)</td></tr>
</table>

For the single particle experiments, influent and effluent particle concentrations were measured by UV absorbance using a UV-Vis spectrophotometer (Shimadzu UV 1650 PC) at 325 nm for TiO_2 and at 262 nm for *P. aeruginosa* (wavelengths were determined from the peak of the individual adsorption spectrum).

For the combined transport of *P. aeruginosa* and TiO_2, various techniques were used to minimize quantification errors due to particle interference (Table IV.1). For the first part of the experiment, when only the suspension of *P. aeruginosa* was pumped through the column, the

bacteria concentration was detected photometrically at 262 nm. When both kind of particles were present in the feed, qPCR was employed to quantify bacteria, while TiO_2 nanoparticles were analyzed by microwave digestion followed by a spectrophotometric method.

qPCR was performed using CFX96 (Bio-Rad, USA) and PowerWater DNA isolation kit (Mo Bio Laboratories Inc., CA, USA) to extract the DNA of the bacteria. A portion of the gene encoding 16S rRNA of *P. aeruginosa* chromosome was amplified. Quantification was made by absolute PCR using SyBr-Green (Bio-Rad, USA).

To determine the TiO_2 concentration, each sample was treated as follows: 3 mL of sample was mixed with 3 mL of H_2SO_4 (18 M) and 0.23 g of $(NH_4)_2SO_4$ and then microwave-assisted digested in a MARS 5 microwave reaction system (CEM, NC, USA). Afterwards, samples were centrifuged at 3,000 rpm for 15 min to remove decanted organic matter, 1 mL of H_2O_2 (30%) added and water up to 10 mL. Finally, sample absorbance was measured at 410 nm (Shimadzu UV 1650 PC).

IV.2.3. DLVO theory

DLVO theory was used to model the attachment of bacterium and TiO_2 to sand grains and the aggregation of both type of particles. TiO_2 nanoparticles and bacteria were considered spheres with diameters equal to their hydrodynamic diameters. In the case of the rod-shaped bacterium, this dimension represents an equivalent diameter that can be related to the average of the two dimensions of the short rod. Sand was regarded as an infinite plate.

Interactions between sphere and plate (TiO_2 and sand, bacterium and sand) were calculated using the following expressions for van der Waals (Eq. IV.1) and electrostatic double layer (Eq. IV.2) interactions:[128, 131]

$$V_{vdWr} = -\frac{A_{iwq}\, a_i}{6\, h}\left[1 - \frac{5.32\, h}{\lambda}\, ln\left(1 + \frac{\lambda}{5.32\, h}\right)\right] \quad \text{(IV.1)}$$

$$V_{EDL} = \frac{128\, \pi\, a_i\, n_\infty}{\kappa^2}\, k\, T\, \gamma_i\, \gamma_q\, e^{-\kappa h} \quad \text{(IV.2)}$$

where V_{vdWr}: retarded van der Waals interaction potential energy (J), V_{EDL}: electrical double layer interaction potential energy (J), A_{iwq}: Hamaker constant for the particle (TiO_2 or bacterium) and quartz surface suspended in water (J), a_i: radius of the sphere (TiO_2 or bacterium) (primary aggregate) (m), h: separation (m), λ: characteristic wavelength of the interaction (assumed to be 100 nm), n_∞: bulk number of ions (ions m^{-3}), κ: Debye-Hückel reciprocal length (m^{-1}), k: Boltzmann constant (J K^{-1}), T: temperature (K), γ_i: reduced surface potential of the sphere (TiO_2 or bacterium), γ_q: reduced surface potential of the plate (quartz).

Interactions between two different spheres (TiO_2 and bacterium) were calculated using Eqs. IV.3 and IV.4 when $h \ll a_i$:[128, 131]

$$V_{vdWr} = -\frac{A_{Twb}\, a_T\, a_b}{6\,(a_T + a_b)\, h}\left[1 - \frac{5.32\, h}{\lambda}\, ln\left(1 + \frac{\lambda}{5.32\, h}\right)\right] \qquad \text{(IV.3)}$$

$$V_{EDL} = \frac{128\,\pi\, a_T\, a_b\, n_\infty}{(a_T + a_b)\,\kappa^2}\, k\, T\, \gamma_T\, \gamma_b\, e^{-\kappa h} \qquad \text{(IV.4)}$$

where A_{Twb}: Hamaker constant for two spheres (TiO_2 and bacterium) in water (J); with the aid of Eqs. IV.5 and IV.6:[1]

$$\gamma_i = Tanh\, \frac{z\, e\, \varphi_i}{4\, k\, T} \qquad \text{(IV.5)}$$

$$\kappa = 2.32\times10^9 \sqrt{\sum C_j\, z_j^2} \qquad \text{in aqueous solutions at 25°C} \qquad \text{(IV.6)}$$

where z: valence of symmetrical (z-z) electrolyte, e: electron charge (C), φ_i: electrical surface potential (V) which cannot be determined and was replaced by ζ_i: zeta potential (V), C_j: ion concentration (mol dm^{-3}), z_j: valence of ion j including sign of charge.

For the case of two equal spheres of TiO_2 or bacteria Eqs. IV.3 and IV.4 were reduced to Eqs. IV.7 and IV.8 respectively:

$$V_{vdWr} = -\frac{A_{iwi}\, a_i}{12\, h}\left[1 - \frac{5.32\, h}{\lambda}\, ln\left(1 + \frac{\lambda}{5.32\, h}\right)\right] \qquad \text{(IV.7)}$$

$$V_{EDL} = \frac{64\,\pi\,a_i\,n_\infty}{\kappa^2}\,k\,T\,\gamma_i^2\,e^{-\kappa h} \quad \text{(IV.8)}$$

where A_{iwi}: Hamaker constant of TiO_2 or bacterium in water (J).

DLVO theory considers the total interaction potential energy as the sum of both van der Waals and electrical double layer potential energies (Eq. IV.9):

$$V_{TOTAL} = V_{vdWr} + V_{EDL} \quad \text{(IV.9)}$$

The Hamaker constants employed were calculated from data obtained in the literature:[23-25, 49, 160] A_{bwq} = 6.5x10^{-21} J, A_{Twq} = 1x10^{-20} J, A_{Twb} = 4.6x10^{-21} J, A_{TwT} = 6x10^{-20} J, A_{bwb} = 1.015x10^{-22} J. Zeta potential of quartz sand was obtained from literature: -40 mV in water, -39 mV in NaCl 1 mM, -22 mV in NaCl 10 mM, -10 mV in NaCl 100 mM.[24]

IV.2.4. Sand bed removal

The attachment of TiO_2 and *Pseudomonas aeruginosa* to the porous bed was evaluated using the classical filtration equation (Eq. IV.10) as well as the particle deposition rate (Eq. IV.11):[45, 46]

$$\frac{dC}{dL} = -\frac{3}{2}\,\frac{1-f}{d_c}\,\alpha_c\,\eta_0\,C \quad \text{(IV.10)}$$

$$k_d = \frac{3}{2}\,\frac{1-f}{f\,d_c}\,U\,\alpha_c\eta_0 \quad \text{(IV.11)}$$

where C: suspended particle concentration, L: bed length (m), f: porosity, d_c: average diameter of the collector (m), α_c: clean-bed collision efficiency factor, η_0: single-collector efficiency, k_d: particle deposition rate coefficient, U: Darcy velocity (m s^{-1}).

The single-collector efficiency, considered to be the addition of Brownian diffusion, interception, and gravitational sedimentation, was calculated using the Tufenkji-Elimelech equation (TEE).[46] For the case of combined transport, a pseudo-collision efficiency factor was

also calculated, considering the initial ("clean") collector to be the bacteria-modified sand particles, at the first stages of nanoparticle influx.

The required parameters for calculating the clean-bed collision efficiency factor, the single-collector efficiency and the particle deposition rate coefficient were calculated from our experimental data obtained during the transport of TiO_2 and *P. aeruginosa*.

IV.3. RESULTS AND DISCUSSION

IV.3.1. Characterization of *Pseudomonas aeruginosa* and TiO_2

The average particle size and zeta potential of the bacterium and TiO_2 were determined for a range of ionic strengths between deionized water and 100 mM, at pH 5.8 (Fig. IV.1).

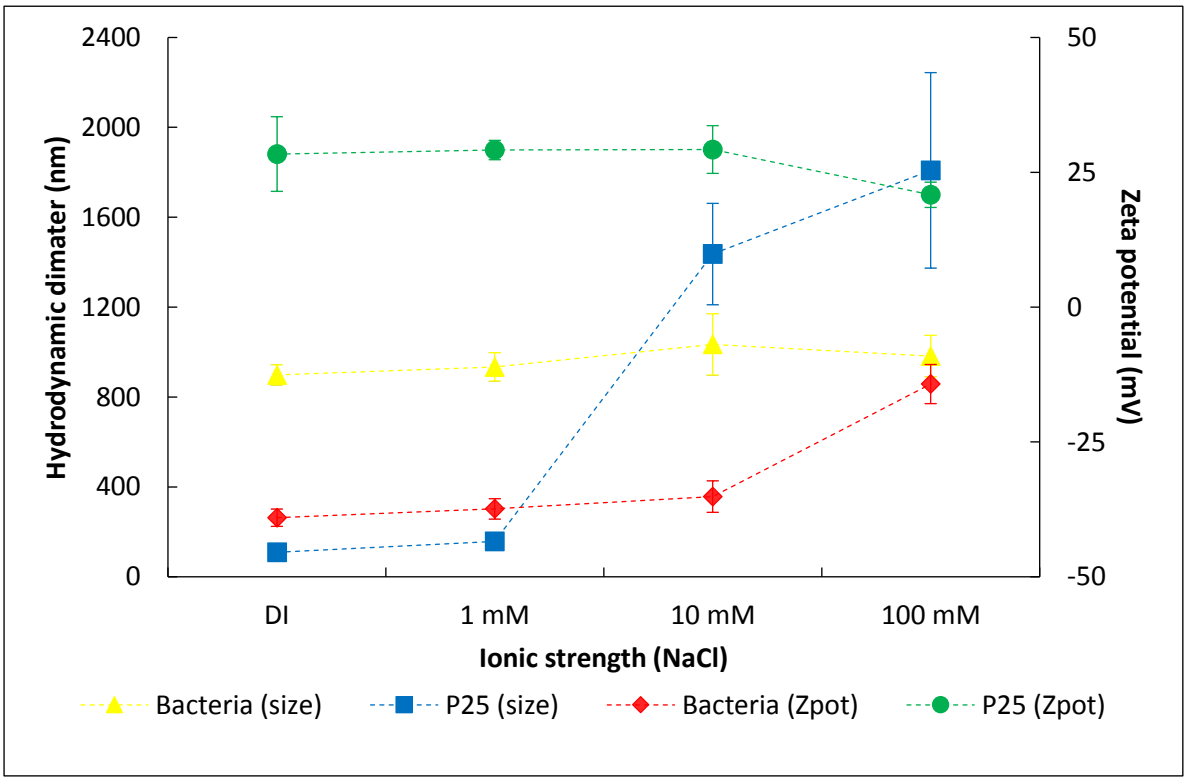

Fig. IV.1: Hydrodynamic diameter and zeta potential of bacteria and TiO_2 nanoparticles suspended in water (18 MΩ.cm) and NaCl solutions; pH=5.8.

P. aeruginosa is a coccobacillus bacterium, not a perfect sphere and then the hydrodynamic diameter obtained by dynamic light scattering (DLS) does not reflect its real size, but accounts for an equivalent diameter that can be related to the average of the two dimensions of the short rod. Moreover, bacteria are not rigid but dynamic in size as they interact with the solvent in which they are suspended. Therefore, the calculated diameter indicates the apparent size taking into consideration attraction and association with water molecules and electrolytes.

The size of the bacterium remained relatively uniform under the different ionic strengths, between 898 $\pm$ 45 and 1,034 $\pm$ 136 nm. Its equivalent diameter is in agreement with isolated bacterium sizes reported in the literature[161] suggesting the absence of aggregation. In contrast, the hydrodynamic size of TiO_2 was significantly affected by the ionic strength. When suspended in pure water, TiO_2 was present as 109 $\pm$ 23nm aggregates, in concordance with previous publications.[156, 162, 163] TiO_2 rapidly aggregated in aqueous solutions, as a consequence of its reactivity and high surface area.[164] Furthermore, ionic strength enhanced attachment efficiency resulting in increase of aggregate size, especially for ionic strengths over 1 mM, reaching sizes well over 1 μm. The samples were subjected to slow mixing during preparation that caused first interactions and then contact between nanoparticles, which, in turn led to aggregation[146] and corresponded to the physical transport mechanisms of the classical aggregation theory.[39]

At the working pH, *P. aeruginosa* was negatively charged while TiO_2 exhibited positive surface charge in agreement with the reported isoelectric point for the metal oxide of 6.7.[146, 165] Zeta potential of the bacterium varied from -39 to -14 mV and between 29 and 21 mV for TiO_2 with increasing ionic strength (DI water to 100 mM).

DLVO theory predicted repulsion between two bacterial particles for all the studied conditions (Fig. IV.2), as it was confirmed experimentally.

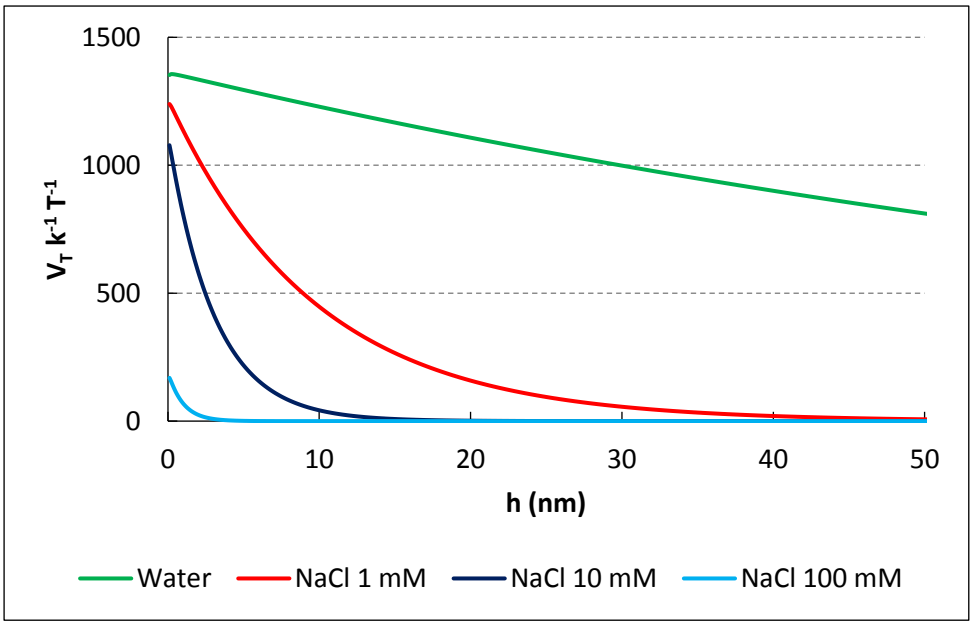

Fig. IV.2: DLVO predicted interaction potential energy for two particles of bacterium.

As ionic strength was increased, larger TiO_2 aggregates were found, in accordance with DLVO modeling (Fig. IV.3). Reduction in zeta potential and compression of the electrical double layer resulted in lower energy barriers at higher electrolyte concentrations, and for NaCl 100 mM only attractive forces between the particles were predicted.

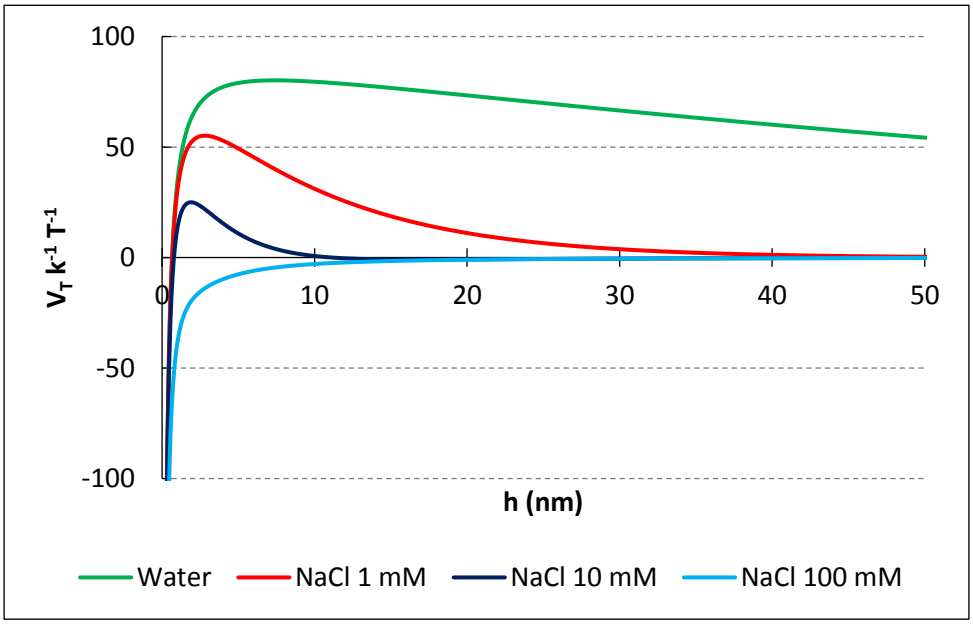

Fig. IV.3: DLVO predicted interaction potential energy for two particles of TiO_2.

IV.3.2. Transport of TiO_2

P25 column experiments were conducted by pumping 5 PV of TiO_2 suspension with the desired ionic strength (water, 1, 10 or 100 mM NaCl), followed by 3 PV of background solution. pH was in the range 5.2-5.8 for all the experiments.

Fig. IV.4 shows the breakthrough curves at each ionic strength investigated (0; 1; 10; 100 mM) for three levels of influent nanoparticle concentration: 30; 50; and 100 ppm. In all cases, tracer solution (NaCl) was circulated prior to transport experiments to determine the column porosity and check the sand packing, also shown in Fig. IV.4. A plateau was reached for water and 1 mM ionic strength respectively (Fig. IV.4.a and b); but for higher ionic strengths (10 and 100 mM) a peak was reached and then concentration at outlet decreased (Fig. IV.4.c and d), which hints to an increasing removal efficiency.

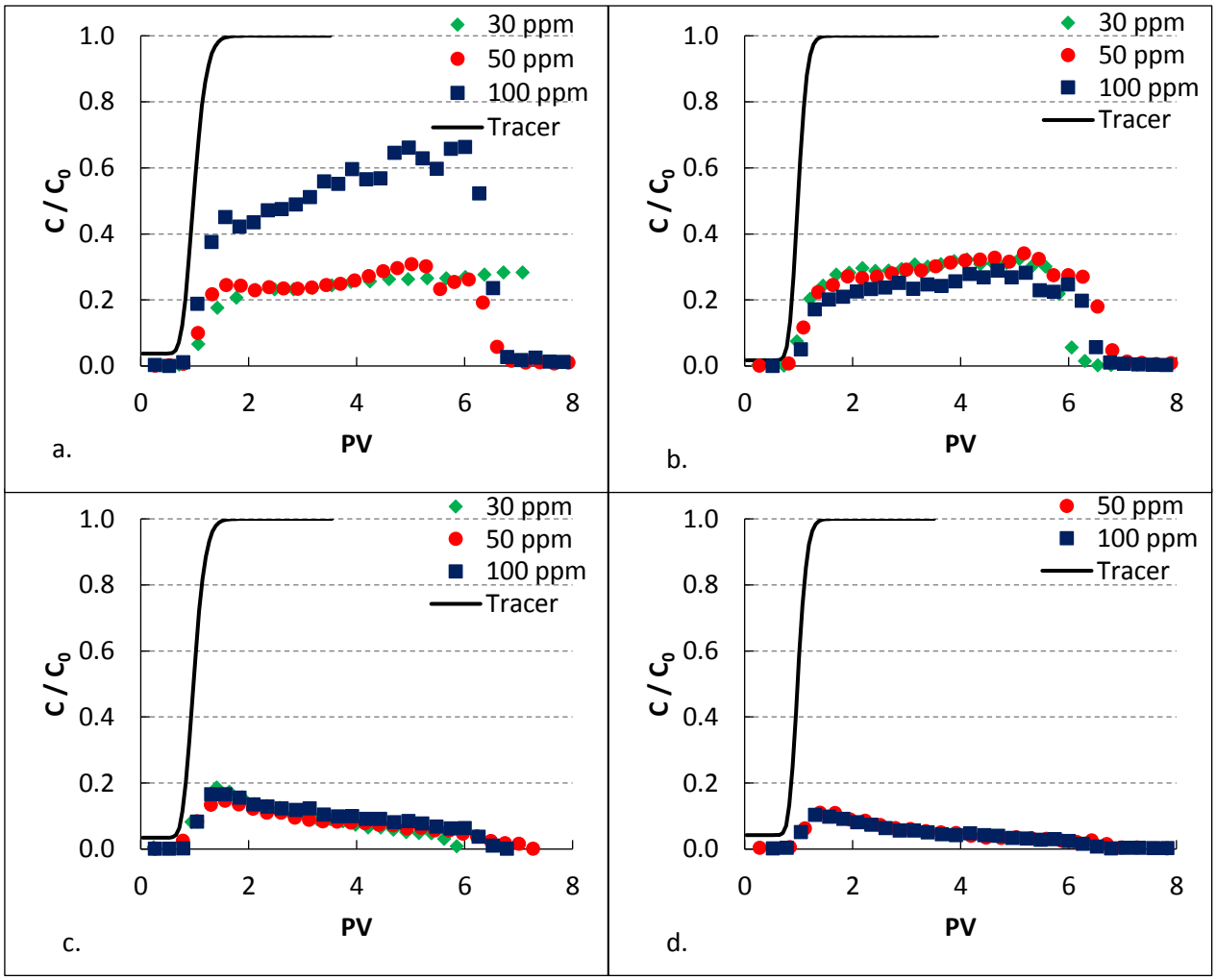

Fig. IV.4: Breakthrough curves for TiO_2 in sand columns suspended in: a. Water (resistivity 18 MΩ.cm), b. 1 mM NaCl, c. 10 mM NaCl, d. 100 mM NaCl.

Three different factors can be responsible for the retention of TiO_2 in the porous media. First, attraction forces between quartz sand and TiO_2 due to the difference in their surface charges (attachment to the clean bed). Second, electrolyte concentration that causes aggregation during the transport of TiO_2 rendering it more difficult for the particles to pass through the pores (straining). Third, attachment of TiO_2 to previously deposited particles due to the attraction forces among them as discussed above (attachment to the ripe bed).

Electrostatic forces take into account surface charge differences between the negative sand and the positive TiO_2. As nanoparticles were retained, the collector's surface became progressively heterogeneous, so some particles would deposit onto the original sand while others would collide with previously attached TiO_2. Scanning electron microscopy (SEM) images showing this heterogeneity are provided in Fig. IV.5 to IV.10; the size of each aggregate and frequency on the surface seems to decrease from the top layers of sand to the deeper grains, indicating less influence of repulsive forces as well as less quantity of TiO_2 to remove due to further retention in the first centimeters of the porous bed.

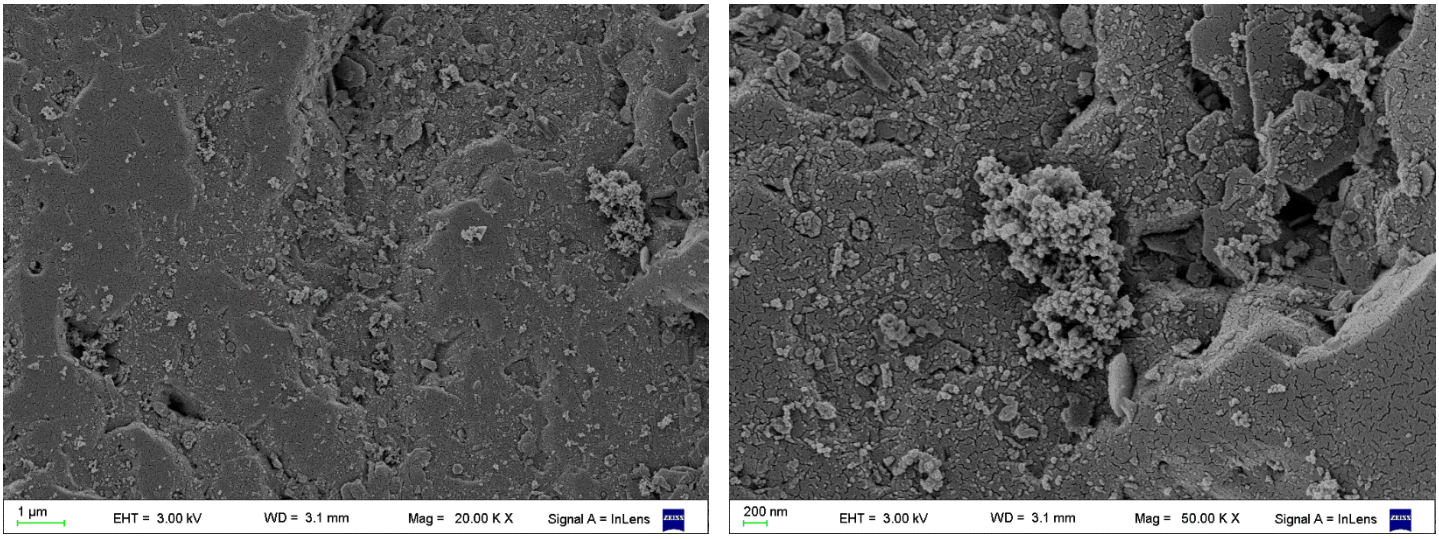

Fig. IV.5: SEM images of TiO_2 aggregate on quartz sand grain after transport experiment (30 ppm TiO_2 in 1 mM NaCl), top of the column.

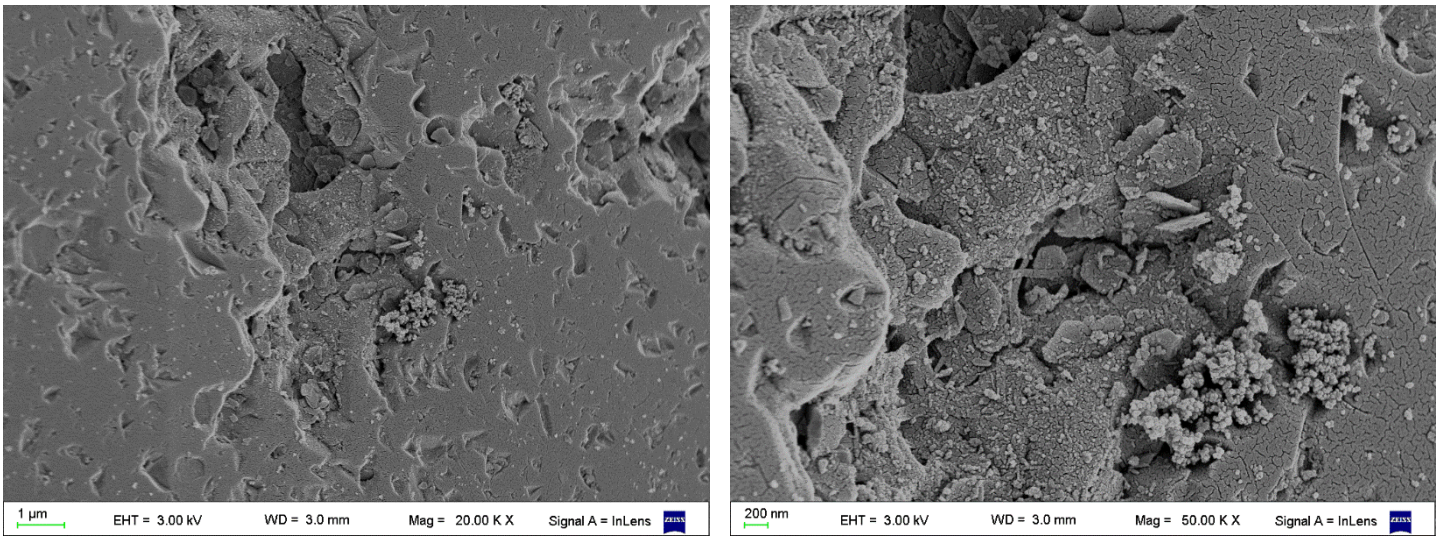

Fig. IV.6: SEM images of TiO_2 aggregate on quartz sand grain after transport experiment (30 ppm TiO_2 in 1 mM NaCl), depth=1 cm.

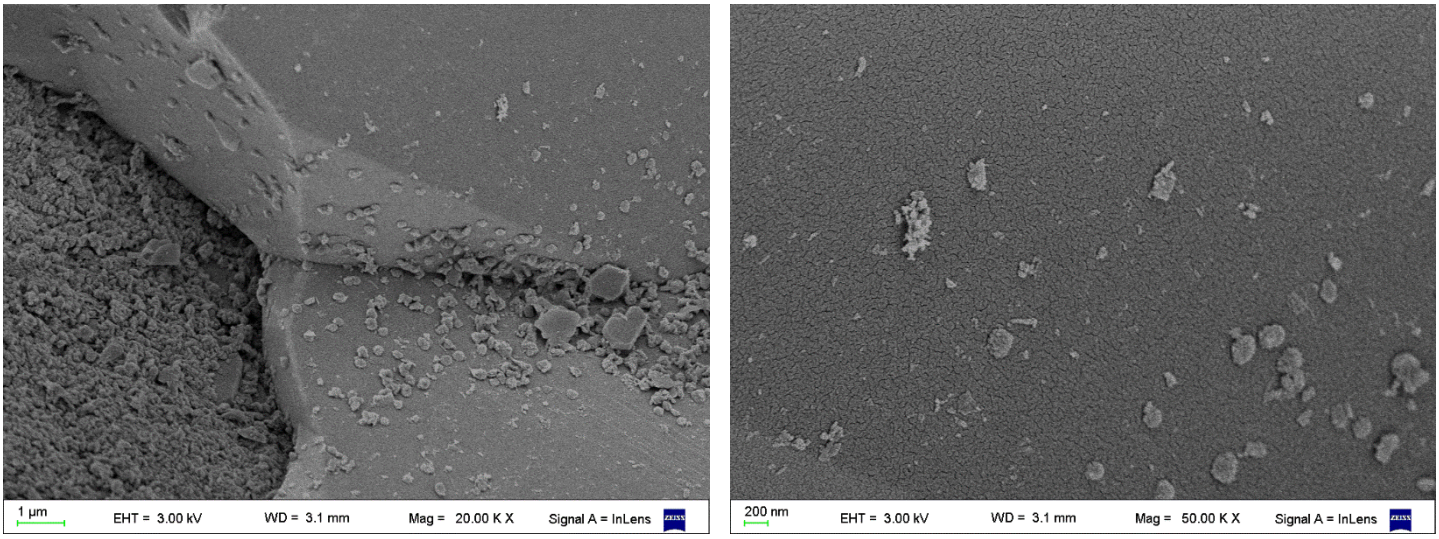

Fig. IV.7: SEM images of TiO_2 aggregate on quartz sand grain after transport experiment (30 ppm TiO_2 in 1 mM NaCl), depth=2 cm.

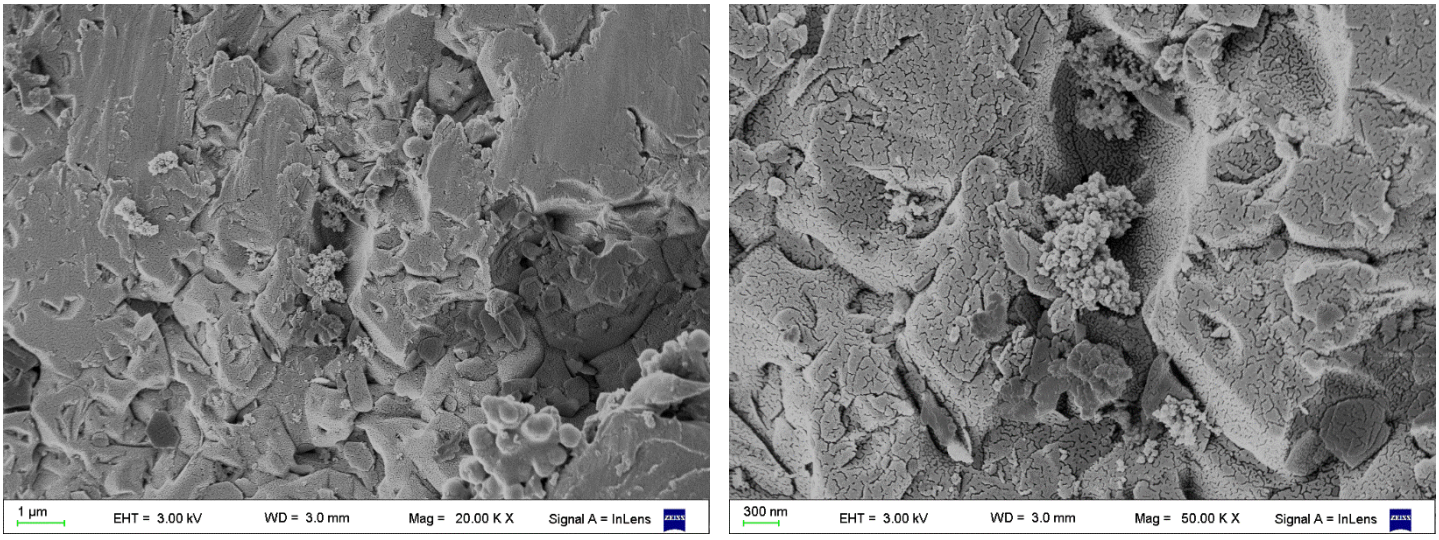

Fig. IV.8: SEM images of TiO_2 aggregate on quartz sand grain after transport experiment (30 ppm TiO_2 in 1 mM NaCl), depth=3 cm.

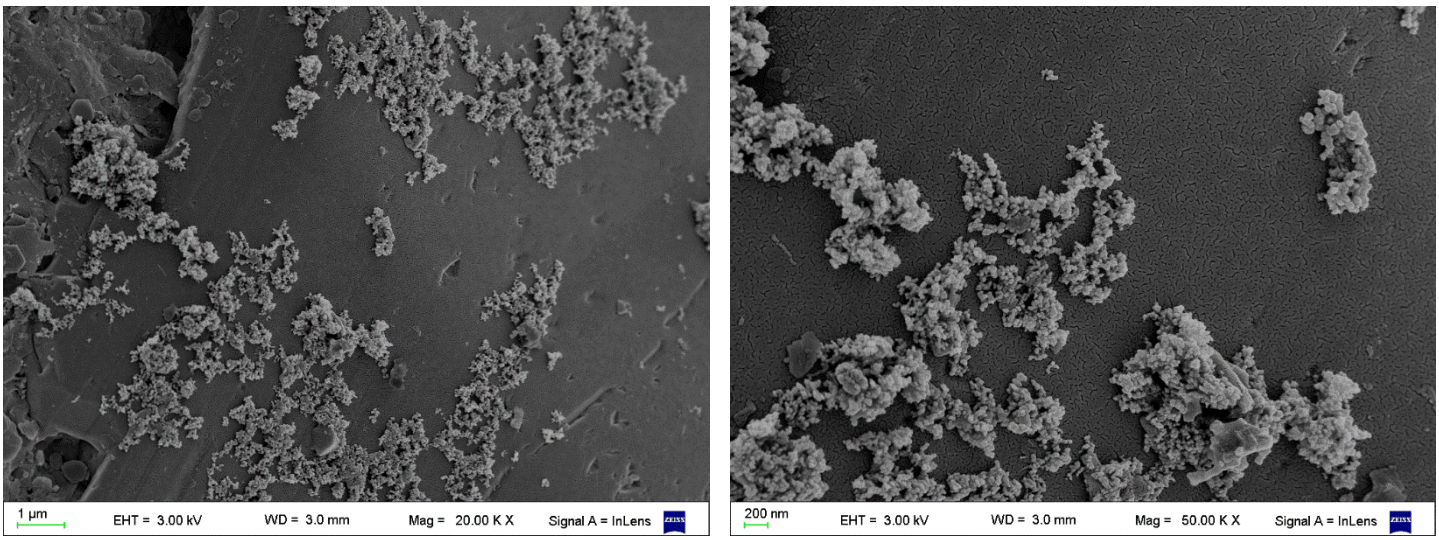

Fig. IV.9: SEM images of TiO_2 aggregate on quartz sand grain after transport experiment (30 ppm TiO_2 in 1 mM NaCl), depth=4 cm.

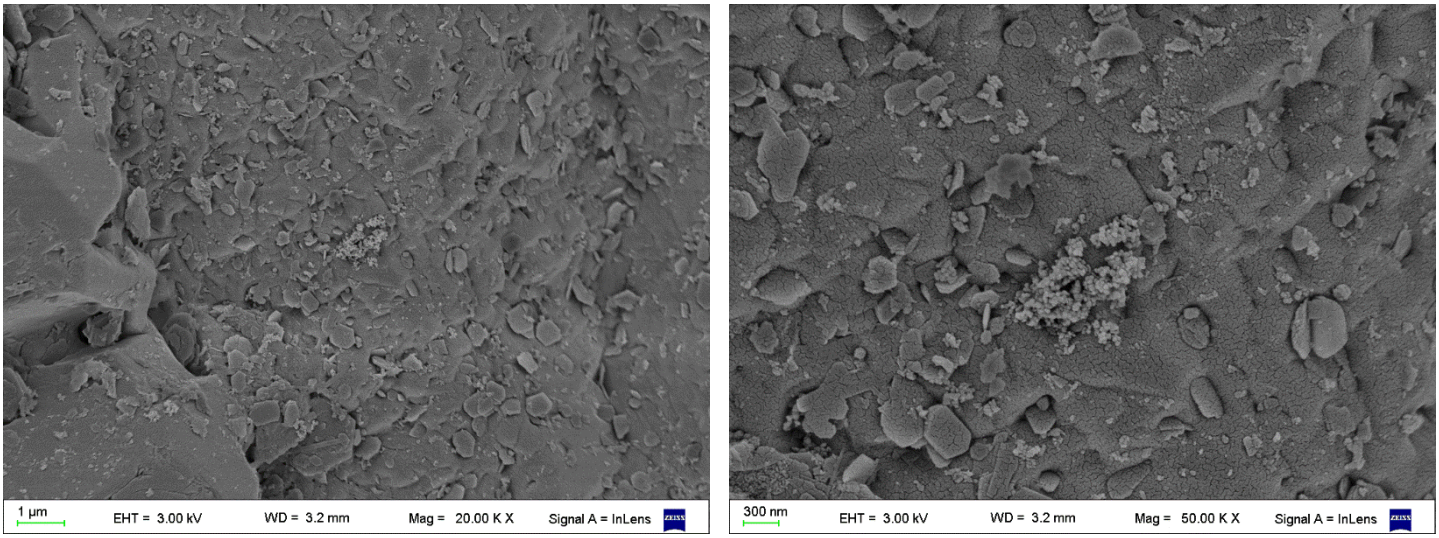

Fig. IV.10: SEM images of TiO_2 aggregate on quartz sand grain after transport experiment (30 ppm TiO_2 in 1 mM NaCl), depth=5 cm.

When particles were suspended in deionized water and repulsion was dominant, collector attachment resulted in a monotonic increase of effluent particle concentration (Fig. IV.4.a). As ionic strength was increased, the attachment efficiency between TiO_2 particles was also increased and the effluent particle concentration dropped (Fig. IV.4.b, c and d). Based on DLVO calculations (Fig. IV.3), repulsion will be present between TiO_2, except when suspended in 100 mM ionic strength. When particles are passing through the column, these dominant repulsion forces will lead to increasing effluent concentration with time.[166, 167] Besides, particles will find less free surface on the collector due to previous deposition; which in turn will contribute to this effect.

The variation of TiO_2 concentration in the feed affected the effluent concentration in the absence of electrolyte (Fig. IV.4.a); making it higher at higher incoming concentration. A strong attachment between TiO_2 and sand was predicted by DLVO theory (Fig. IV.11), and deposition was expected as long as there was free collector surface available. When the surface was more covered in nanoparticles, it created repulsion between this layer and new incoming TiO_2; DLVO modeling of TiO_2-TiO_2 interactions (Fig. IV.3) showed a significant energy barrier. For the highest feed concentration (100 ppm), collectors were covered in nanoparticles sooner due to enhanced chances of collisions, which in turn prevented new deposition and effluent concentration augmented.

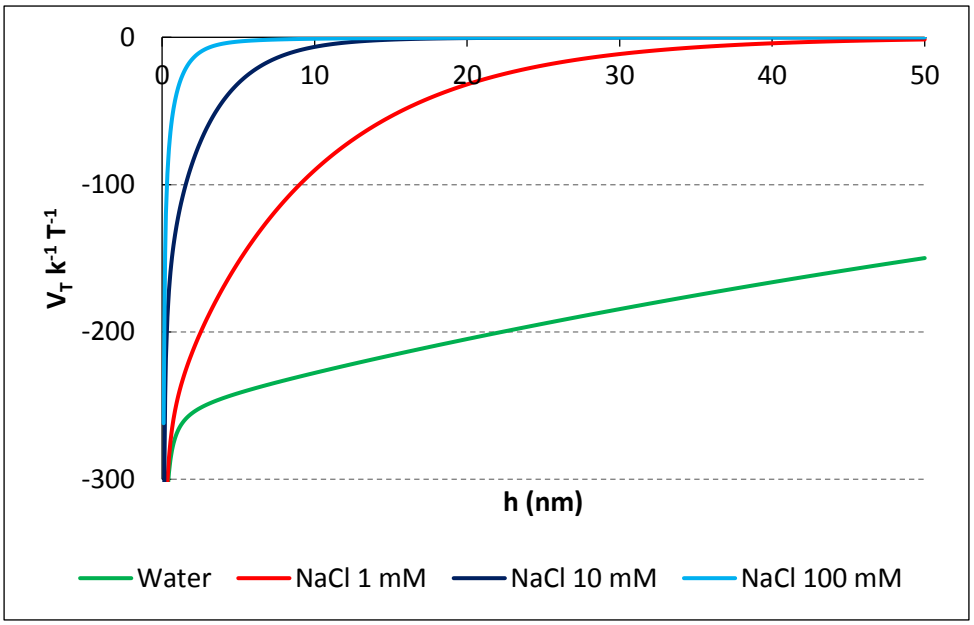

Fig. IV.11: DLVO predicted interaction potential energy for a particle of TiO_2 and the quartz sand.

At 1 mM ionic strength, DLVO showed a moderate energy barrier (Fig. IV.3) and the system was closer to its critical coagulation concentration,[146] so increased attachment efficiency was attained and deposition resulted independent of particle concentration.

For the highest ionic strengths, TiO_2 easily aggregated and attachment to sand and previously deposited particles was a consequence of the high attachment efficiency and particle size growth, independent of feed concentration.

DLVO calculations for the interactions between TiO_2 particles and sand collectors (Fig. IV.11) resulted in strong attractive but no repulsion forces due to the opposite sign of the surface charges. As ionic strength increased, the electrical double layer interactions tend to a zero value, diminishing their relative importance when compared to the van der Waals attraction.

The experiments showed that for low to moderate ionic strengths (10 to 100 mM), TiO_2 retention levels in saturated sand were independent of incoming concentration.

IV.3.3. Transport of *Pseudomonas aeruginosa*

Pseudomonas aeruginosa transport experiments were conducted by pumping 5 PV of bacterial suspension with the desired ionic strength, followed by 3 PV of background solution. pH was in the range 5.2 - 5.8 for all the experiments. Breakthrough curves are shown in Fig. IV.12.

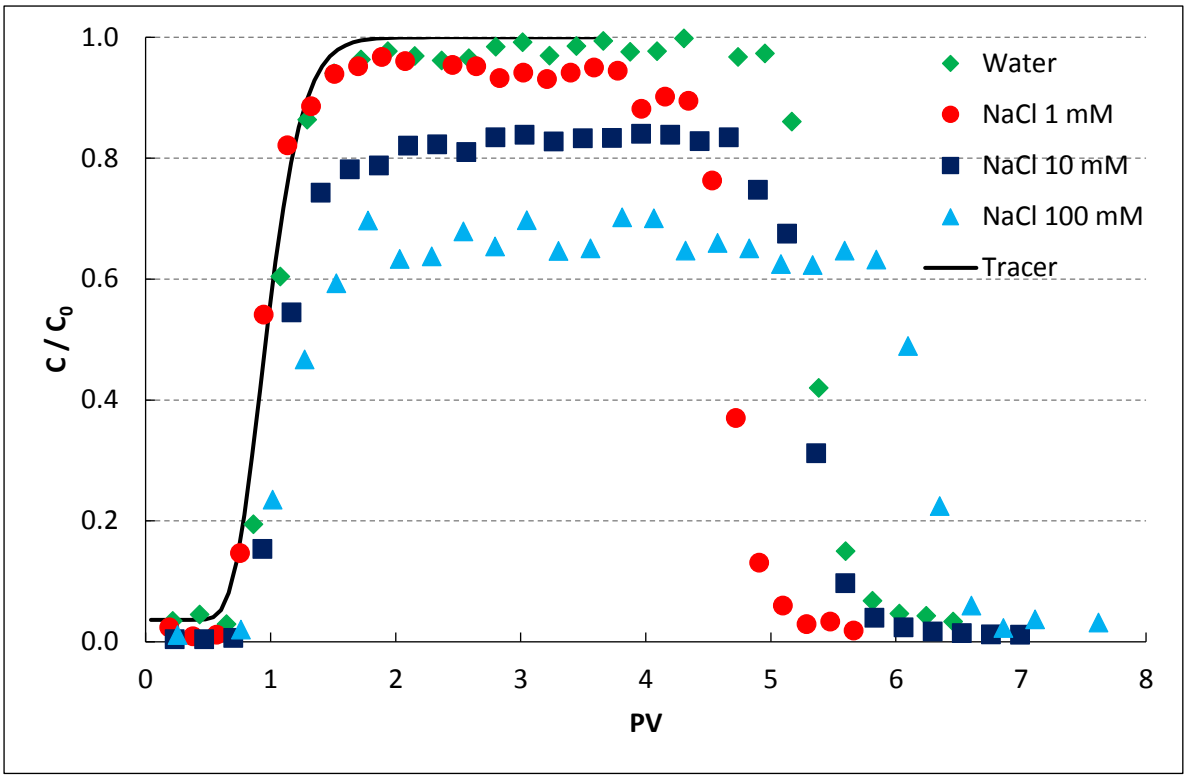

Fig. IV.12: Breakthrough curves for *Pseudomonas aeruginosa* in water (18 MΩ.cm), NaCl 1 mM, 10 mM, 100 mM.

Surface charge of bacteria was always negative and therefore, not expected to be significantly retained by the also negatively charged sand. However, as ionic strength increased, some retention was observed. This effect can be explained by DLVO theory (Fig. IV.13). For ionic strengths up to 10 mM, no net attracting forces were present and a high energy barrier was predicted. The energy barrier diminished as ionic strength increased because of the compression of the electrical double layer and of the reduction of the zeta potentials. For ionic strength of 100 mM, the energy barrier disappeared completely and the net forces were attractive, favoring attachment.

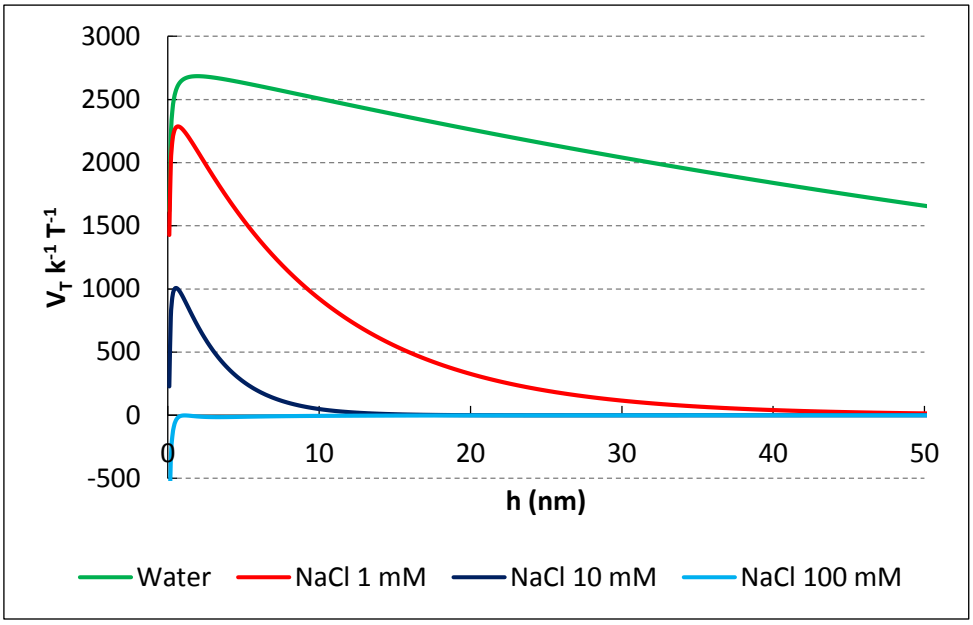

Fig. IV.13: DLVO predicted interaction potential energy for a particle of bacterium and the quartz sand.

IV.3.4. Combined transport of *Pseudomonas aeruginosa* and TiO_2

In the combined transport experiments, 4 PV of *Pseudomonas aeruginosa* suspension were first pumped through the sand bed with the desired ionic strength, followed by 3 PV of a suspension containing both *P. aeruginosa* and TiO_2, and finally 3 PV of the original suspension of *P. aeruginosa*.

Fig. IV.14 shows the breakthrough curves for *P. aeruginosa* in the presence of TiO_2. These concentrations were determined by qPCR. The detection limit was 24.1 CFU and the quantification limit was 241 CFU. For the reaction, the efficiency was 101.4% and R^2=0.996. Agarose gel electrophoresis was performed to corroborate the reaction products and the quality of the standard for the calibration curve (Fig. IV.15) and for the results (Fig. IV.16). Additionally, it was determined that the presence of TiO_2 nanoparticles did not generate inhibition of the polymerase chain reaction, through a control test using a standard corresponding to a DNA fragment of *Arabidopsis thaliana*.

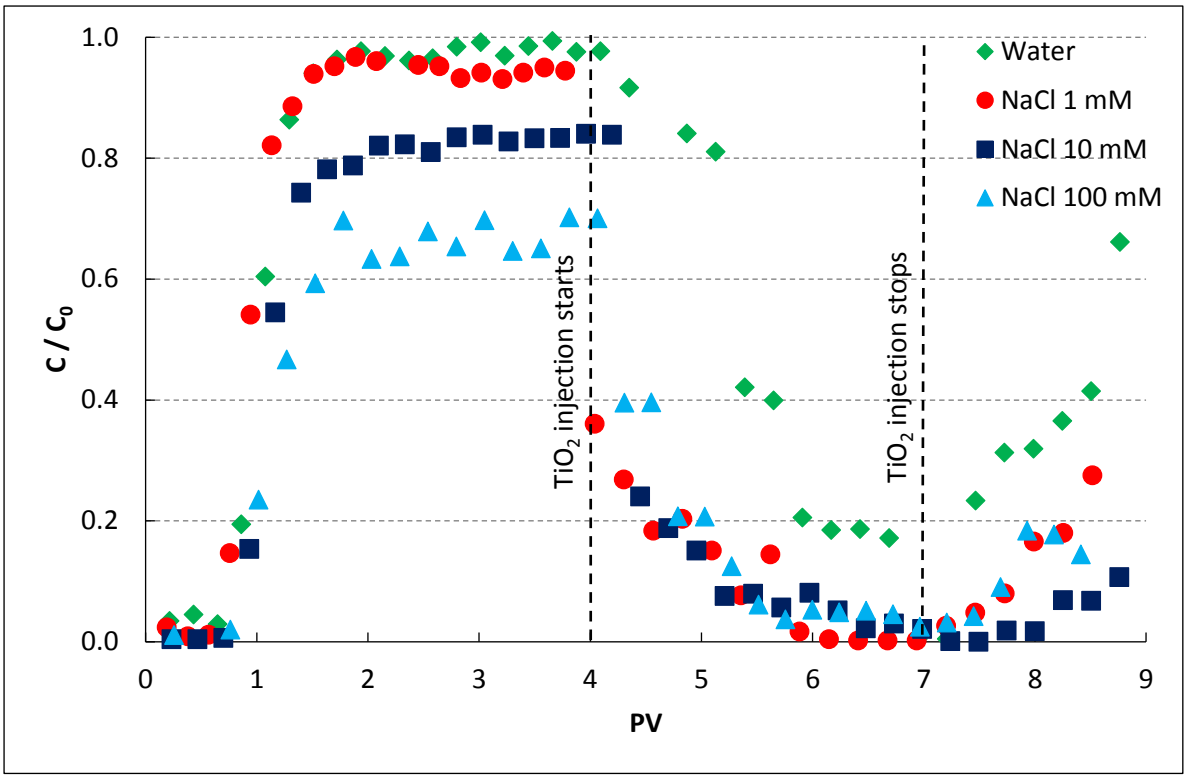

Fig. IV.14: Breakthrough curves for bacteria, measured by qPCR between 4 and 9 PV, in co-transport of bacteria and TiO_2.

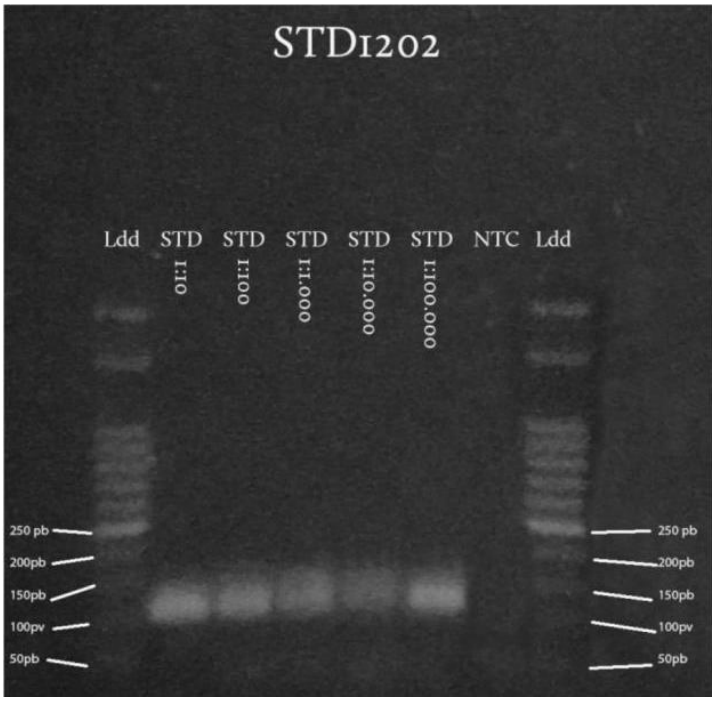

Fig. IV.15: Agarose gel 1.5% electrophoresis to corroborate the reaction products and the quality of the standard for the calibration curve.

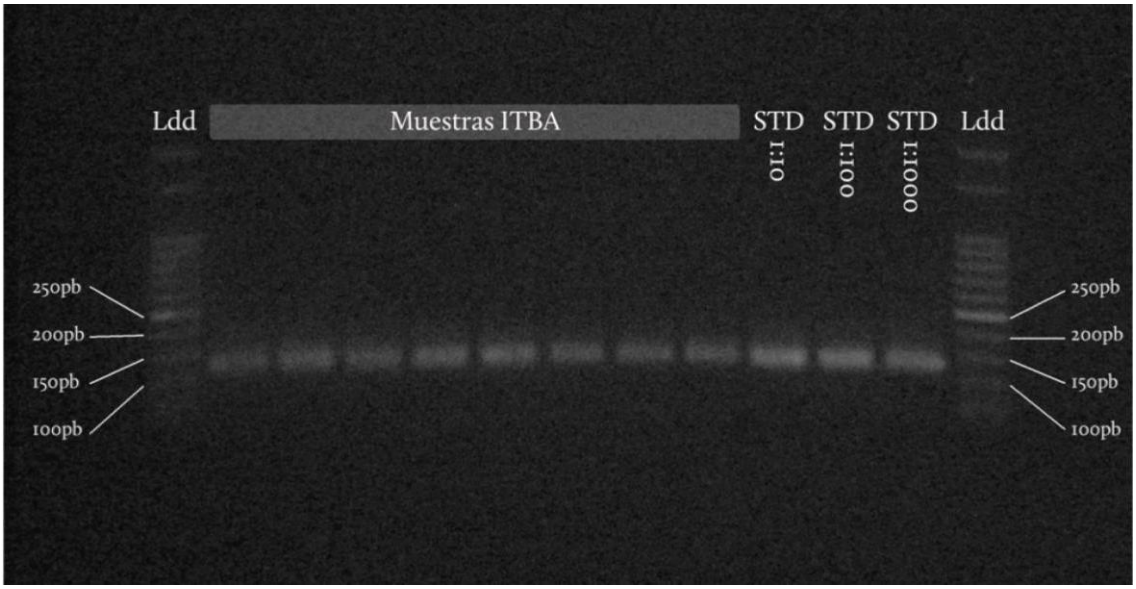

Fig. IV.16: Agarose gel 1.5% electrophoresis to corroborate the reaction products and the quality of the standard for the results.

The transport characteristics of the bacteria were highly modified by the presence of TiO_2. Retention in the sand bed was observed, in contrast to the bacteria flow observed in the single particle experiments. The quantity of bacteria retained was increased with ionic strength, probably as a consequence of the formation of large TiO_2-bacterium aggregates that clogged the pores.[152]

Fig. IV.14 shows that after reaching the initial plateau, effluent bacteria concentration suffered a sharp decrease coincident with the injection of TiO_2. This effect was important even for pure water suspensions and retention remained very high for the duration of the TiO_2 injection. After TiO_2 injection stopped, bacteria concentration at outlet showed an increasing trend indicating that the microorganisms were transported through the sand bed again. DLVO theory predicted the attachment between TiO_2 and bacteria due to the difference in surface charges (Fig. IV.17), although non-DLVO Lewis acid-base interactions and hydrogen bonds could also be partially responsible for the increasing attachment efficiency.[151, 168, 169]

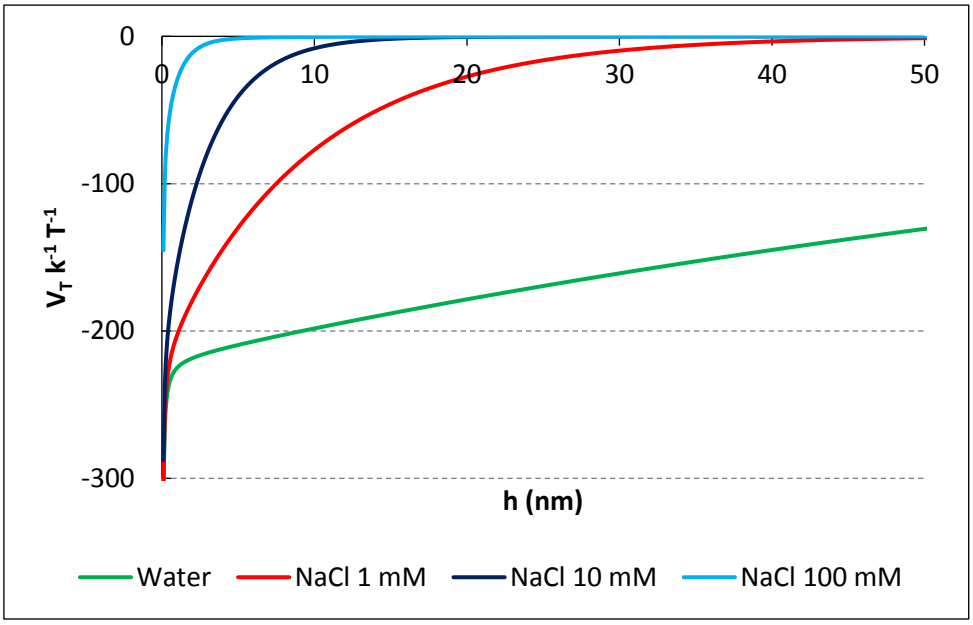

Fig. IV.17: DLVO predicted interaction potential energy for a particle of TiO_2 and a particle of bacterium.

Fig. IV.18 shows the breakthrough curves for TiO_2 in the presence of bacteria. The breakthrough of TiO_2 only suspensions is shown for comparison. The retention of TiO_2 by the sand was highly increased by the presence of bacteria, probably due in part to the formation of larger aggregates of nanoparticles and bacteria. The first layer of TiO_2 attached to the sand was responsible for adhering incoming microorganisms, which can in turn attract new particles of TiO_2. This process continued as long as both kinds of particles were injected. It can also be seen that in both cases, with and without the presence of the bacteria, the concentration of TiO_2 at the outlet was modified by the ionic strength, showing an increase in retention with increasing ionic strength, as predicted by DLVO theory and discussed above. This last observation suggests that electrostatic repulsion, modulated by the electrolyte concentration, played a fundamental role in the retention of the nanomaterial. Moreover, it can be clearly observed that concentrations of bacteria and TiO_2 at outlet diminished when both of them were present together, compared to the case when only one of them was in the stream; this suggests attachment of TiO_2 to both bacteria and sand, causing retention of microorganisms due to heteroaggregation.

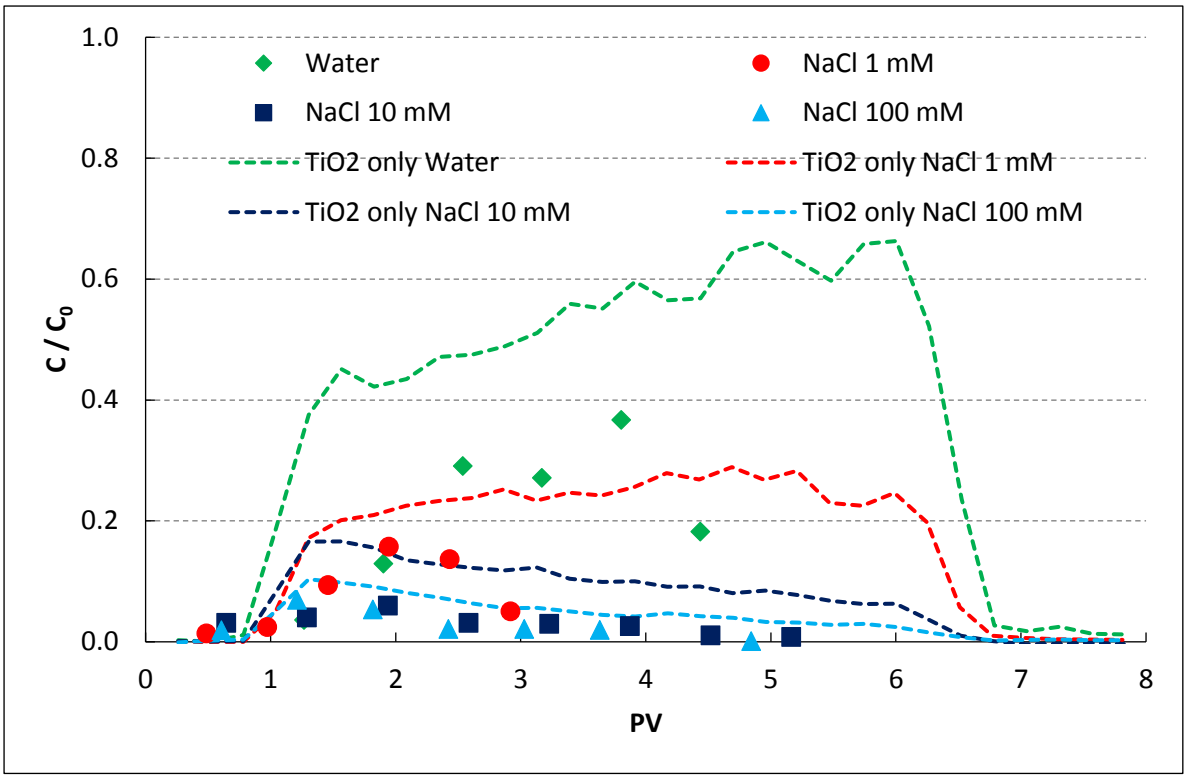

Fig. IV.18: Breakthrough curves for titanium measured by spectrophotometry at 410 nm after digestion and addition of H_2O_2 in co-transport of bacteria and TiO_2. Breakthrough curves for TiO_2 only for comparison.

IV.3.5. Sand bed removal

The average single-collector efficiency (η_0), clean-bed collision efficiency factor (α_c) and particle deposition rate coefficient (k_d) for TiO_2 and for *Pseudomonas aeruginosa* were calculated (Table IV.2).

Efficiency factors for bacteria and TiO_2 attachment to the collectors gave higher values for increasing ionic strength; and thus, increased retention in the porous bed, as confirmed in the laboratory experiences and in agreement with attachment controlled by classical DLVO interactions.[170]

Table IV.2: Average single-collector efficiency (η_0), clean-bed collision efficiency factor (α_c) and particle deposition rate coefficient (k_d) for TiO_2 and quartz sand and for *P. aeruginosa* and quartz sand.

	Water		NaCl 1 mM		NaCl 10 mM		NaCl 100 mM	
	TiO_2-Sand	Bacteria-Sand	TiO_2-Sand	Bacteria-Sand	TiO_2-Sand	Bacteria-Sand	TiO_2-Sand	Bacteria-Sand
η_0	0.0181	0.00321	0.0184	0.00320	0.0191	0.00348	0.0197	0.00325
α_c	0.792	0.127	1.118	0.339	1.473	0.602	1.661	1.418
$k_d \cdot 10^3$ (s^{-1})	4.79	0.109	5.96	0.305	8.07	0.637	9.95	1.33

Collision efficiency factors above unity are theoretically impossible, but those between 1 and 1.25 are not considered rare. Discrepancies between the actual shape of collectors and the perfect spheres considered in the TEE can cause these overestimated values, as well as the size of the TiO_2 particle employed which is subject to aggregation.[171] It is important to note however, that the TEE was derived based on experimental data and was widely validated and employed, offering valuable parameters to compare different situations. Moreover, high values of collision efficiency factors suggest coexistence of straining along with physicochemical filtration.[172]

To compare the attachment of TiO_2 with and without concurrent flow of bacteria, a pseudo-collision efficiency factor was calculated (considering the individual plateau concentration for each particle obtained from the breakthrough curves in Fig. IV.18). These values were significantly higher (between 32 and 53%) than those found in the single particle experiment for all ionic strengths, hinting to a synergistic effect on the retention in the combined transport (Fig. IV.19).

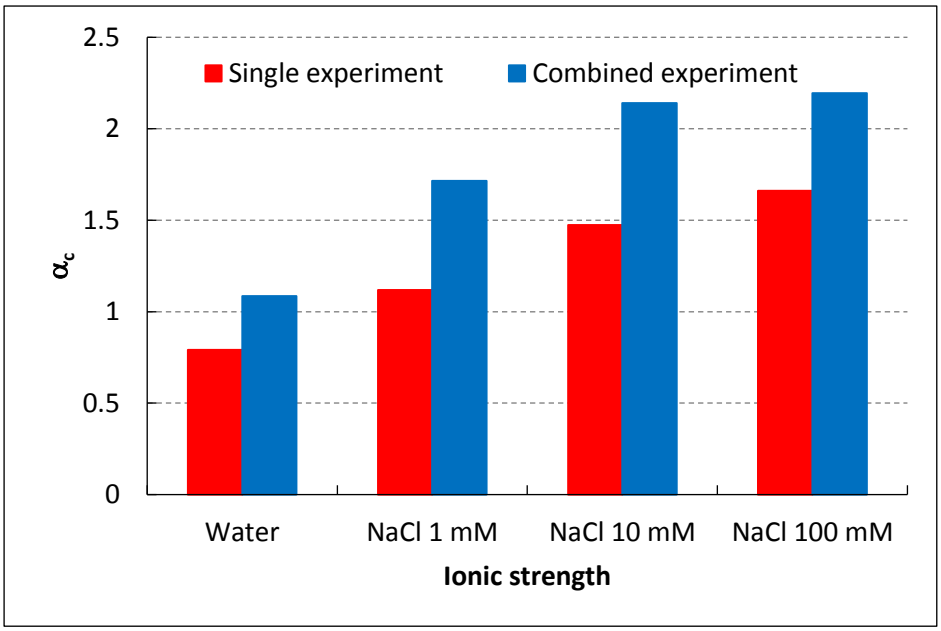

Fig. IV.19: Collision efficiency factor (α_c) for TiO_2 in the single experiment and pseudo-collision efficiency factor for TiO_2 in the combined experiment.

IV.4. CONCLUSIONS

Groundwater quality is seriously affected by the irruption of microorganisms and engineered nanoparticles. Nonetheless, the inclusion of novel materials and resources for controlling the presence of bacteria can be developed.

In this work, we showed that P25 TiO_2 was retained by the quartz sand due to aggregation and electrostatic attraction leading to attachment. At low ionic strengths, the attachment to the sand grains was low but it increased over time when ionic strength augmented. Bacteria were transported through the porous media, with minimal retention; however, a completely different scenario arose when nanoparticles were present in the water matrix, and bacteria were retained up to 99.99%. This observation is probably due to a combination of straining due to heteroaggregation of bacteria and TiO_2 nanoparticles in the incoming suspension and a more favorable condition for removal given by a ripening effect in the sand bed caused by previously deposited particles. Besides, electrostatic repulsion, controlled by ionic strength, played a fundamental role in the retention of the nanomaterial.

The transport of microorganisms in porous media (groundwater, aquifers, sand filters) is an important issue in both natural and engineered systems. We have shown that the transport of bacteria in saturated porous media is severely hampered by the presence of TiO_2

nanoparticles. Inclusion of these nanoparticles in sand beds offers the possibility to design an effective barrier for microorganisms, as a preventing measure, as a drinking water filter enhancer, or as a mean for retention of active bacteria and biofilm growth during a bioremediation process within the boundaries of the contaminant plume. However, this addition of nanoparticles should be designed carefully, considering the potential consequences brought by the incorporation of nanoparticles in the system.

Ecology of soils and water reservoirs can be modified by the emergence of nanoparticles as environmental contaminants. The outcomes of this work suggest that TiO_2 could be used to develop new methods for retaining bacteria in a well delimited subsurface area; but conversely, the pulse-like influx of nanomaterials in natural environments (sand aquifers) may be responsible for potential hazardous high concentrations of bacteria in the groundwater due to release of previously retained organisms after the nanoparticle input stops.

Chapter V

VIRUS REMOVAL BY IRON OXIDE CERAMIC MEMBRANES

Nomenclature

a: radius of virus (m)

A_{132}: combined Hamaker constant for bacteriophage P22 and hematite in water (J)

A_{131}: Hamaker constant for bacteriophage P22 in water (J)

A_{11}: Hamaker constant of virus (J)

A_{22}: Hamaker constant of hematite (J)

A_{33}: Hamaker constant of water (J)

C_i: ion concentration (mol dm^{-3})

e: electron charge (C)

h: separation between surfaces (m)

k: Boltzmann constant (J K^{-1})

n_∞: bulk number of ions (ions m^{-3})

T: temperature (K)

U: electrophoretic mobility (m^2 V^{-1} s^{-1})

V_{EDL}: electrical double layer interaction potential energy (J)

V_{TOTAL}: total colloidal interaction potential energy (J)

V_{vdW}: unretarded van der Waals interaction potential energy (J)

z: valence of symmetrical (z-z) electrolyte

z_i: valence of ion i including sign of charge

γ: reduced surface potential

ε: dielectric constant (F m^{-1})

ζ: zeta potential (V)

κ: Debye-Hückel reciprocal length (m^{-1})

μ: viscosity (Pa s)

ϕ: electrical surface potential (V)

V.1. INTRODUCTION

The availability of a safe water supply is an increasingly important priority for the welfare and development of human populations, challenged by the combined growth of demography, development, and waste. Parallel to this, researchers and authorities have been paying more attention in the last decades to the link between disease outbreaks and the presence of viral pathogens in drinking water sources.[173]

The removal or inactivation of viruses in water treatments is a challenging task: the technical difficulty resides in the fact that viruses and bacterial spores are much harder to eliminate -by common techniques such as microfiltration or chlorination for example- than bacterial pathogens due to their smaller size and simpler physiology. Although bacteria and larger microorganisms can be removed by ultrafiltration or microfiltration, the removal of smaller viral particles is mainly controlled by electrostatic interactions and attachment.[34, 174] Nanofiltration membranes meet the requirements for nanosized particle removal, but its use represents a significant increase in cost due to higher pressure requirements and lower produced water yields.[68] Consequently, there is a need to develop cost-efficient methods to achieve these goals, not only for large urban agglomerations but also for smaller rural populations and mobile applications.

Adsorption processes can effectively remove small contaminants as well as ionic constituents from water, avoiding energy consumption associated with pumping and disposal issues of concentrated streams generated.[175, 176] Furthermore, bulk porous adsorbents, as opposed to suspended colloidal particles and co-precipitation schemes, offer the additional advantage of not requiring an extra separation stage added to the treatment process, and thus, rendering the system safer to handle, easier to use, and applicable to mobile devices. In order for an adsorbent to be an efficient and economically sound option while still maintaining the above mentioned characteristics, it must be readily available on site, have a relatively high

specific surface area, low cost, and no toxicity associated with its fabrication, use, or final disposal of the material itself or its degradation products.

Previous work successfully led to the developing of iron oxide nanostructured ceramic membranes,[177, 178] which have proven to be an efficient treatment for the removal of natural arsenic contamination[99] and promising for other ionic contaminants as well. These membranes are especially suited for their use as filters of both inorganic/organic and biological contaminants in rural settings where access to electricity or specialized supplies is compromised. There is evidence[179-181] that iron and iron oxides can effectively retain and/or inactivate viral particles. Furthermore, iron oxides or minerals having a substantial proportion of iron oxides have shown very high affinity for viruses, that seems to be independent of their type or structure,[179, 181-183] and therefore, can become a general method for the removal of viruses from natural waters, where microorganisms exhibit seasonal and spatial variability.[184, 185] Metal oxide coatings on sand,[144, 186-188] glass fiber,[189, 190] ceramic filters,[191, 192] and diatomaceous earth[193] have been used in the removal and inactivation of viruses from water.

Bacteriophages are recognized as model organisms for human viruses.[100, 103] P22[110] and MS2[183] phages have been used in attachment experiments as well as other phages.[194] P22 phage has an icosahedral capsid and an approximate diameter of 70 nm, which is within the same order of magnitude as picornaviruses, the wide family to which human enteroviruses belong (approximately 30 nm).[195-197]

The nanostructured iron oxide ceramic filter investigated in this work presents numerous advantages over previously studied systems: ease of operation, low fabrication cost, more compact due to the higher specific active area available, and no sludge generation. The attachment kinetics and equilibrium isotherm of bacteriophage P22 was investigated. The virus was characterized with respect to size and surface charge, as they are expected to play a key role in the removal process. A flow through ceramic filter was fabricated and tested for the continuous treatment of contaminated water. The mechanism and limitations of the processes were analyzed and discussed in light of the DLVO theory of colloidal interaction, as well as the aggregation conditions of the phage in natural waters.

V.2. MATERIALS ANS METHODS

All chemicals were of reagent grade, except $FeCl_2$ used in the synthesis of the iron nanoparticles that was technical grade. Solutions were prepared in all cases with Type I water (resistivity 18 MΩ.cm).

P22 phage stock suspensions had a concentration of approximately $2x10^{10}$ PFU/mL. Viral solutions and subsequent dilutions were made by dissolving NaCl (Anedra, Argentina) in DI water to obtain a 15 mM concentration. The culture media used in these experiments were LB broth Lennox and LB Agar Lennox with two different concentrations of agar-agar as presented in Table V.1. In order to provide the inoculum for each plaque, *Salmonella typhimurium* strain DA1468, was spiked in 10 mL of LB broth Lennox, and then incubated for 24 h at 37°C.

Table V.1: Culture media and solutions used in virus experiments.

	L Broth	Soft L Agar	L Agar	Brand	Lot
Tryptone (g/L)	10	10	10	Britania	687
Yeast extract (g/L)	5	5	5	Britania	550,3
Agar-agar (g/L)	0	7.5	15	Britania	238
NaCl (g/L)	5	5	5	Anedra	17872-1

Glassware, tips, Eppendorf tubes, adsorbent and inert solutions were sterilized by autoclaving at 121°C for 15 minutes. Micropipettes were thoroughly rubbed with ethanol 70% prior to usage.

V.2.1. Purification of bacteriophage P22

After replication, the viral suspension was centrifuged at 15,000 rpm for 60 minutes. Then, the supernatant was filtered through a 0.22 µm PVDF membrane (Millipore GVW P02500). This suspension was dialyzed through a 100 kDa MWCO membrane (SpectraPor Biotech CE, Spectrum Laboratories, USA) twice: first, against Milli-Q water, and second, against a 15 mM NaCl solution for 20 hours each. The final suspension was filtered again and kept at 4°C.

V.2.2. Synthesis of ferroxane nanoparticles

Iron oxide nanoparticles were synthesized in the laboratory following a previously published procedure.[99] Briefly, lepidocrocite was obtained by oxidation of $FeCl_2$ (PPE, Argentina) under controlled pH. NaOH (Anedra, Argentina) was used for pH adjustments. Secondly, the prepared lepidocrocite was reacted with anhydrous acetic acid (Anedra, Argentina) to yield ferroxane nanoparticles by the attack of the acid on the hydrogen bonds of the mineral structure. These nanoparticles are precursors to ceramic membranes; they can be either deposited onto support matrices or used as a self-standing material. Finally, the ferroxane particles were sintered at 450°C and converted to iron oxide ceramic (hematite).

V.2.3. Characterization of materials

The ceramic ferroxane were characterized by X-ray diffraction (XRD) using a PW1730-10 Diffractometer (Phillips). The specific surface area was measured by Brunauere-Emmette-Teller (BET) N_2 method and the pore size was calculated by the Barrett, Joyner, and Halenda (BJH) N_2 adsorption/desorption isotherm method at 77 K using a Coulter SA 3100 (Beckman Coulter, USA) analyzer.

The size of the bacteriophage P22 was determined by transmission electron microscopy (TEM) on a Philips EM301, and by dynamic light scattering using a Zetasizer Nano ZS (Malvern); the same equipment was used for laser Doppler velocimetry measurements to characterize the electrophoretic mobility (EPM) of the bacteriophage and iron oxide particles. Measured EPMs were converted to zeta potential using the Smoluchowski equation.

V.2.4. Attachment experiments

V.2.4.1.Attachment kinetics

The kinetic investigation of virus deposition onto hematite was performed in 45 mL sterile centrifuge tubes. A mass of 0.100 g of iron oxide was added to the tubes. Stirred and unstirred control experiments, without iron oxide, were also conducted. An orbital shaker (M-23, Vicking)

was set at a speed of 75 rpm, placing the tubes horizontally. The initial phage concentration in each tube was in the order of 10^7 PFU/mL. Samples were taken at different time intervals for 48 hours.

V.2.4.2.Adsorption isotherms

Attachment experiments were carried out in sterile centrifuge tubes of 45 mL, where a determined mass of iron oxide ceramic was added, ranging from 0.010 g to 0.150 g. Each tube was then filled with NaCl (Anedra) solution and sterilized. After this, the samples were inoculated with 0.100 mL of virus stock suspension of 10^{10} PFU/mL, reaching a concentration of approximately 10^7 PFU/mL. In parallel, two control experiments were carried out without the addition of iron oxide, one stirred and one unstirred, in order to evaluate the natural inactivation of the bacteriophages and quantify the effect of shear in the reduction of the number of PFUs. The tubes were shaken in horizontal position in an orbital shaker (M-23, Vicking) at 75 rpm at room temperature for 7 hours. Samples were taken from each batch at the beginning and at the end of each experiment.

V.2.4.3.Filtration experiments

The operational set-up used for the attachment during filtration experiments is shown schematically in Fig. V.1. It consisted of an alumina-supported iron oxide ceramic tube with a dead end. This type of membrane was fabricated by depositing the iron oxide particles onto the alumina supports and was previously applied to the adsorptive filtration of inorganic contaminants.[99] Briefly, a suspension of the nanoparticles was filtered inside-out through the support tubes with one end closed so that all the water was forced through the ceramic, while the iron oxide particles were retained (Fig. V.1.a). The filter was then dried and sintered at 450°C, before treatment of virus suspensions. Between 250 and 300 mL of viral solution was passed through a supported filter as shown in Fig. V.1.b.

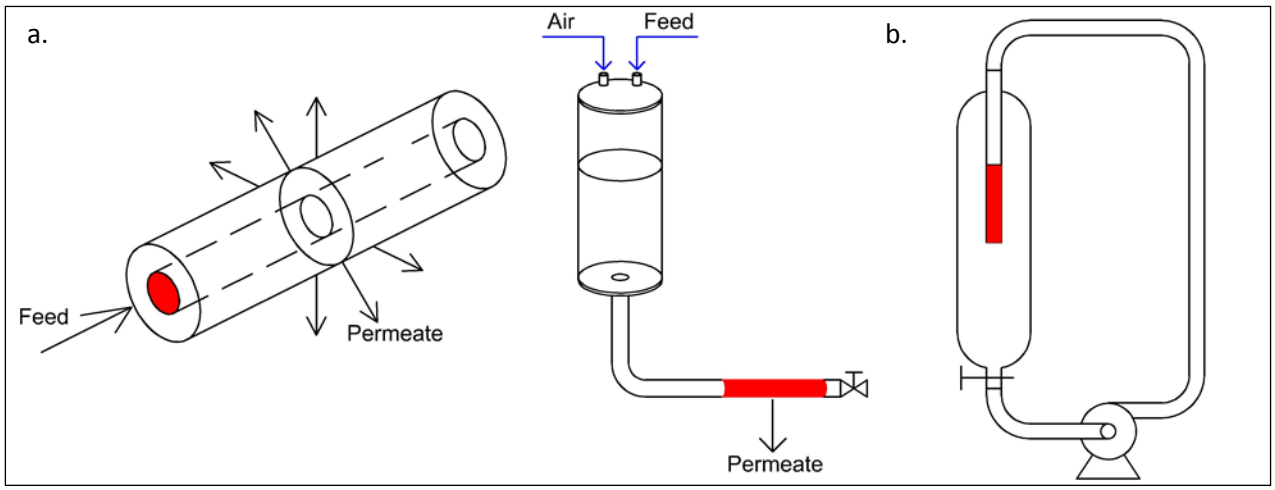

Fig. V.1: Experimental set up for: a. supported filter fabrication. b. dynamic filtration experiments.

The feed solution entered inside the tube, forcing it to flow tangentially through the iron oxide coated walls. The permeate was sampled and tested for viral concentration.

The original apparatus consisted of a 350 mL glass burette with Teflon stopcock and a short silicon hose attached to its bottom end. The supported filter could be attached at the distal end of the silicon hose. The top end of the burette was covered with a 22 µm Whatman filter and wrapped with aluminum foil to keep it in place. The tube filter was alternatively placed into different Erlenmeyer flasks to obtain the subsequent aliquots, and was covered at all times by aluminum foil to minimize exposure to airborne contaminants.

For the recirculation experiments, the same apparatus was used with some modifications. The hose was in this case long enough to pass through the peristaltic pump and then return to the top end of the burette. The supported filter could be attached at the distal end of the silicon hose, or alternatively the distal end could be left without any tube attached, according to the type of experiment performed. The top end of the burette was wrapped in sterile aluminum foil to prevent airborne particles from contaminating the system. The flow was set at a rate of about 0.38 mL/min, accounting for about 4 recirculation cycles per hour during a 48-hour period. Samples were taken at different times during the experiment to assess the temporal evolution of viral concentration in the solution. The potential inactivation effect of the alumina tube itself was investigated in an experiment using an alumina tube with the same dimensions and characteristics of the sintered tube, but with no iron loaded onto it. In order to

rule out viral inactivation due to stresses generated during the recirculation process, another run was performed with no tube in place.

V.2.5. Analytical methods

Two methodologies were applied to the determination of the concentration of P22 phage in the samples: double agar layer method[30] and quantitative polymerase chain reaction (qPCR).

For the double layer method, 3 mL of melted soft agar L was cooled to 45°C and inoculated with 50 µL of concentrated suspension of *Salmonella typhimurium* DA1468 strain. Secondly, 0.1 mL of the phage suspension was added and the entire mixture was poured over the surface of a Petri dish with agar L. When needed, dilutions of the bacteriophage aliquots were made based on estimations and previous results. Once the top agar layer had solidified, the plate was incubated for 24 hours at 37°C. Finally, the plaques were counted, taking as valid those displaying between 30 and 300 plaques per dish.

The qPCR method was performed extracting DNA from 200 µL of P22 suspensions using the Pure Link Viral RNA/DNA Mini Kit (Invitrogen, Carlsbad, CA). The DNA was detected using a GeneAmp 5700 Sequence Detection System (Applied Biosystems). The genomic sequence of the primers and probe used is described in Table V.2.[198] PCR mixtures (20 µL in total) contained 5 µL of DNA sample, 12.5 µL of 2X PCR master mix (TaqMan Universal Master Mix II, no UNG; Applied Biosystems, Indianapolis, IN), 500 nM each of forward and reverse primers, and 150 nM of the TaqMan probe. Amplification was initiated using the hot start method at 95°C for 10 minutes; 40 cycles of 95°C for 15 seconds, and 60°C for 1 minute. The detection limit was calculated to be 10 bacteriophages per sample.

Table V.2: Primer and probe sequences for detection of P22.

Target	Name	Sequence
P22	P22-2F	CTT AAC AAG CTC TGA CTG CTC ATC A
	P22-2R	CCA TCG CCT GTG ACT GGA T
	P22-2P	FAM-TCG CAA CGA TGC AGA ACG ACT CG-TAMRA

V.2.6. DLVO modeling

DLVO theory, developed independently by Derjaguin and Landau (1941) and by Verwey and Overbeek (1948), explains colloid stability as well as attachment between colloids and surfaces, based on the van der Waals attraction and the electrical double layer repulsion.

When there is a particle in aqueous suspension that presents surface charge, as for example due to ionization of surface chemical groups, a layer of counterions will develop to balance the charge in the solution adjacent to the surface and an electrical double layer surrounding the particle will appear. As two particles approach, the double layers overlap, giving origin to interaction forces.

The electrical double layer interaction potential energy between two spheres can be calculated by the following expression:[128]

$$V_{EDL} = \frac{128\pi a_1 a_2 n_\infty kT}{(a_1+a_2)\kappa^2}\gamma_1\gamma_2 e^{-\kappa h} \quad \text{(V.1)}$$

$$\gamma = Tanh\frac{ze\varphi}{4kT} \quad \text{(V.2)}$$

where V_{EDL}: electrical double layer interaction potential energy (J), a: radius of virus (m), n_∞: bulk number of ions (ions m^{-3}), k: Boltzmann constant (J K^{-1}), T: temperature (K), κ: Debye-Hückel reciprocal length (m^{-1}), γ: reduced surface potential, z: valence of symmetrical (z-z) electrolyte, e: electron charge (C), ϕ: electrical surface potential (V), h: separation between surfaces (m). This equation is valid when $h << a$ and $\kappa h > 5$; in a symmetric electrolyte solution.

In aqueous solutions at 25°C, κ can be calculated as:[1]

$$\kappa = 2.32\times10^9\sqrt{\sum C_i z_i^2} \quad \text{(V.3)}$$

where C_i: ion concentration (mol dm^{-3}).

If there is a large difference between the particle sizes, the bigger one is perceived as an infinite plate, and Eq. V.1 reduces to:

$$V_{EDL} = \frac{128\pi a n_{\infty} kT}{\kappa^2}\gamma_1\gamma_2 e^{-\kappa h} \quad \text{(V.4)}$$

The electrical surface potential (φ) is commonly approximated by the zeta potential (potential at the shear plane) due to the impossibility to experimentally determine the first.

Attractive van der Waals interactions are the result of short-term magnetic forces that form between identical or different particles that may have the same, different or no net charge, due to transition dipoles, and depend on the geometry, properties of the particles and the medium in which they interact.

For two identical interacting spheres, the potential can be calculated according to:[199]

$$V_{vdW} = -\frac{A_{131}}{6}\left(\frac{2a_1a_2}{h^2+2a_1h+2a_2h} + \frac{2a_1a_2}{h^2+2a_1h+2a_2h+4a_1a_2} + ln\frac{h^2+2a_1h+2a_2h}{h^2+2a_1h+2a_2h+4a_1a_2}\right) \quad \text{(V.5)}$$

where V_{vdW}: unretarded van der Waals interaction potential energy (J), A_{131}: Hamaker constant for two spheres of material 1 suspended in a medium 3 (J).

For a sphere-plate geometry:[199]

$$V_{vdW} = -\frac{A_{132}}{6}\left(\frac{a}{h} + \frac{a}{h+2a} + ln\frac{h}{h+2a}\right) \quad \text{(V.6)}$$

where A_{132}: combined Hamaker constant for the sphere 1 and the plate 2 in a specific medium 3 (J).

DLVO theory considered the total potential energy of interaction as the sum of both electrical double layer and van der Waals potentials:

$$V_{TOTAL} = V_{EDL} + V_{vdW} \quad \text{(V.7)}$$

Additional non-DLVO interacting forces (e.g., Born repulsion, hydration forces, hydrophobic and/or steric forces, polymer bridging) may also exist but they can be assumed to be negligible in many cases in comparison with electric double layer and van der Waals potential energies.

The bacteriophage P22 was considered to have a perfect spherical geometry; the interaction between two spheres was modeled with Eqs. V.1, V.5, and V.7. The needed parameters were calculated with Eqs. V.2 and V.3.

The ceramic membrane was regarded as an infinite plate compared to the P22 and the interaction between the plate and one sphere was calculated using Eqs. V.4, V.6, and V.7, with the aid of Eqs. V.2 and V.3 to calculate the required parameters.

The Hamaker constants were calculated from data obtained in literature:[1, 200-202] A_{11} = 8.54×10^{-20} J, A_{22} = 1.59×10^{-19} J, A_{33} = 3.70×10^{-20} J, A_{132} = 2.06×10^{-20} J, A_{131} = 9.98×10^{-21} J.

V.3. RESULTS AND DISCUSSION

V.3.1. Materials characterization

The ferroxane particles were sintered at 450°C, in order to convert to the nanoporous ceramic, and characterized. XRD showed that the iron oxide was completely converted to hematite, α-Fe_2O_3. BET specific surface area from nitrogen adsorption isotherms was determined to be 29.3 ± 1.5 m^2/g. Pore size distribution calculated from the adsorption branch of isotherm yielded a mean pore size of 62 nm and a standard deviation of the distribution of 40 nm.

P22 and ferroxane-derived iron oxide surface charge was measured as a function of pH (Fig. V.2). The isoelectric point, represented by the pH at which the phages have no net surface charge, was estimated from the data points where the electrophoretic mobility changes from positive to negative. With an IEP of 3.4, the virus is expected to be negatively charged under the conditions of environmentally relevant pHs, reaching a value of -27.9 mV at pH 7, and remaining relatively stable for alkaline solutions. The ferroxane derived ceramic showed a point of zero charge (PZC) of 6, in agreement with previously published values for hematite.[203] Consequently, the bacteriophage will be subjected to attractive interaction forces at pHs below 6, while attachment is expected to be hampered by electrostatic repulsion at higher pHs.

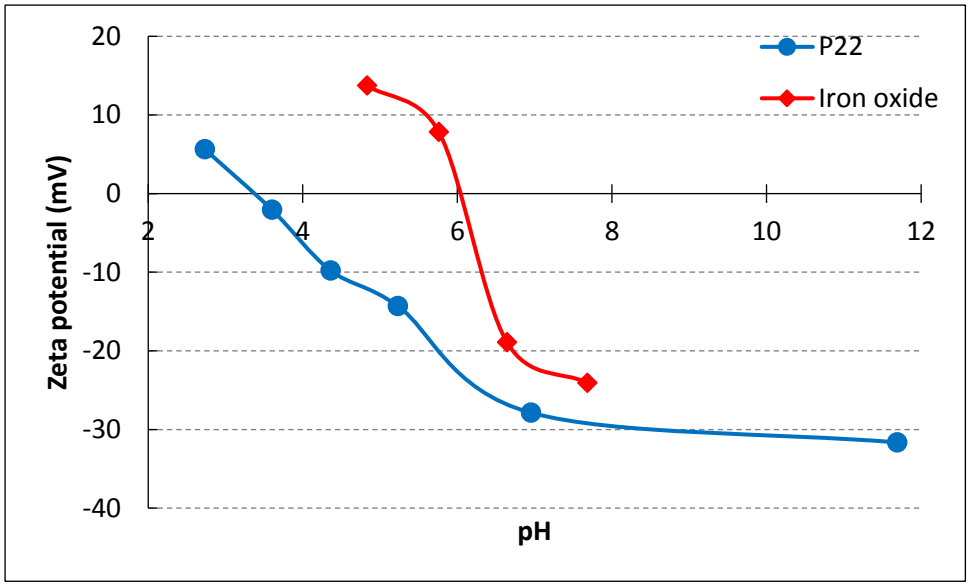

Fig. V.2: Zeta potential as a function of pH for P22 bacteriophage and nanostructured iron oxide (ionic strength 15 mM NaCl, 20°C).

Virus size was measured by DLS and TEM. DLS analysis gave a hydrodynamic diameter of 71 ± 0.8 nm, while analysis of TEM images suggested a size of 58 ± 9 nm.

V.3.2. Virus attachment

Viral concentration was determined by two methodologies: PFU and qPCR. The former was applied to all samples, due to availability of the technique in our laboratory and relevancy.

PFU determinations only accounts for active or infective organisms, since it relies on the quantification of the damage caused by the phage suspension to the host bacteria. However, the technique suffers from the drawback of possible underestimating the real viral concentration, if the microorganisms happen to be aggregated in the sample, and therefore, the assumption that each plaque correspond to a single viral particle would not hold.[30]

The qPCR measurements are sensitive to all P22 genetic material, and report on both infective and inactivated viruses, which may lead to an overestimation of the infective capability of the suspension but it is not affected by the physico-chemical properties of the media or the aggregation state of the viral particles.[204]

In order to analyze the quality of the PFU determinations conducted in this work, a P22 suspension was analyzed under changing conditions of pH and ionic strength, given in all cases by the NaCl, and the results from both methods compared.

Fig. V.3 shows measurements of P22 concentration by qPCR and PFU for pH values between 4 and 7. For the full range of pHs investigated, P22 have a net negative surface charge as evidenced by the zeta potential measurement (Fig. V.2). This surface potential would result effective in preventing aggregation at all investigated pHs but pH 4, where the zeta potential absolute value is only slightly over 5 mV. Virus quantification by PFU technique gave steady results over a range of pHs of 5 to 7, and less than an order of magnitude lower for pH 4. This difference may be due in part to some aggregation of the viral particles when repulsion forces are weaker. The comparison with qPCR results showed excellent agreement for pH 7. At neutral conditions, pH related inactivation is expected to be negligible; also, the highest absolute value of zeta potential is observed at pH 7, and therefore, aggregation should be minimal, if any. Based on these considerations and the experimental error associated with the data, we concluded that the measurements for both techniques were equivalent. At lower pHs, a reduction in the concentration determined by PFU compared to the qPCR obtained values is observed, especially for pH 4, probably as a combination of two effects: partial aggregation as surface potential become less negative, and the acidic conditions affecting the organism viability.[205, 206]

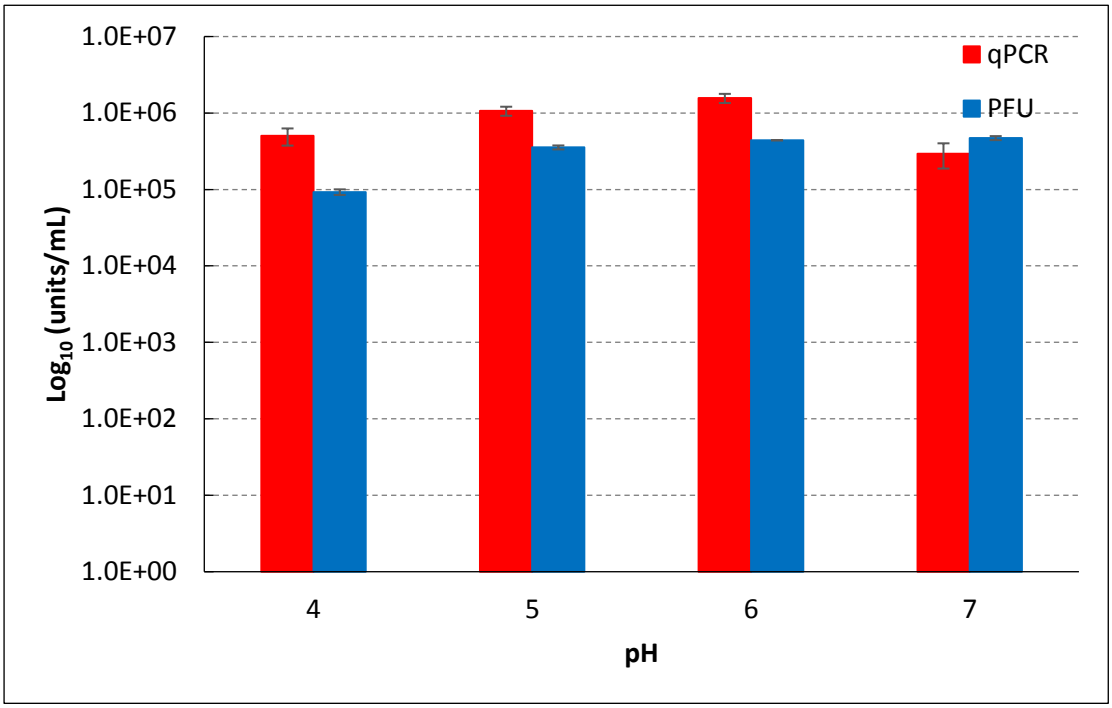

Fig. V.3: Determination of viral concentration under different pHs; results by qPCR and by PFU.

The effect of ionic strength on the quantification method was also investigated, and plotted in Fig. V.4. Results showed good agreement between analytical methods, and no appreciable difference can be observed between 0.1 mM and 1 M NaCl suspensions. Increasing ionic strength is expected to induce aggregation as electric double layer compression results in shorter-range repulsive forces and overall dominance of van der Waals attractive interaction, but no significant virus aggregation can be inferred form the experimental results. Furthermore, qPCR determinations were in all cases uniformly higher than PFUs, hinting to the presence of some inactive viruses in all of the measured samples.

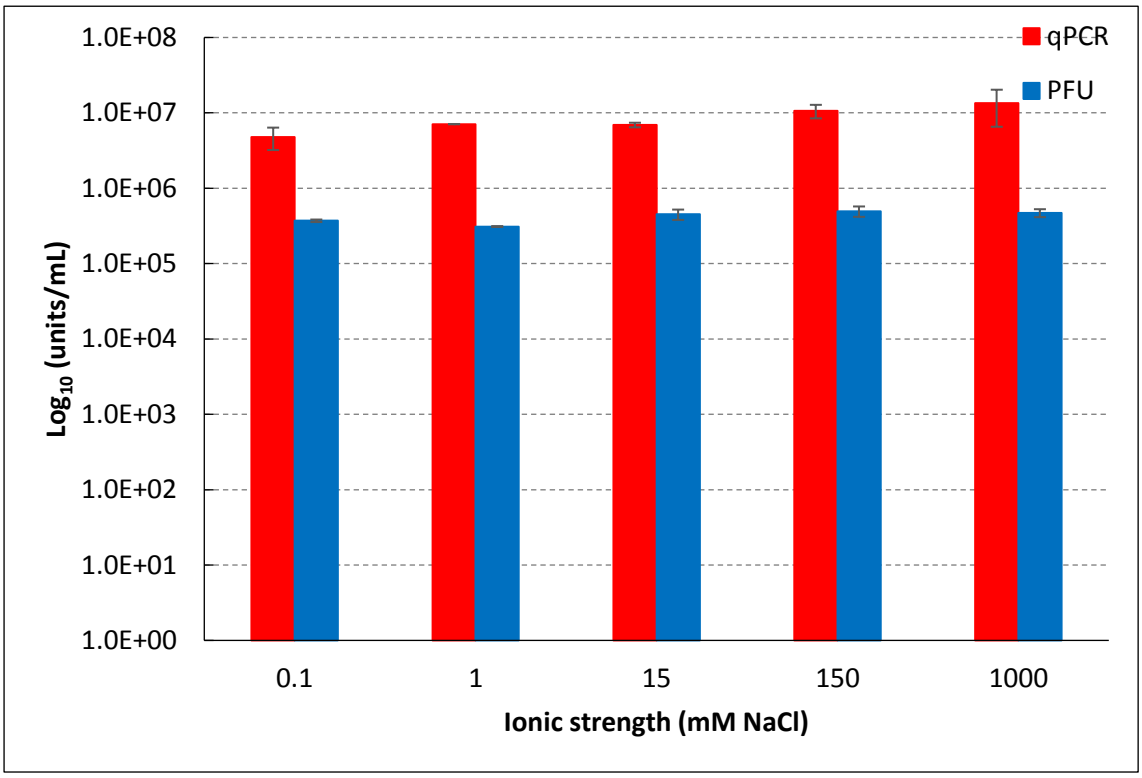

Fig. V.4: Determination of viral concentration under different ionic strength levels; results by qPCR and by PFU.

Overall, it can be concluded that both techniques can be applied to accurate quantification of viral concentration in the present study with minor underestimations by PFU method at lower pH levels.

V.3.2.1.Attachment kinetics

Attachment kinetics experiments were conducted in order to investigate the time and evolution of the attachment process as well as to determine the appropriate equilibration time to be used in the isotherm determination.

Samples were analyzed by PFU and qPCR techniques. Given that some degree of inactivation may occur when viruses are subjected to stirring or room temperature, two control experiments were added to determine the relative contribution to the loss of viral activity due to these factors.

Fig. V.5 presents the results from the kinetics experiments. Samples containing viruses and iron oxide were obtained (E); SC data points correspond to the stirred viral suspension without the addition of adsorbent and UC relates to the same sample composition without stirring. In the first seven hours an average log removal of 1.4 was observed for the samples containing the adsorbent, while no detectable reduction in viral concentration was observed for the control experiments. The decrease in log reduction values (LRV) of viral concentration continued, but inactivation in the control samples started at 24 hours, and therefore, the LRV could not be attributed entirely to attachment to the iron oxide particles.

Fig. V.6 depicts the net amount of viruses expected to be adsorbed on the iron oxide, calculated from the measured viral concentration and subtracting the effect of room temperature and shear due to stirring on inactivation as determined by the control experiments.

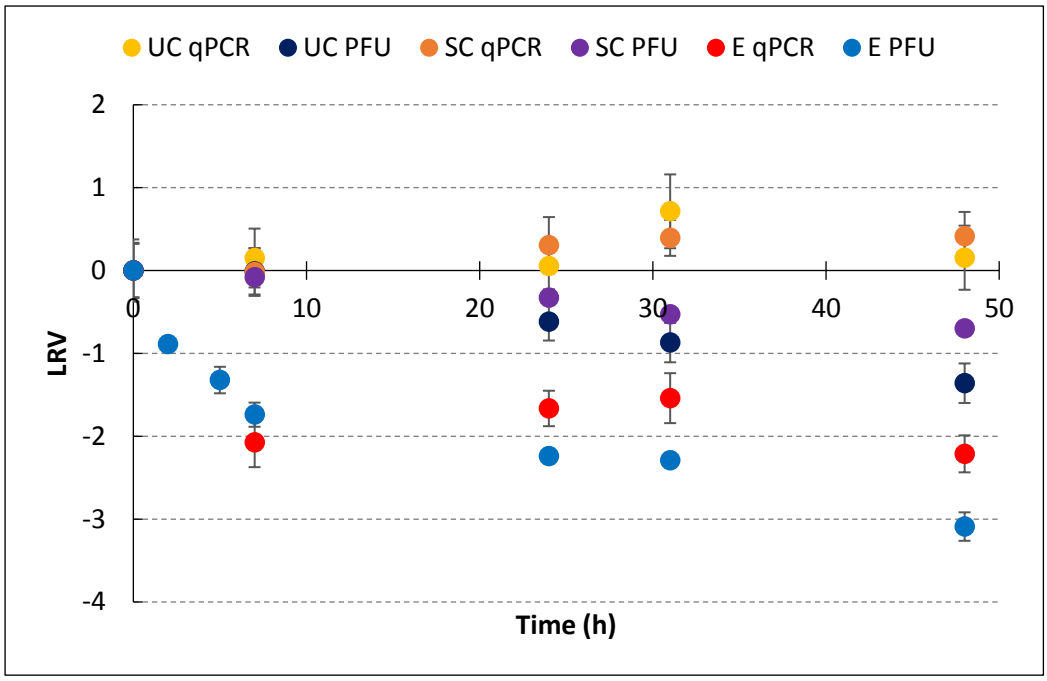

Fig. V.5: Logarithmic reduction value (LRV) of bacteriophage P22 concentration (C_0=10^7 PFU/mL) as a function of time in the presence of iron oxide (2 mg/ml), analyzed by qPCR and PFU methods; E: virus and adsorbent; SC: stirred control samples without adsorbent, UC: unstirred control samples without adsorbent.

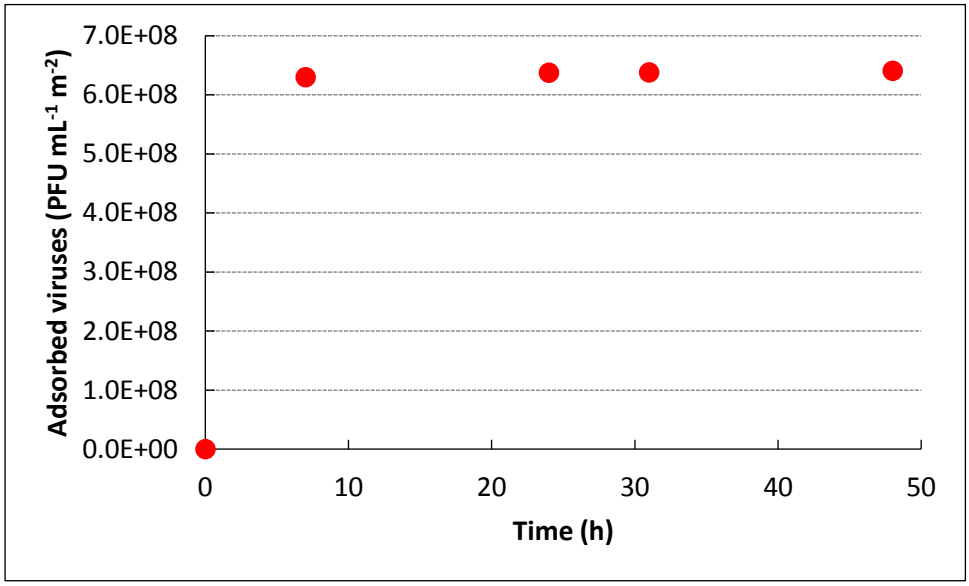

Fig. V.6: Adsorption kinetics of bacteriophage P22 concentration (C_0=10^7 PFU/mL) on iron oxide particles (2 µg/mL); inactivation due to environmental conditions was subtracted to obtain net adsorption values.

A rapid decrease in viral concentration is observed in the first seven hours, followed by a marginal increase in removal up to the 48-hour time frame of the experiment. This may hint to a two phase process, when a rapid removal is observed corresponding to the readily available easier to reach surface sites for the iron oxide, and a second, much slower stage in which the adsorbate diffuses into the internal structure of the iron oxide particles finding new sites. A similar behavior has been observed for ionic species adsorbing to nanoporous materials[207, 208] and in particular, for arsenite adsorption onto this same iron oxide particles.[99] In fact, BJH pore volume distribution from nitrogen adsorption isotherms showed that about one third of the total pore volume of the iron oxide particles is given by pores larger than 65 nm, and 27% of those are within the 54 - 120 nm range. Thus, this internal surface area is available at least in part to the bacteriophage that given its size of approximately 70 nm, as measured in this work and in consistency with the literature,[195-197] is able to diffuse into the nanostructure and adsorb into the pore walls. However, the process is expected to be much slower than for the ionic species due to the limited diffusion and possible pore clogging by previous adsorbed particles, and therefore, a very slow reduction in concentration is observed, rendering this stage not suitable for engineering applications. We have therefore assumed that a pseudo-equilibrium state is reached after 7-hour contact time and adopted this time for all subsequent experiments.

The results are similar or better than previously reported adsorbent materials for virus removal. For example, with an initial viral concentration of 10^7 PFU, Gutiérrez et al. reported adsorption of MS2 on hematite nanoparticles to be less than 2 log removal units after 3-hour contact time from simulated groundwater and similar adsorbent dose to the one used in this work;[189] in another work, iron oxide magnetic nanoparticles achieved 0.36 log removal units in 60 minutes at 2 g/L concentration.[209]

V.3.2.2.Adsorption isotherm

Attachment experiments were carried out adding a determined mass of iron oxide ceramic ranging from 0.010 g to 0.150 g to a sterile NaCl solution following by inoculation with 0.100 mL of virus stock suspension of 10^{10} PFU/mL to reach a concentration of approximately 10^7 PFU/mL. Experiments without iron oxide addition and unstirred were also implemented as controls to quantify inactivation by mechanical shear and exposition at room temperature. Samples were taken at the beginning and after 7 hours of contact time.

The obtained attachment isotherm at 25°C is shown in Fig. V.7, at two different levels of ionic strength, 15 mM and 100 mM NaCl.

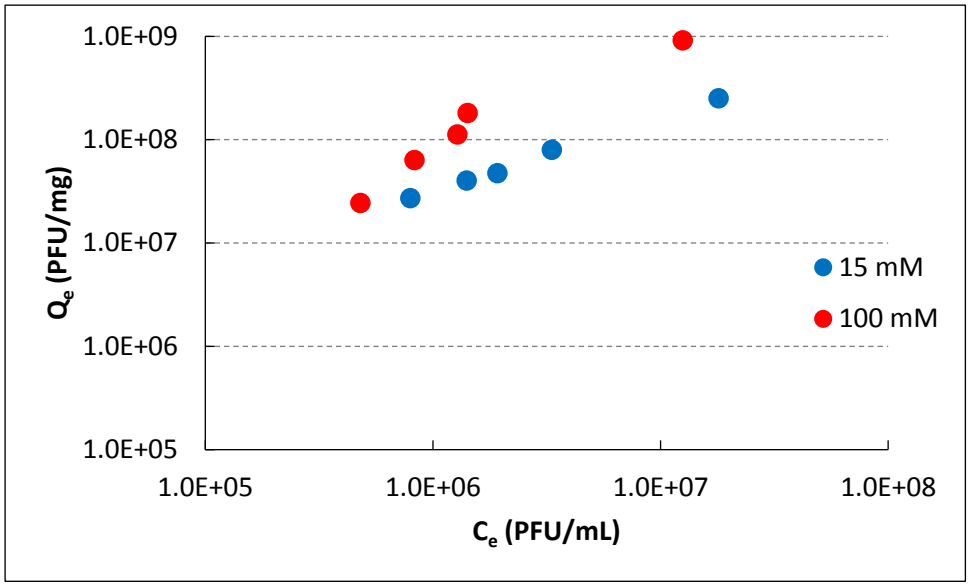

Fig. V.7: Adsorption isotherm for P22 bacteriophage on nanostructured iron oxide (electrolyte concentration 15 mM and 100 mM NaCl, 25°C).

Viruses may be present in different waters: surface water, groundwater, seawater, wastewaters, and they all present different levels of ionic strength. Moreover, being the attachment of virus to iron oxide electrostatic in nature, ionic strength is expected to play a fundamental role, making its investigation highly relevant. The data points showed the net loss of virus activity due to attachment onto iron oxide, as the inactivation levels observed in the controls have been subtracted to the reported values. The results showed increases of the adsorbed concentration with increasing liquid equilibrium concentration for the range of conditions tested. A plateau was not reached, although the slope showed a slight decrease for the highest concentration point. The isotherms were fit to the linearized form of three model isotherms: Langmuir, Freundlich, and Temkin and the corresponding coefficients of determination (R^2) calculated (Table V.3).

Table V.3: Model fits for virus adsorption isotherms.

	Ionic Strength (mM NaCl)	Langmuir	Temkin	Freundlich		
		R^2	R^2	R^2	K_f	n
P22	15	0.9776	0.9373	0.9974	144	0.724
	100	0.9355	0.9549	0.9415	39.0	1.02

The three proposed equations depict relatively well the experimental data, the Freundlich isotherm showing the highest goodness of fit. Additionally, the absence of a plateau in the curves that could be related to the surface sites saturation suggests the inappropriateness of both Langmuir and Temkin equations, even though the data fit relatively well the first linear portion of the corresponding isotherms. The Freundlich equation is often used to describe cation adsorption data on iron oxides;[203] however this equation is purely empirical and provides no information on the adsorption mechanism. The data analysis is useful for comparison purposes: the ferroxane-derived ceramics showed higher adsorption when ionic strength, given by NaCl, is increased from 15 mM to 100 mM; the increased affinity in the 100 mM case is also reflected in a higher *n* value.

This dependence hints to an electrostatic interaction mechanism for virus attachment, regulated by van der Waals and electrostatic repulsion forces, which can be altered by the concentration of salts in the water matrix.

V.3.2.3. Filtration experiments

A virus suspension with similar concentration as tested for the batch experiments, was filtered through ferroxane-coated alumina filters.

This breakthrough experiment as originally conceived did not yield a measurable reduction in the viral load of the solution. This may be due to a low attachment efficiency of the P22 under the conditions tested, that cause a significant number of particles to pass through the ceramic filter without being retained; another reason for the poor performance may be related to the relatively open pore structure of the ceramic support, that offers short cuts for the particles to flow through the filter and drastically diminished the occurrence of collisions with potential attachment sites. Consequently, a rearrangement of the supported filter setup was carried out. A peristaltic pump was added to the circuit in order to recirculate the filtrate back

to the feed burette. The speed was set in such a way that approximately 4 recirculation cycles were performed every hour, increasing the residence time.

Results showed that viral attachment/inactivation is strongly dependent on the time elapsed since the beginning of the experiment (Fig. V.8).

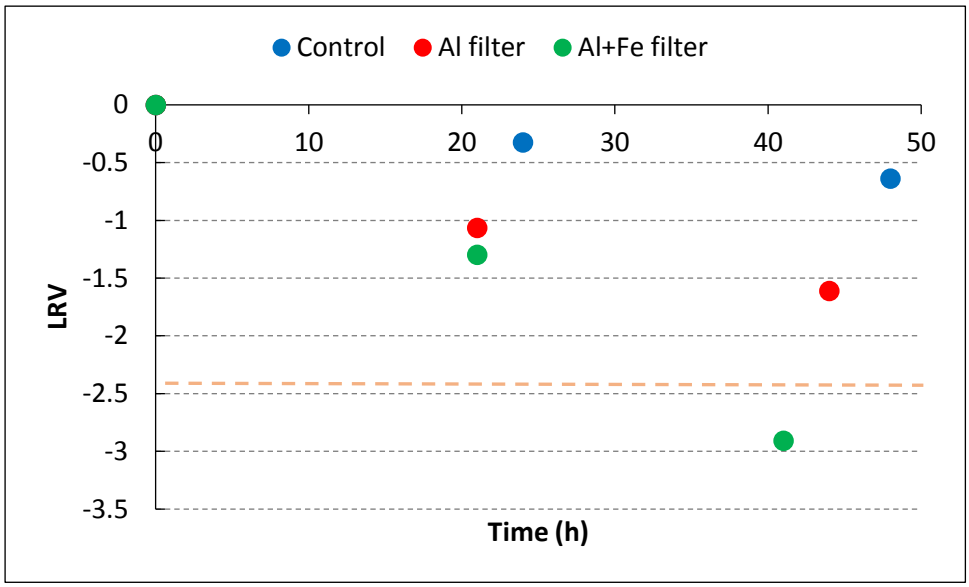

Fig. V.8: LRV of P22 by recirculation of a feed solution through a ferroxane-coated alumina filter.

In the case of the ferroxane-loaded tube, the concentration of viable viral particles dropped close to the detection limit at the end of the 48-hour test period. The alumina tube seems to be effective as well in reducing the viable viral load of the solution, although less than in the case of the iron-oxide loaded tube. In comparison, the experiments performed without filter showed a much lesser degree of inactivation, within a range of values that can wholly or partly be due to the expected measurement error, indicating that shear due to pumping is not a significant contributor to virus inactivation.

V.3.3. DLVO theory analysis of virus attachment

Since electrostatic interactions are expected to dominate the virus attachment to metal oxide surfaces, DLVO theory was applied to the analysis of the attachment data as well as the virus stability and aggregation conditions.

Bacteriophage P22 particles were modeled as spheres with a diameter of 71 nm, while the adsorbent was modeled as a plate due to its larger dimension in comparison with the P22.

Fig. V.9 shows the interaction potential energy for two bacteriophage P22 particles in a pH range of 3 to 7, and a background ionic strength of 15 mM NaCl.

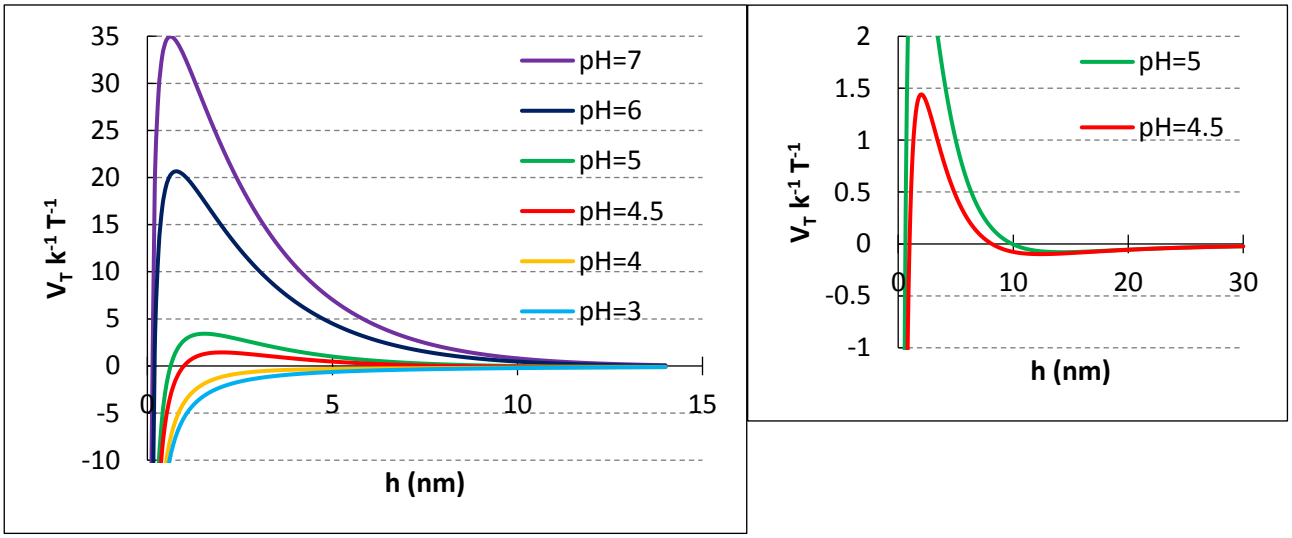

Fig. V.9: DLVO predicted interaction potentials for two P22 bacteriophages. Detail on the right shows secondary minimum present at pH 4.5 and 5.

At low values of pH (i.e. 3 and 4), van der Waals attraction energy completely overweighs electrical double layer repulsion energy; and thus, a net attraction potential leading to aggregation between the particles is expected. At pHs close to neutral, an energy barrier develops such that aggregation may be effectively prevented. At intermediate pHs, illustrated here by the pH 4.5 and 5 calculations, a low barrier in the total energy is present. A fraction of the particles may overcome this barrier due to energy associated with Brownian motion and aggregate in the primary minimum in a similar fashion as in the low pH conditions; additionally, particles may aggregate in a secondary minimum that develops at these intermediate pH values but these weaker structures are highly likely to release individual particles.[1] The comparison of concentration measurements by PFU and qPCR techniques (Fig. V.3) showed equivalent determinations at pH 7, and relatively lower values given by PFU for pH 4; 5; and 6, the former showing the larger difference. In light of the DLVO calculations, we can explain the difference at the two middle points by limited aggregation due to a moderate to low energy barrier; however, the predicted instability at pH 4 does not agree with the measured results, that did not reveal a significant difference between both techniques and therefore, not extensive aggregation can be

concluded. The results suggested an underestimation of the repulsive forces by the DLVO theory as applied in this study.

The interaction potentials between the iron oxide ceramic and the P22 particles were analyzed based on DLVO calculations for pHs between 4 and 7 (Fig. V.10). The results showed a strong dependence of attachment on pH. For pH values 4 through 6, a deep primary minimum in the interaction energy is predicted, and strong attachment is expected. As pH gets closer to the point of zero charge of the adsorbent, repulsive forces arise. A moderate energy barrier is predicted at pH 6.5, while unfavorable conditions for deposition develop at pH 7. If virus repulsive forces are underestimated as suggested by the discussion above, the applicability of the method could be further limited to pHs below 6.5.

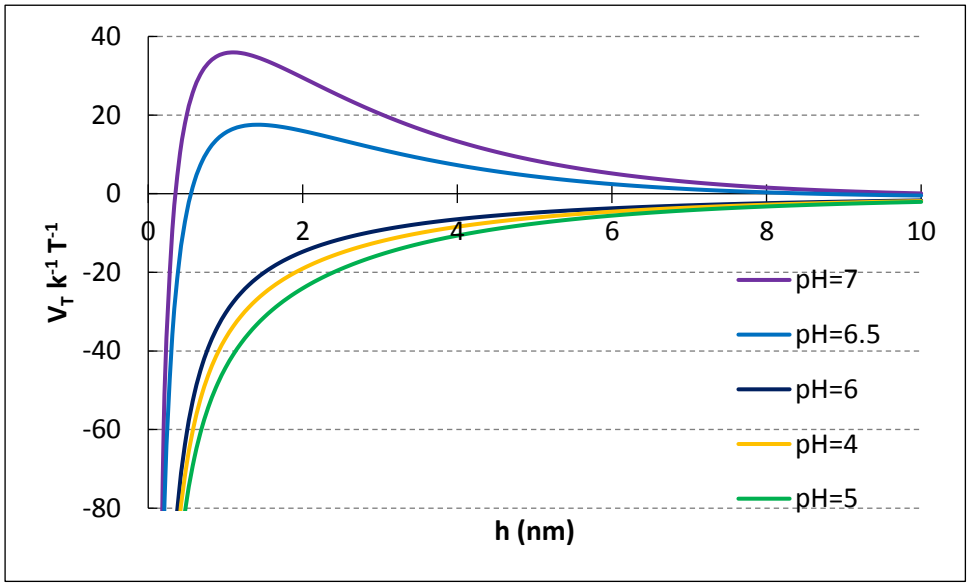

Fig. V.10: DLVO predicted interaction potentials for P22 bacteriophages and the iron oxide membrane.

Divergence between DLVO predicted stability and experimental observations are commonly attributed to non-DLVO interactions, e.g., Born repulsion, hydration forces, hydrophobic and/or steric forces, polymer bridging. Of these, only hydration forces may be postulated. Although their effect is anticipated to be comparable to double layer repulsion at higher ionic strengths than those considered in this study,[210] they explained MS2 and ϕX174 attachment to clay particles.[31] Another limitation to the application of the DLVO theory arises from the fact that virus particles can be defined as soft particles, e.g., particles covered with ion-

penetrable surface layer of polyelectrolytes, as opposed to hard particles where the surface is clearly defined and no electrolyte ions can penetrate it.[133]

V.4. CONCLUSIONS

Iron oxide ceramic membranes were successfully applied for the removal of viruses from water. Iron oxide coated alumina filters showed improved removal capacity compared to the stand-alone material tested in batch mode, as inner pore sites, that otherwise would be considered inaccessible due to long diffusion times, become operational. Additional improvement can be achieved by the design of a support material with more uniform porosity, avoiding the possibility of wide channels inside the pore structure that result in inefficiency in the attachment process.

The recirculation required in the filtration experiments constitutes a barrier for cost-effective application of the technology in a water treatment plant scenario. Therefore, an increase in the efficiency of the removal at each cycle is needed. This can be achieved by an improved the support porosity, that enhances the contact between the solution and the iron oxide-coated walls.

The mechanism of removal was observed to be electrostatic in nature. DLVO analysis of the attachment predicted it to be effective up to a pH of 6.5. The filters are especially applicable as a mobile drinking water treatment device, due to their low cost, ease of use and extra capabilities of the membrane, such as the removal of organic contaminants or heavy metals.

Chapter VI

STUDY OF INTERACTIONS IN ULTRAFILTRATION FOR VIRUS REMOVAL

Nomenclature

a: radius of virus particle (m)

A_{131}: Hamaker constant of virus particle in water (J)

A_{132}: combined Hamaker constant of virus particle and PES membrane in water (J)

C_e: salt concentration (mol m^{-3})

C_h: hydration constant (J)

C_j: ion concentration (mol dm^{-3})

e: electron charge (C)

h: separation between surfaces (m)

k: Boltzmann constant (J K^{-1})

K: hydrophobic constant (J)

n_∞: bulk number of ions (ions m^{-3})

N_A: Avogadro number

T: temperature (K)

V_{AB}: Lewis acid-base interaction potential energy (J)

V_B: Born interaction potential energy (J)

V_{EDL}: electrical double layer interaction potential energy (J)

V_H: hydration interaction potential energy (J)

V_{DLVO}: DLVO interaction potential energy (J)

V_{TOTAL}: total interaction potential energy (J)

V_{vdW}: unretarded van der Waals interaction potential energy (J)

z: valence of symmetrical (z-z) electrolyte

z_j: valence of ion j including sign of charge

Φ: reduced potential

ζ: zeta potential (V)

θ: contact angle of surface (°)

κ: Debye-Hückel reciprocal length (m^{-1})

λ_{AB}: decay (Debye) length of water (m)

σ_B: collision parameter (m)

φ: electrical potential (V)

$\Phi_{AB\ (h=h0)}$: Lewis acid-base free interaction potential energy between surfaces at contact (J m^{-2})

VI.1. INTRODUCTION

Access to safe water is a primary objective for public health policies worldwide. The reduction and inactivation of viral pathogens in natural waters is therefore a major goal to achieve, due to the intimate relationship between this kind of organisms and disease outbreaks.[173] Available treatments based on bacteriological criteria are not always effective, since viruses are more resistant and difficult to remove.[104, 211]

Ultrafiltration membranes, with pore size between 1 and 100 nm,[34] are increasingly used in potabilization to remove viral particles and are considered a good barrier in the nanometer scale.[73] The removal of virus particles is controlled by different mechanisms, such as electrostatic repulsion, attachment, and size exclusion.[34, 71-73, 174] The outer surface of viruses and its charge play a key role in interactions with other surfaces. Therefore, conditions under which viruses are prepared, purified and conserved at laboratory scale should be taken into consideration prior to assess this kind of interactions in ultrafiltration processes.[29]

Bacteriophages are viruses that infect bacteria. Some of them have similar structure, composition, and size to human enteric viruses; thus, they are valuable as models or surrogates.[100] Bacteriophages PP7,[115] P22,[110, 139] MS2,[31, 183, 212] and φX174[31] have been used in filtration, transport, adhesion, and adsorption experiments. In particular, PP7 was chosen for this work because it can be a surrogate for poliovirus in water treatment processes, since both

are icosahedral and have similar diameter (25 - 30 nm).[115] Besides, PP7 is non-infective to humans, easy to enumerate and offers challenging conditions for membrane testing in virus filtration due to its small size.

Virus-membrane interactions in an ultrafiltration process can be modeled in the light of DLVO theory,[31] which is often applied to predict colloidal stability.[154, 155] Although the widespread use of this theory, it makes assumptions (particles are dense, solid spheres with homogenous surface) that sometimes lead to failure in explaining the interactions. Extended-DLVO theory is subject of research to overcome these limitations, considering additional interacting forces (Born repulsion, hydration forces, and Lewis acid-base forces among others).[31]

In this work, we characterized bacteriophage PP7 and polyethersulfone membrane with respect to size and surface charge, under a broad range of relevant conditions of pH and ionic strength, and assessed the removal of bacteriophage at laboratory scale by ultrafiltration. The mechanism and limitations were analyzed and discussed under DLVO and X-DLVO theories.

VI.2. MATERIALS AND METHODS

Bacteriophage PP7 (ATCC 15692-B2) belongs to *Leviviridae* family, *Levivirus* genus and infects *Pseudomonas aeruginosa*. It is naked, has icosahedral capsid and consists of single-stranded RNA. This coat protein has a molecular weight of 13,874 and contains 42% of hydrophobic residues.[37]

Reagent grade $NaNO_3$ (J. T. Baker, Mexico), NaCl, $MgCl_2 \cdot 6H_2O$, $NaHCO_3$, $CaCl_2 \cdot 2H_2O$ (Anedra, Argentina) were employed. Solutions were prepared with Type I water (18 MΩ.cm). The nutrient broth (Britania, Argentina) was prepared mixing 8 g in 1 L of deionized water. The soft nutrient agar for bacteriophage titration was prepared mixing 8 g of nutrient broth and 7.5 g of agar-agar technical for microbiology (Merck, Germany) in 1 L of deionized water. The nutrient agar for Petri dishes was prepared mixing 8 g of nutrient broth, 8 g of NaCl and 15 g of agar-agar technical for microbiology in 1 L of deionized water. Materials and reagents were sterilized by autoclaving at 121°C for 20 minutes. A modified polyethersulfone (PES) flat sheet ultrafiltration membrane was used (Pall Corp., USA), with MWCO 50 kDa as reported by the manufacturer, and average pore size of 0.067 μm determined by porosimetry.

VI.2.1. Size and zeta potential measurements

First, the host bacteria *Pseudomonas aeruginosa* were incubated in nutrient broth for 24 hours at 37°C on an orbital shaker at 120 rpm. PP7 was then inoculated and incubated under the same conditions. Afterwards, the virus suspension was centrifuged at 1,000 xg for 15 minutes and the supernatant filtered through a 0.22 μm PVDF membrane (Millipore GVW P02500). This suspension was dialyzed through a 100 kDa MWCO membrane (SpectraPor Biotech CE, Spectrum Laboratories, USA) twice: first, against water, and second, against the appropriate solution (fifteen in total: NaCl, $NaNO_3$, $NaHCO_3$, $CaCl_2$, $MgCl_2$ of 1 mM, 10 mM, 100 mM ionic strength) for 20 hours each. The final suspension was again filtered and kept at 4°C overnight before measuring the zeta potential and hydrodynamic diameter.

The concentration of each bacteriophage suspension was determined after the last filtration, with the double agar method. A plate containing only melted soft agar served as negative control for bacteria. A plate only seeded with bacteria served as negative control for bacteriophage. The plates were incubated at 37°C for 24 hours. The concentrations were between $6x10^7$ and $7x10^8$ PFU/ml.

The hydrodynamic diameter and the zeta potential of the bacteriophage were measured by DLS and laser Doppler micro electrophoresis respectively, using a Zetasizer Nano ZS (Malvern, UK) at 25°C as described elsewhere.[139]

The membrane surface zeta potential was obtained using a zeta potential accessory and a suspension of tracer particles in order to measure electro-osmosis near to the surface, from which membrane zeta potential can be derived.[121]

VI.2.2. Filtration experiments

The host bacteria in nutrient broth was inoculated with PP7 and incubated for 18 hours at 37°C. Afterwards, the viral suspension was centrifuged at 1,000 xg for 15 minutes and the supernatant filtered through a 0.22 μm filter.

The experimental set up consisted of a membrane filtration unit, connected to a feed tank through a peristaltic pump, a permeate tank on a scales, and control instruments (two pressure gauges and a flowmeter); all components were sterilized prior to use and pH was measured but not modified. Synthetic aqueous matrixes were prepared mixing: $CaCl_2.2H_2O$ (5.8

g/L), $MgCl_2.6H_2O$ (5.9 g/L), $Ca(NO_3)_2.4H_2O$ (3 g/L), $Mg(NO_3)_2.6H_2O$ (3 g/L), $NaHCO_3$ (8.94 g/L) in deionized water.

The concentrations of the bacteriophage suspensions were determined by qPCR (quantitative polymerase chain reaction) by taking samples of the inlet, permeate and retentate. The bacteriophage concentration in the feed was kept between $1.7x10^5$ and $1.1x10^6$ PFU/ml.

VI.2.3. DLVO

DLVO theory explains colloid stability and attachment between colloids themselves and between colloids and surfaces, based on two predominant forces, electrical double layer repulsion and van der Waals attraction.[154, 155]

The electrical double layer interaction potential energy between two spherical particles can be calculated as:[1]

$$V_{EDL} = \frac{2\pi a_1 a_2 n_\infty kT}{(a_1+a_2)\kappa^2}(\Phi_1^2 + \Phi_2^2)\left[\frac{2\Phi_1^2\Phi_2^2}{\Phi_1^2+\Phi_2^2} ln\frac{1+e^{-\kappa h}}{1-e^{-\kappa h}} + ln\left(1-e^{-2\kappa h}\right)\right] \quad \text{(VI.1)}$$

$$\Phi = \frac{ze\varphi}{kT} \quad \text{(VI.2)}$$

$$\kappa = 2.32x10^9\sqrt{\sum C_j z_j^2} \text{ in aqueous solutions at 25°C} \quad \text{(VI.3)}$$

where V_{EDL}: electrical double layer interaction potential energy (J), a: primary aggregate radius of sphere (m), n_∞: bulk number of ions (ions m^{-3}), k: Boltzmann constant (J K^{-1}), T: temperature (K), κ: Debye-Hückel reciprocal length (m^{-1}), Φ: reduced potential, z: valence of symmetrical (z-z) electrolyte, h: separation between surfaces (m), e: electron charge (C), ϕ: electrical potential (V), C_j: ion concentration (mol dm^{-3}), z_j: valence of ion j including sign of charge.

If there is a large difference between the particle sizes, the bigger one is perceived as an infinite plate, and Eq. VI.1 will reduce to:

$$V_{EDL} = \frac{2\pi a n_\infty kT}{\kappa^2}(\Phi_1^2 + \Phi_2^2)\left[\frac{2\Phi_1^2\Phi_2^2}{\Phi_1^2+\Phi_2^2} ln\frac{1+e^{-\kappa h}}{1-e^{-\kappa h}} + ln\left(1-e^{-2\kappa h}\right)\right] \quad \text{(VI.4)}$$

The electrical surface potential (φ) is commonly approximated by the zeta potential (ζ) (potential at the shear plane) due to the impossibility to experimentally determine the first.

The attractive van der Waals interaction potential energy between two identical spherical particles can be calculated as:[1]

$$V_{vdW} = -\frac{A_{131}}{6}\left(\frac{2a^2}{h^2+4ah} + \frac{2a^2}{h^2+4ah+4a^2} + ln\frac{h^2+4ah}{h^2+4ah+4a^2}\right) \quad \text{(VI.5)}$$

where V_{vdW}: unretarded van der Waals interaction potential energy (J), A_{131}: Hamaker constant for two spheres of material 1 suspended in a medium 3 (J). And for a sphere and an infinite plate:[1]

$$V_{vdW} = -\frac{A_{132}}{6}\left(\frac{a}{h} + \frac{a}{h+2a} + ln\frac{h}{h+2a}\right) \quad \text{(VI.6)}$$

where A_{132}: combined Hamaker constant for the sphere 1 and the plate 2 in a medium 3 (J).

The DLVO interaction potential energy is the sum of electrical double layer and van der Waals interactions:

$$V_{DLVO} = V_{EDL} + V_{vdW} \quad \text{(VI.7)}$$

Additional interacting forces (Born repulsion, hydration forces and Lewis acid-base forces among others) may also exist, giving raise to extended-DLVO theory.

Born short-range repulsion is originated from the repulsion between electrons of different atoms when their shells interpenetrate each other. For a sphere interacting with a plate, Born repulsion energy can be obtained as:[137]

$$V_B = \frac{A_{132}\sigma_B^6}{7560}\left[\frac{8a+h}{(2a+h)^7} + \frac{6a-h}{h^7}\right] \quad \text{(VI.8)}$$

where V_B: Born interaction potential energy (J), σ_B: collision parameter (m).

Lewis acid-base interactions arise from migration of electrons between the surfaces, adsorbed species, and the solvent; and can be calculated as follows for two spheres:[31]

$$V_{AB} = 2\pi\frac{a_1 a_2}{a_1+a_2}\lambda_{AB}\Phi_{AB\ (h=h0)}e^{\frac{h0-h}{\lambda_{AB}}} \quad \text{(VI.9)}$$

$$\Phi_{AB\ (h=h0)} = -\frac{K_{132}}{2\pi h_0 \lambda_{AB}} \quad \text{(VI.10)}$$

$$\log K = -3.5(Cos\theta_1 + Cos\theta_2) - 18 \quad \text{(VI.11)}$$

where V_{AB}: Lewis acid-base interaction potential energy (J), λ_{AB}: decay (Debye) length of water (m), $\Phi_{AB\ (h=h0)}$: Lewis acid-base free interaction potential energy between surfaces at contact (J m^{-2}), K: hydrophobic constant (J) θ_i: contact angle of surface i (°). And for a sphere and a plate:[31]

$$V_{AB} = 2\pi a\lambda_{AB}\Phi_{AB\ (h=h0)}e^{\frac{h0-h}{\lambda_{AB}}} \quad \text{(VI.12)}$$

Particles and surfaces that have superficial charges may be hydrated in a solution, and this water will hinder the approximation of the mentioned surfaces. Then, the extra hydration repulsion origins when particles need to eliminate the water to be in contact between them, and diminishes exponentially with distance:[132]

$$V_H = \pi a N_A C_h C_e \lambda_{AB}^2 e^{-\frac{h}{\lambda_{AB}}} \quad \text{(VI.13)}$$

where V_H: hydration interaction potential energy (J), N_A: Avogadro number, C_h: hydration constant (J), C_e: salt concentration (mol m^{-3}).

Therefore, the total interaction potential energy is obtained as the sum of:

$$V_{TOTAL} = V_{EDL} + V_{vdW} + V_B + V_{AB} + V_H \quad \text{(VI.14)}$$

The bacteriophage PP7 was considered as a sphere due to its icosahedral shape[34] and the flat sheet membrane was regarded as an infinite plate. The Hamaker constants were: A_{11} = 8.55x10^{-20} J, A_{22} = 7.45x10^{-20} J, A_{33} = 3.70x10^{-20} J, A_{131} = 1x10^{-20} J, A_{132} = 8.06x10^{-21} J, which were derived from literature.[1, 200, 202, 213]

Hydrated ions prevent separation between surfaces of less than 0.3 nm, thus, Born repulsion forces were neglected.[1, 31] Lewis acid-base interaction was calculated according to Eqs. VI.9 and VI.12 and the needed parameters from Eqs. VI.10 and VI.11. Hydration repulsion was calculated from Eq. VI.13 using C_h = 1.6x10^{-20} J and λ_{AB} = 0.6 nm[132] regarding the bacteriophage as a colloid with a protein capsid. Total interaction energies were calculated using Eq. VI.14.

VI.3. RESULTS AND DISCUSSION

VI.3.1. Bacteriophage size

No significant change in size was observed when varying salt or ionic strength. Average hydrodynamic diameter of the bacteriophages ranged between 44 and 84 nm (Fig. VI.1), which differs from the diameter of an isolate virus of around 27 nm reported in the literature.[214]

The hydrodynamic diameter is the diameter of a rigid hypothetical sphere whose velocity of diffusion is the mean of the velocities of diffusion of its different spatial orientations. It is calculated from data of diffusion coefficients obtained by DLS. Macromolecules are not rigid and spherical, but dynamic and they can interact with the solvent in which they are suspended. Therefore, the calculated diameter indicates the apparent size taking into consideration attraction and association with solvent molecules. In the light of filtration membrane processes, the membrane cut-off accounts for the molecular weight but not for the tridimensional structure of the molecule. This is particularly important for proteins, bacteria, and viruses, since their apparent size may change as a result of the water matrix chemistry.

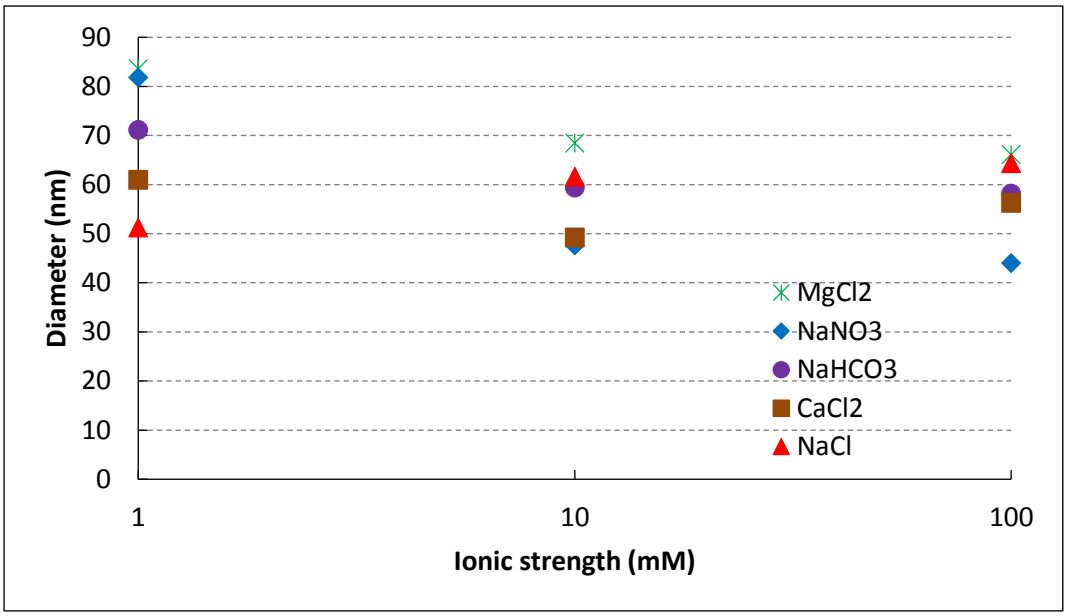

Fig. VI.1: Hydrodynamic diameter of bacteriophage PP7.

The aggregation of viral particles is important when evaluating and comparing retention efficiencies of different membranes so as to avoid overestimating removal. Perfectly disperse viral particles represent the most challenging scenario.[215] However, this condition can only be obtained in low ionic strength solutions; whereas in environmental waters many factors (such as pH, ionic strength, and presence of colloids and organic matter) affect the ideal isolation state, and aggregation occurs.[216, 217]

VI.3.2. Bacteriophage and membrane zeta potentials

Zeta potential for both phage and membrane surface was measured at 1; 10; and 100 mM ionic strength (Fig. VI.2 to Fig. VI.11). pH was varied between 5 and 8 in order to imitate pH of natural waters[29] and its effect studied for the phage at all ionic strengths and at 10 mM for the membrane.

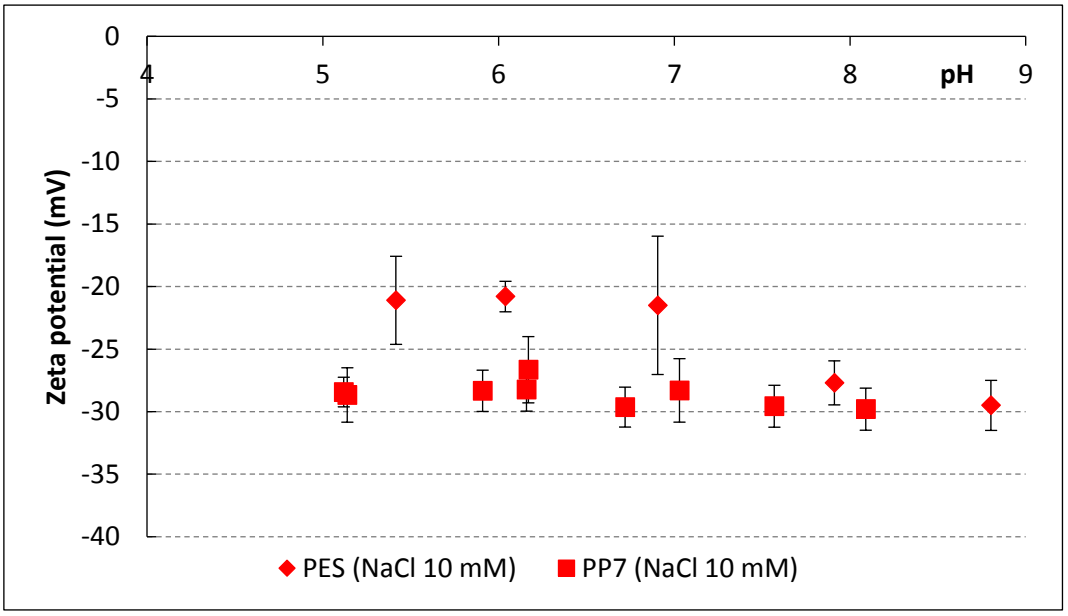

Fig. VI.2: Zeta potential of bacteriophage and membrane at NaCl 10 mM ionic strength.

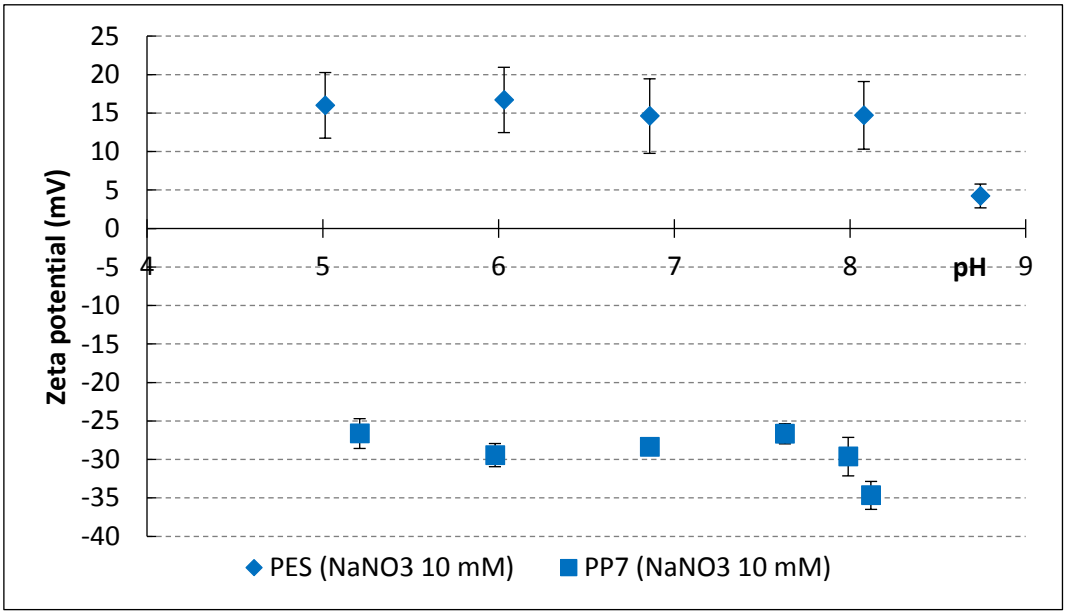

Fig. VI.3: Zeta potential of bacteriophage and membrane at $NaNO_3$ 10 mM ionic strength.

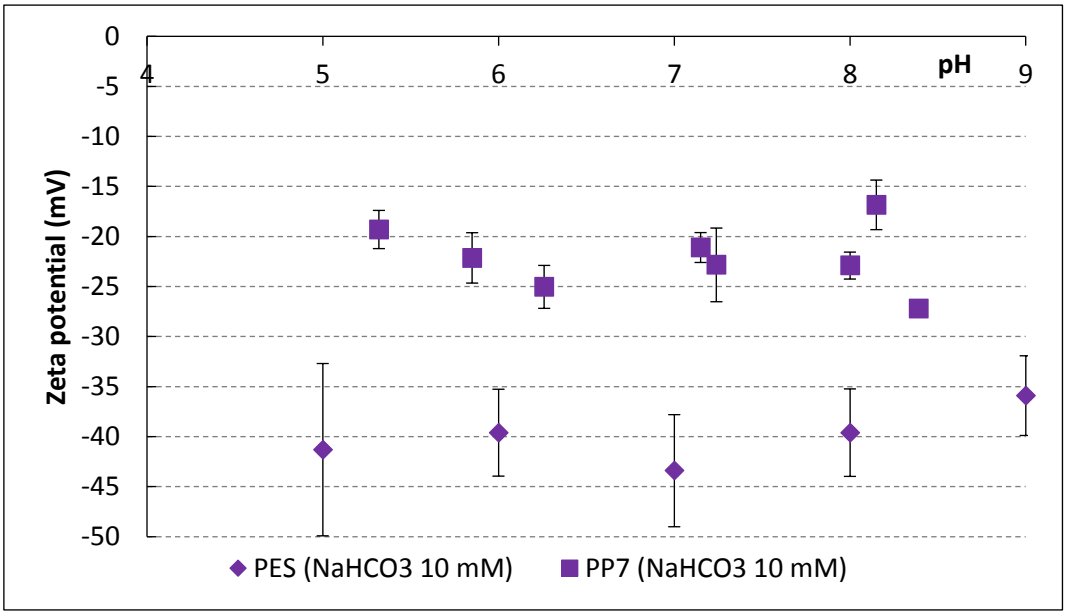

Fig. VI.4: Zeta potential of bacteriophage and membrane at $NaHCO_3$ 10 mM ionic strength.

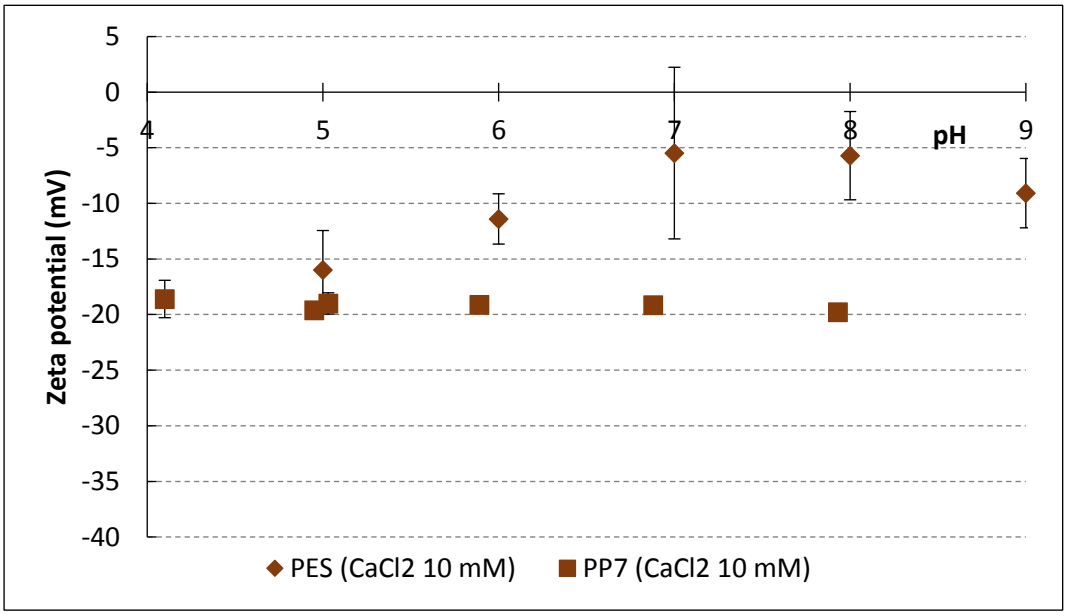

Fig. VI.5: Zeta potential of bacteriophage and membrane at $CaCl_2$ 10 mM ionic strength.

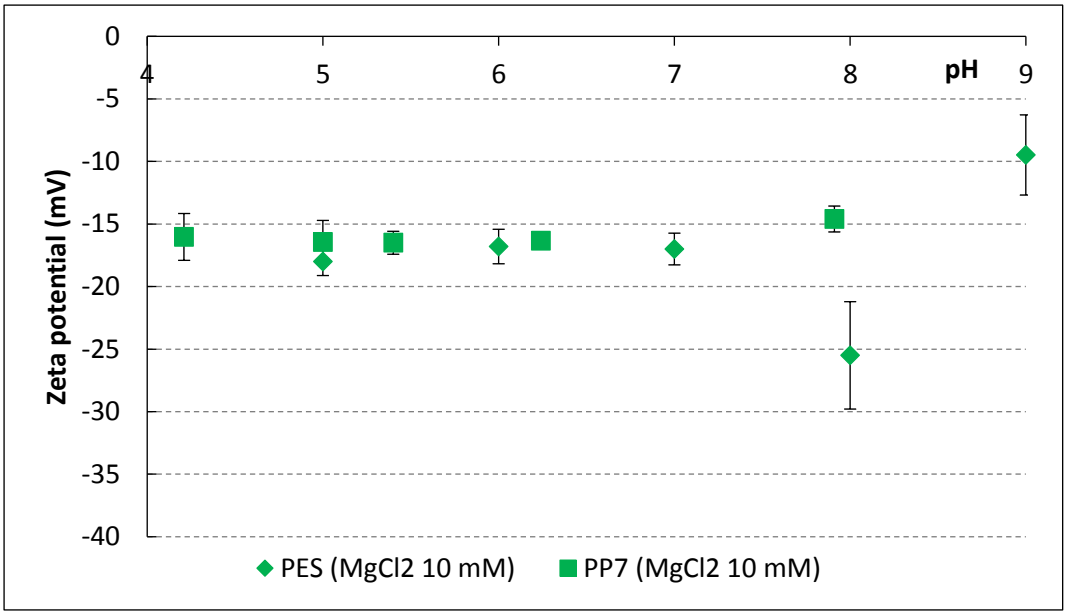

Fig. VI.6: Zeta potential of bacteriophage and membrane at $MgCl_2$ 10 mM ionic strength.

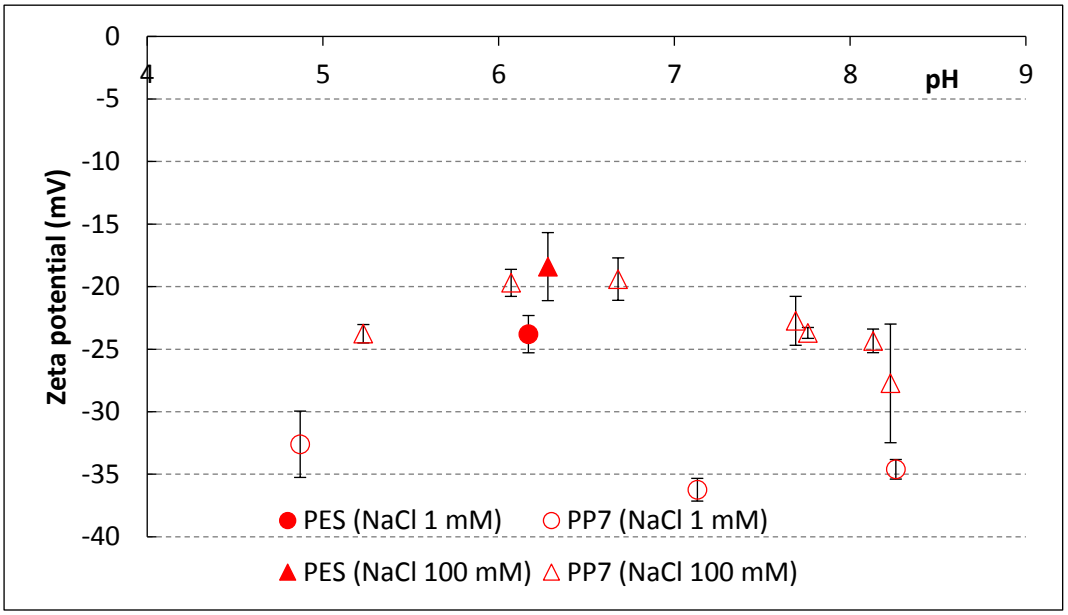

Fig. VI.7: Zeta potential of bacteriophage and membrane at NaCl 1 mM and 100 mM ionic strength.

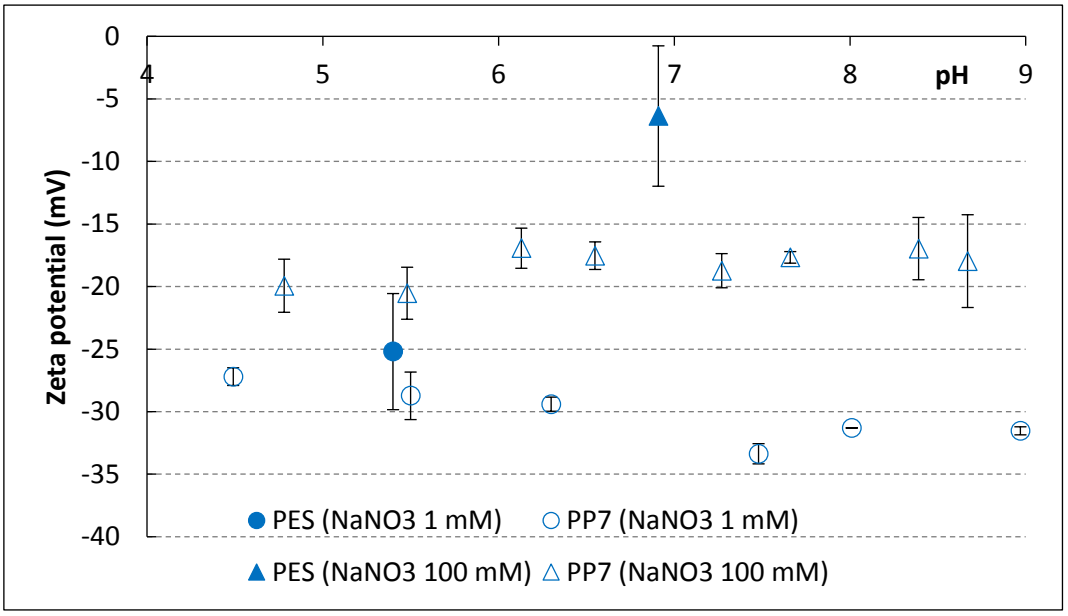

Fig. VI.8: Zeta potential of bacteriophage and membrane at $NaNO_3$ 1 mM and 100 mM ionic strength.

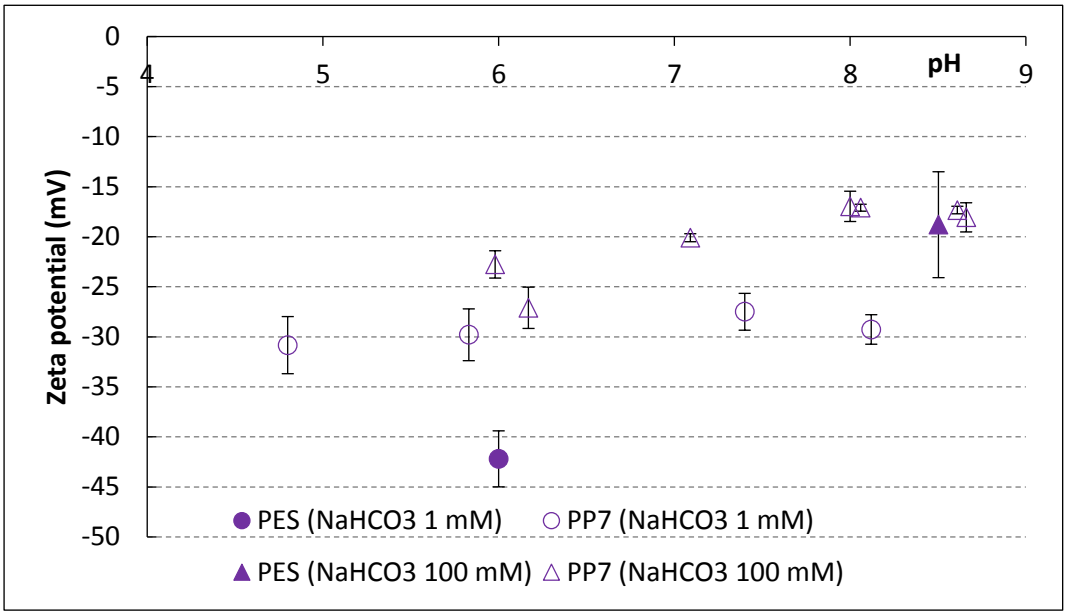

Fig. VI.9: Zeta potential of bacteriophage and membrane at $NaHCO_3$ 1 mM and 100 mM ionic strength.

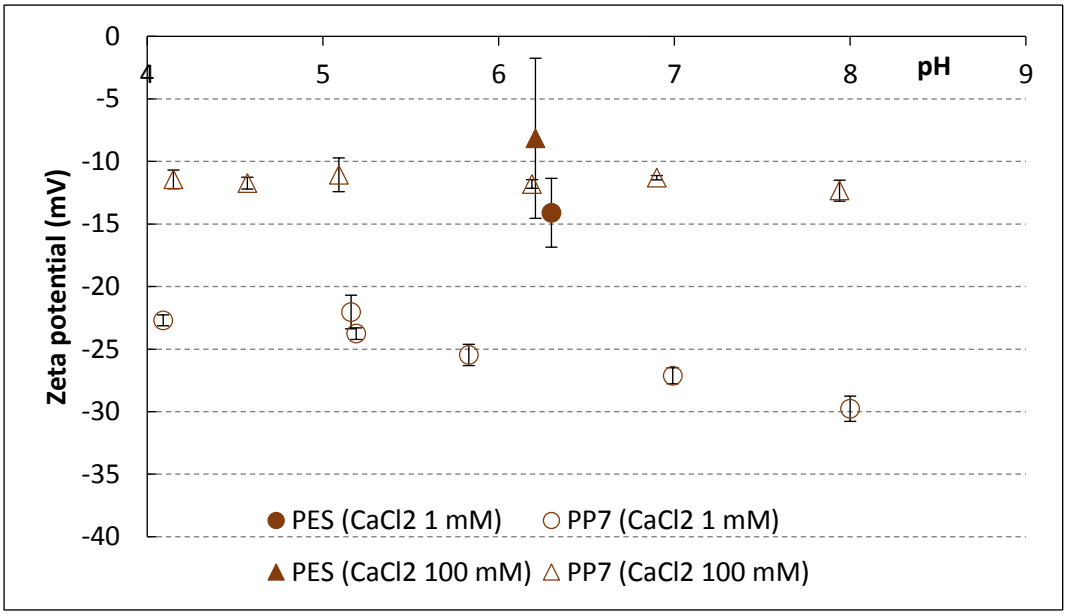

Fig. VI.10: Zeta potential of bacteriophage and membrane at $CaCl_2$ 1 mM and 100 mM ionic strength.

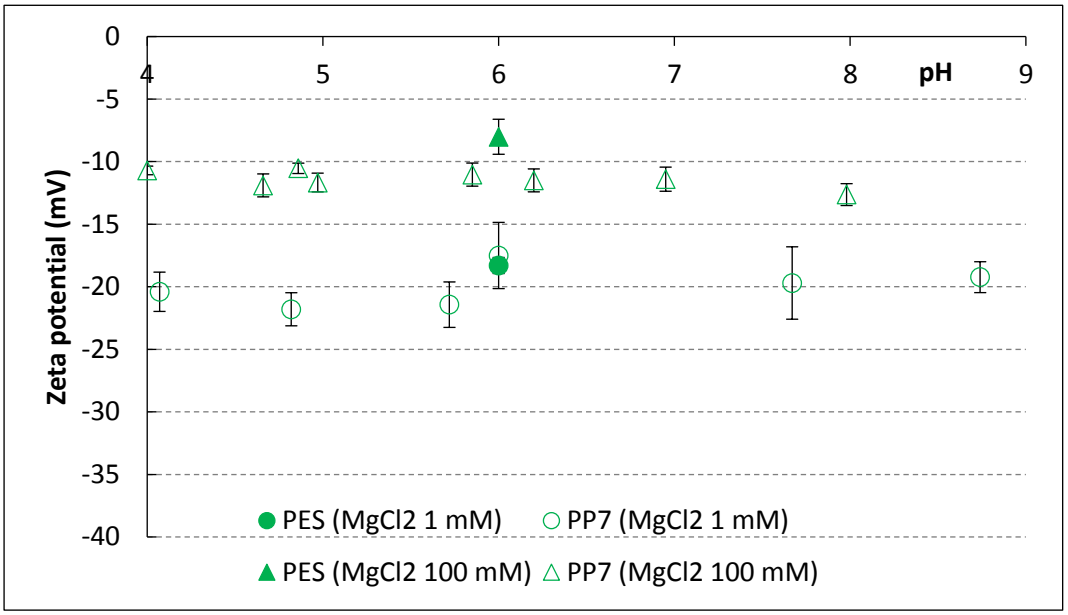

Fig. VI.11: Zeta potential of bacteriophage and membrane at $MgCl_2$ 1 mM and 100 mM ionic strength.

Zeta potential of the bacteriophage PP7 was very negative. For each salt and ionic strength level, there was no significant change over the considered pH range. This fact is in agreement with previous modeling of the phage's surface charge at NaCl 100 mM[27] where this stability was predicted for pH 6 and higher. Increasing ionic strength produced an increase in

the zeta potential of the bacteriophage, as expected due to compression of the ionic double layer.

For the flat membrane, the zeta potential showed negative values, with the exception of $NaNO_3$ 10 mM which was positive for the whole range of pH considered.

The membrane was less negatively charged than the virus for the case of NaCl and $NaNO_3$ 1 and 10 mM, $CaCl_2$ 1; 10; and 100 mM, $MgCl_2$ 100 mM ionic strength, more negatively charged for $NaHCO_3$ 1 mM and 10 mM ionic strength, and both had approximately the same charge for NaCl, $NaNO_3$, and $NaHCO_3$ 100 mM, $MgCl_2$ 1 and 10 mM ionic strength (Fig. VI.12).

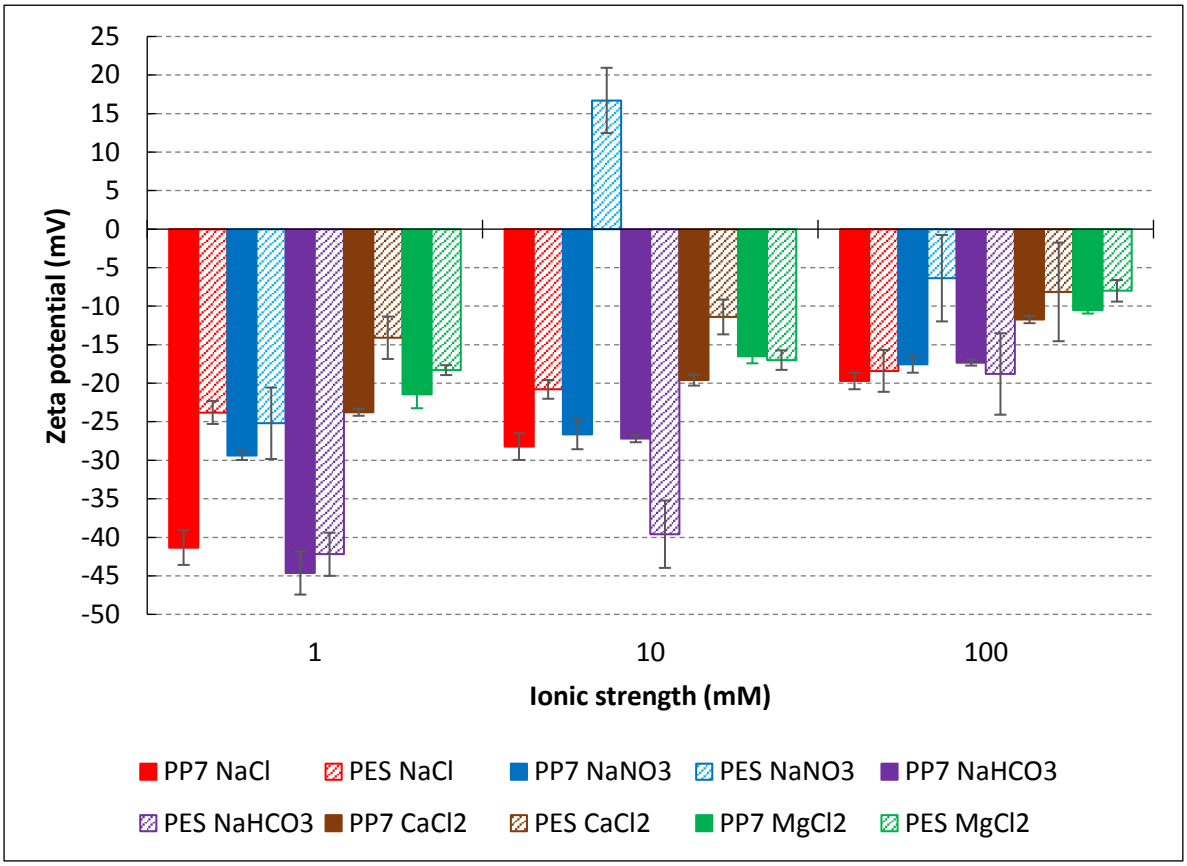

Fig. VI.12: Zeta potential of bacteriophage and membrane at different ionic strengths.

VI.3.3. Filtration results

Ultrafiltration of bacteriophage PP7 was performed using a polyethersulfone membrane (MWCO 50 kDa). Logarithmic removal values (LRV) varied between 1.50 and 2.83 and are presented in Table VI.1. The least removal was obtained in the cases where Mg^{2+} and Ca^{2+} were

dominant, an intermediate removal was obtained when NO_3^- was dominant, and the highest removal was when Na^+ and HCO_3^- were the dominant species together. To be consistent with quantities of selected ions in natural waters, different high concentrations were employed for different species.

Table VI.1: LRV for PP7 using polyethersulfone membrane.

Ionic strength					LRV
Na^+	HCO_3^-	NO_3^-	Ca^{2+}	Mg^{2+}	
high (1.23 mM)	high (1.23 mM)	low	low	low	2.83
low	low	high (0.48 mM)	low	low	1.91
low	low	low	high (2.50 mM)	low	1.53
low	low	low	low	high (1.24 mM)	1.50

The lowest LRVs were observed for the divalent cations, which have the largest hydrated radiuses (Na^+: 0.4 nm, Ca^{2+}: 0.6 nm, Mg^{2+}: 0.8 nm).[218] The highest removal was obtained when an indifferent ion such as Na^+ was present, suggesting its electrostatic nature. Besides, adsorption or proximity of cations to the negatively charged membrane can act as bond with the virus to the surface and could be the reason for the low existent removal.

VI.3.4. DLVO analysis

Attachment of viruses to surfaces is generally due to electrostatic interactions.[21] The van der Waals potential energies are equal at all conditions for two given surfaces, since they depend on the geometry and on properties of the interacting macroscopic bodies and of the medium. The electric double layer potential energies for two given surfaces change as function of the solution ionic strength and the zeta potential of both bacteriophage and membrane. Lewis acid-base and hydration repulsion energies were calculated and incorporated to the total interaction potential energy, though they could be neglected if compared to DLVO interactions.

VI.3.4.1. DLVO analysis of viral particle stability

Interaction potential energies were analyzed for the bacteriophages in different background solutions (Fig. VI.13). An energy barrier preventing aggregation was predicted in all cases except for the divalent cations at 100 mM ionic strength. This barrier was smaller with increasing ionic strength.

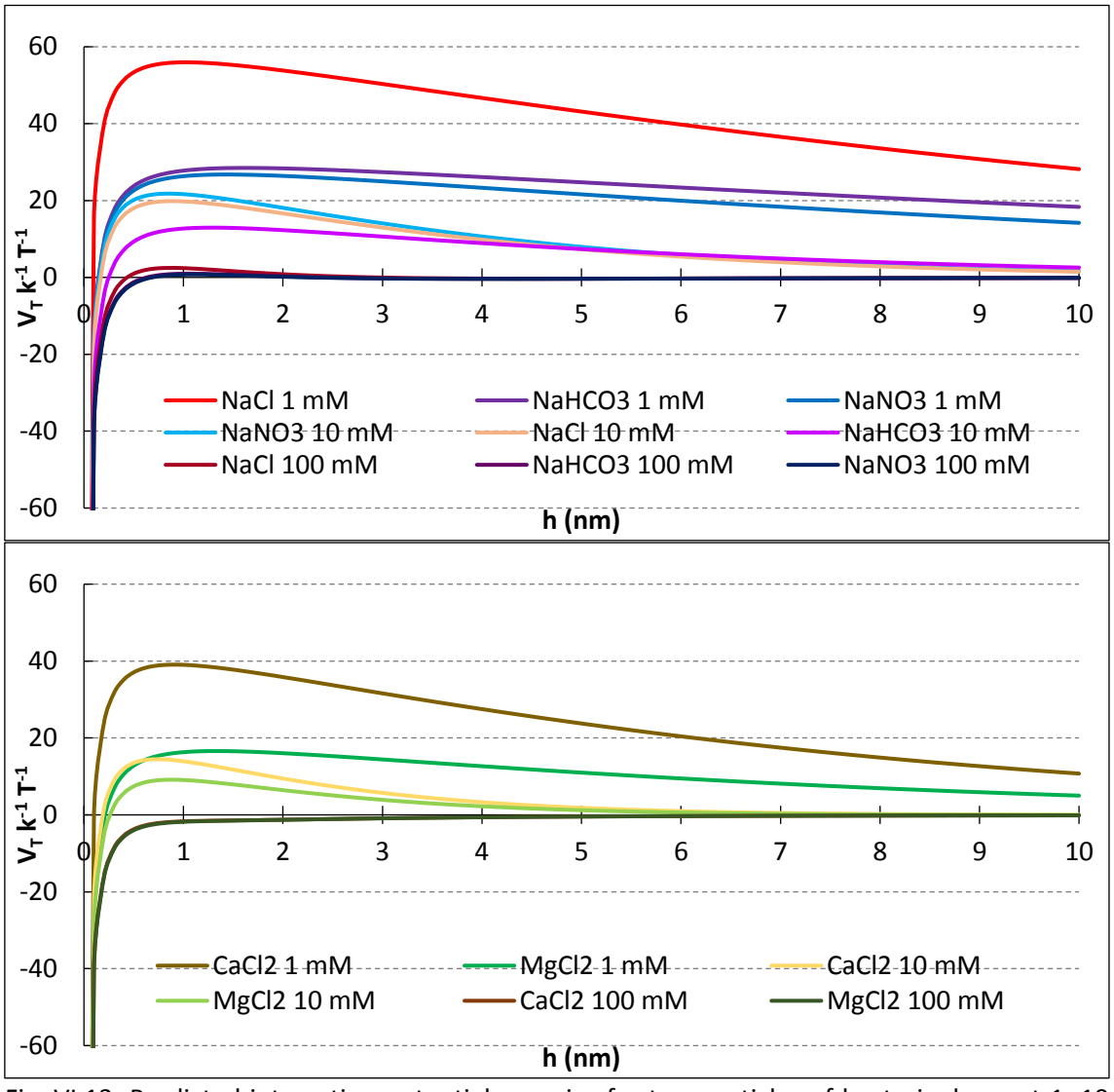

Fig. VI.13: Predicted interaction potential energies for two particles of bacteriophage at 1, 10 and 100 mM ionic strength.

Experimentally we did not observe difference in size when varying ionic strength and aggregates of only up to 84 nm were found (Fig. VI.1).

DLVO modeling was also performed for interactions under variable pH and all ionic strengths. The total interactions did not show significant differences since the variations of zeta potentials were very small. The analysis suggests that pH would not affect the stability of viral aggregates, which was in agreement with experimental observations.

VI.3.4.2. DLVO analysis of virus-membrane interactions

Interaction potential energies were analyzed for the bacteriophage and the membrane in different background solutions (Fig. VI.14). Net attraction was predicted for $NaNO_3$ 10 mM solution since the bacteriophage was negative and the membrane positive. Attraction forces were also predicted for the highest ionic strength conditions (100 mM) for $NaNO_3$, $CaCl_2$, and $MgCl_2$. Low energy barriers were obtained (2 to 4 k T) for NaCl and $NaHCO_3$ at 100 mM, not expected to prevent attachment to the membrane. For all other background solutions (1 and 10 mM), energy barriers were obtained and electrostatic repulsion expected.

When both the virus and the membrane were negative, higher removal rates would be expected due to electrostatic repulsion and therefore, viruses will not reach and attach to the membrane surface, but remain in the retentate. The membrane average pore diameter of 67 nm makes size exclusion an important mechanism for removal in natural waters where viruses are not usually present as individual particles but small aggregates.[71] Additional mechanisms such as electrostatic repulsion and adsorption are expected to play major roles both in natural and synthetic solutions.

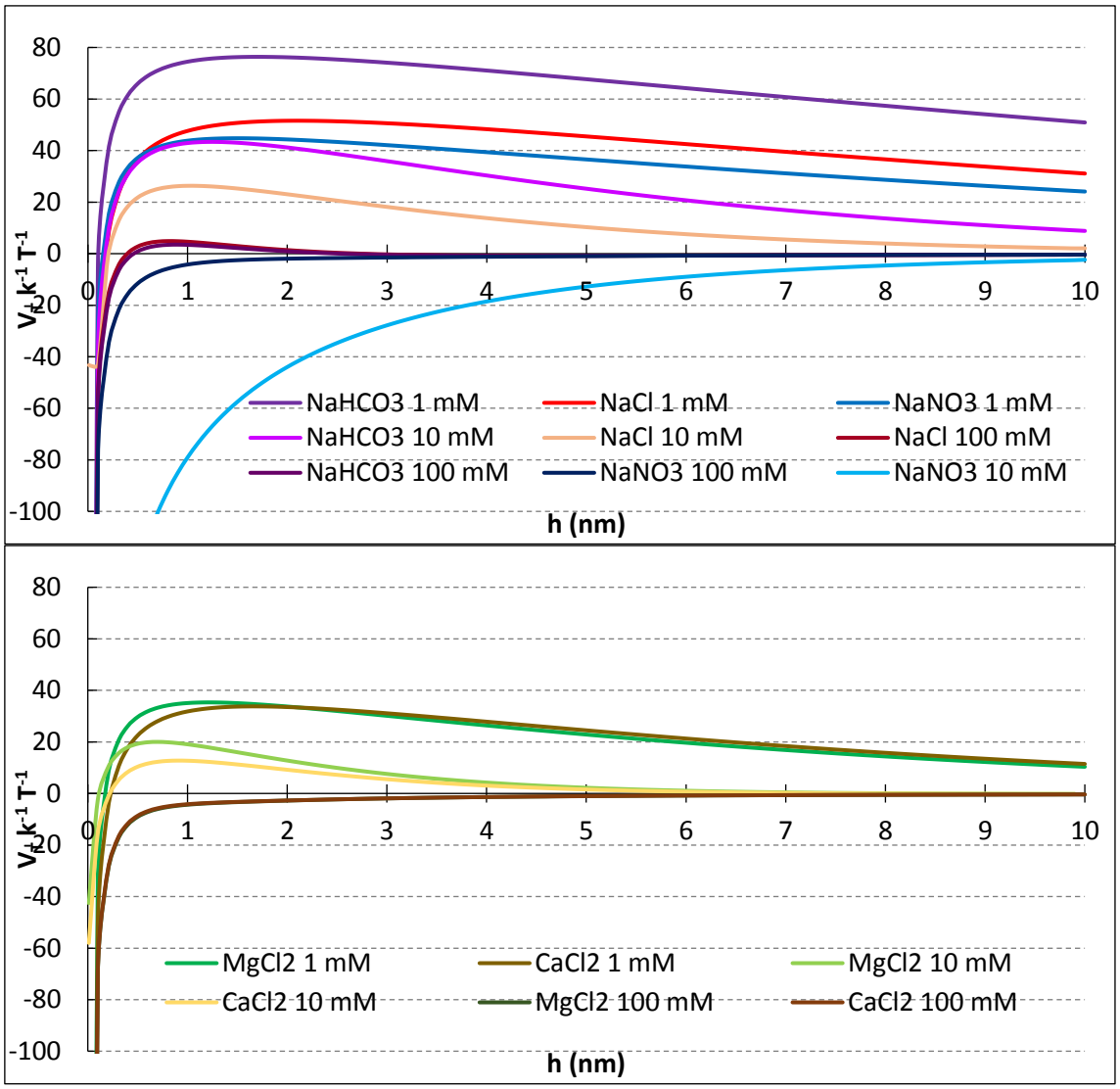

Fig. VI.14: Predicted interaction potential energies for a particle of bacteriophage and PES membrane at 1; 10; and 100 mM ionic strength.

The high ionic strength condition used in the laboratory scale ultrafiltration experiments was very close to or barely exceeded 1 mM; therefore, DLVO modeling for 1 mM solutions was applied to the interpretation the results (Fig. VI.15). The highest energy barriers corresponded to $NaHCO_3$ and NaCl giving rise to repulsion which would enhance the effectiveness of filtration. A slightly lower energy barrier was predicted for $NaNO_3$ and lesser values were obtained for divalent cations. The presence of Ca^{2+} and Mg^{2+} reduced the repulsion but in turn, prevented attachment to the membrane due to the enhanced hydrated radiuses. Filtration removal rates were expected to be reduced, as observed experimentally.

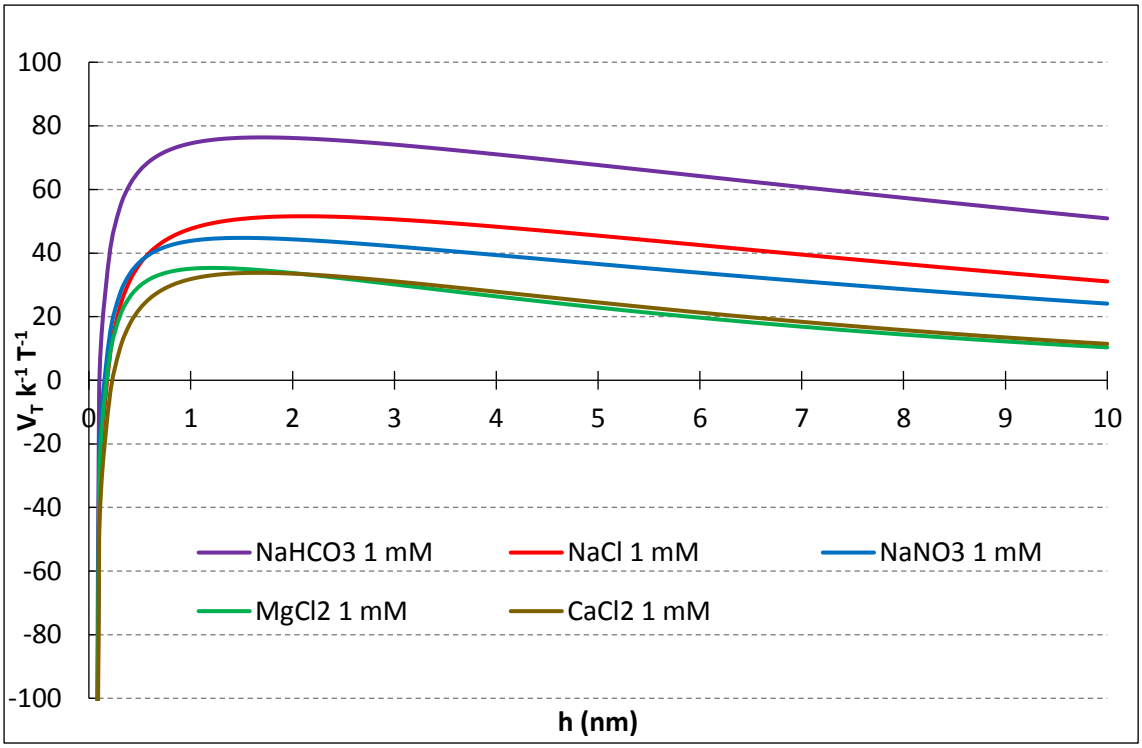

Fig. VI.15: Predicted interaction potential energies for a particle of bacteriophage and PES membrane at 1 mM ionic strength.

Theory predicted no significant changes when varying pH at 10 mM ionic strength. For the case of $NaNO_3$, attachment was predicted at all pH values but in all other cases energy barriers prevailed, due to the small variation in zeta potentials with pH.

VI.4. CONCLUSIONS

Size of the bacteriophage did not vary considerably with ionic strength nor pH. Both the bacteriophage and the membrane (except for $NaNO_3$ 10 mM) were negatively charged; their zeta potential increased with higher ionic strengths and did not substantially vary with pH.

The ultrafiltration experiments showed partial removal of PP7. This procedure to disinfect waters proved to be efficient, but the process was affected by the aqueous matrix. The presence of divalent cations diminished the effectiveness as opposed to monovalent cations and species with amphoteric behavior such as bicarbonate.

DLVO and X-DLVO modeling was applied to predict PP7-PP7 and PP7-PES interactions. In particular, the role of different electrolytes and the effect of pH were investigated. Modeling

of interactions between two PP7 particles predicted stability for the whole range of studied conditions, as it was confirmed by DLS measurements. For PP7-PES interactions, attraction was predicted for $NaNO_3$ 10 mM due to opposite charges and for $NaNO_3$, $CaCl_2$, and $MgCl_2$ at the highest ionic strength level. Low energy barriers were obtained for NaCl and $NaHCO_3$ at 100 mM. For 1 and 10 mM background solutions electrostatic repulsion was expected.

The removal increased in the following order: Mg^{2+}, Ca^{2+}, NO_3^-, Na^+ with HCO_3^-. The same trend was observed for the height of the energy barriers predicted by DLVO modeling. These results highlighted the importance of electrostatic interactions in virus-membrane filtration. Changes in pH or ionic strength did not alter the modeling predictions regarding stability and attachment; therefore, removal improvements are not expected.

Some limitations to the modeling arise from the fact that viruses are not perfect, rigid spheres with homogeneous surface, but soft particles where the surface is not clearly defined and electrolyte ions can penetrate it.[133] Therefore, the electrical double layer is not limited to the outside of the virus but it develops within the surface charge layer. Consequently, the zeta potential importance and meaning might be questioned.[134, 135] Moreover, commercial polyethersulfone membranes are not smooth and homogenous in their surface as considered in DLVO calculations.

Chapter VII

SIMULATING PRESSURE RETARDED OSMOSIS IN THE NEGRO RIVER MOUTH

Nomenclature

A: water permeability coefficient (m s^{-1} kPa^{-1})

J_w: water flux per unit of membrane area (m s^{-1})

W: power density (W m^{-2})

ΔP: hydrostatic pressure difference (kPa)

$\Delta\pi$: osmotic pressure difference (kPa)

VII.1. INTRODUCTION

The great dependence on fossil fuels as energy source originated different research works on alternative forms to generate energy due to economic and environmental factors as well as resource availability. In particular, the close relationship between CO_2 emissions and global warming is a key point to motivate the search and development of new green energy technologies.

Pressure retarded osmosis (PRO) process is a promising technology that is under study since the 1970's. It is based on the possibility of obtaining electricity from two solutions of different osmotic pressure which are separated by a semipermeable membrane.[94] One of the solutions has high osmotic pressure due to its elevated salt content (draw solution), the other one has low salt content, and therefore, low osmotic pressure (feed solution). Water will permeate from the feed solution to the draw solution, which has been previously pressurized. Afterwards, the draw solution can be depressurized through a hydroturbine to obtain electricity.[74] In this way, not only an alternative, renewable, and clean method for energy generation is obtained, but also water of a certain quality to develop new pharmaceutical or

food products. Environmentally, the process is of great relevance since there are no gaseous emissions and it is more stable in terms of power generation than solar or wind energy.[80]

There is an intimate dependence between water and energy. For the production of water, energy is required and in turn, natural waters can be employed for power generation.

The objective of this study was to investigate the application of PRO for energy generation in Argentina. In order to achieve this objective, we simulated the process and predicted the net power density taking into account natural water qualities and equipment needed.

The selected place to simulate a PRO plant was the mouth of the Negro River (Río Negro Province, Argentina) in the Atlantic Ocean, due to its proximity to the city of Viedma and because the hydrographic system is the most important in the Argentinian Patagonia and has the largest flow in the country.

VII.2. MATERIALS AND METHODS

The simulation software used was UniSim Design R390 with OLI Electrolyte fluid package for the osmotic pressure calculation. PRO simulation included a membrane module (where the mass transfer takes place), a high pressure pump (for the draw solution), a low pressure pump (for the feed solution), a recycle pump (for part of the diluted draw solution after osmosis), a pressure exchanger, and a hydroturbine. Fig. VII.1 shows the configuration and Fig. VII.2 the UniSim simulation layout.

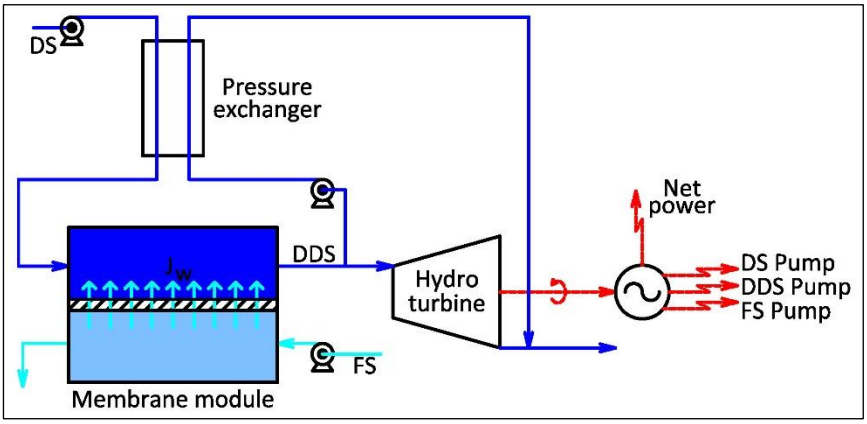

Fig. VII.1: PRO plant configuration.

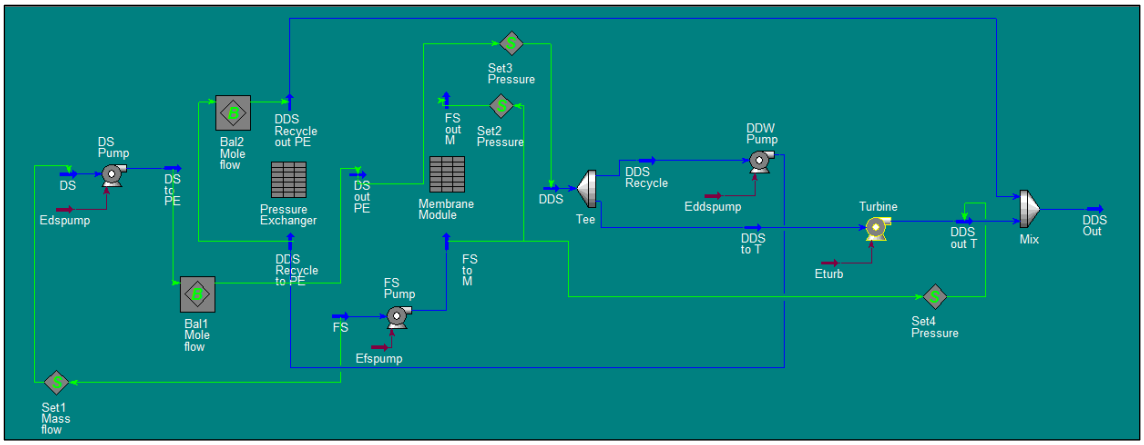

Fig. VII.2: Simulation layout.

Ideally, the best location for the system would be where a large salinity gradient is found in a short geographical distance and is constant all year-round.[81] Therefore, the feed solution is usually a river that flows into the sea and this salty water constitutes the draw solution. The difference in osmotic pressures is usually high enough, with standard salinity compositions of 0 for the river water and 3.5% w/w for the seawater;[219] giving an osmotic pressure of approximately 29 bar for the last one.

The flux across the membrane was calculated using Eq. VII.1 and the power generated in the membrane module was obtained from Eq. VII.2:[74, 75]

$$J_w = -A(\Delta P - \Delta\pi) \qquad \text{(VII.1)}$$

$$W = J_w \, \Delta P \qquad \text{(VII.2)}$$

where J_w: water flux per unit of membrane area (m s^{-1}), A: water permeability coefficient (m s^{-1} kPa^{-1}), ΔP: pressure difference (kPa), $\Delta\pi$: osmotic pressure difference (kPa), W: power density per unit area of membrane (W m^{-2}). The water permeability coefficient was obtained from literature: 1.87×10^{-9} m s^{-1} kPa^{-1}.[74]

River water is at ambient pressure. Seawater has to be pressurized because the hydraulic pressure for the best power output is half the difference in osmotic pressures of both solutions, as it can be seen as follows:

$$W = J_w \, \Delta P = \, -A(\Delta P - \Delta\pi)\Delta P \quad \text{(VII.3)}$$

$$\frac{\partial W}{\partial \Delta P} = -A(2\Delta P - \Delta\pi) = 0 \text{ for obtaining maximum power} \quad \text{(VII.4)}$$

$$\text{Consequently, } \Delta P = \frac{\Delta\pi}{2} \quad \text{(VII.5)}$$

Thus, optimal pressure for the seawater is between 11 and 15 bar. This is equivalent to 100 - 145 m water head in a hydroelectric plant, enabling the generation of 1 MW per m^3/s of water.[80, 91, 220]

Mole flow balances were used to set composition, temperature and flows of the two streams exiting the pressure exchanger. The pressure of the draw solution (DS) exiting the pressure exchanger and going to the membrane module was 12 bar.[75, 79, 91] The pressure of the diluted draw solution (DDS) going out of the pressure exchanger was equal to the pressure of the DS entering the unit.

The reason for using the pumps depended on each specific stream. DS and FS pumps allowed the fluids to move. DDS pump was necessary to compensate the pressure exchanger efficiency: DDS needed to enter the unit at a higher pressure than the required at the exit of DS. This fact implies that having a better efficiency in the pressure exchanger will reduce the pump's consumption of energy, generating an advantage in terms of produced net power.

The pressure exchanger may be an isobaric or a centrifugal device that transfers pressure from a high- to a low-pressure flow. In particular, isobaric devices transfer pressure in a rotor that is in a sleeve that, when filled with high-pressure water, creates an almost frictionless hydrodynamic bearing. This technology is economically more accessible than high-pressure pumps.[221] In a PRO plant, this is vital to reduce costs since the high pressure of the DDS is used to pressurize the inlet of the DS to the membrane module.

The pressure exchanger and the membrane module were not available among the equipment in UniSim, so two spreadsheets were used to simulate them by introducing the equations for mass balances.

In a first approximation, the pressure drop in the membrane module was considered to be null, although some pressure loss is expected in real conditions.[79] The composition of the DDS was calculated by mass balance.

Hydraulic turbines are used to recover energy from high-pressure liquid flows. Gas expansion is an isentropic process, which is not applicable to expansion of liquids, so the expander module provided by the software cannot be employed because the resulting exit temperature would be unrealistically low and the energy recovered too excessive. The hydraulic turbine acts more like a reverse pump; thus, a pump with negative head was used instead. As far as energy utilization, power recovered can be used to generate electricity, which complements the electric requirements for other services.

The fact that power generated in the osmosis was actually obtained in the hydroturbine was key to set the pressure at the exit of the hydroturbine. It was chosen to be the same as that of the FS entering the membrane module. In this way, the decrease of pressure in the hydroturbine was equal to the difference of pressures between the two flows feeding the membrane module.

The temperature and concentrations were chosen upon hydrological and climate data for the selected Negro River and the Atlantic Ocean respectively.

Flow measurements for the period 1997-2010 are presented in Fig. VII.3 and with further detail in Appendix A.[222] Monthly mean flows (average of daily registered values during a month) are grouped by hydrologic year, which is defined as the 12-month period that comprises a complete hydrologic cycle, beginning from the month when minimum values of the variable are observed. Maximum and minimum daily mean flow correspond to the observed maximum and minimum mean daily. Annual mean flow for a hydrologic year is the average of the monthly mean flows.

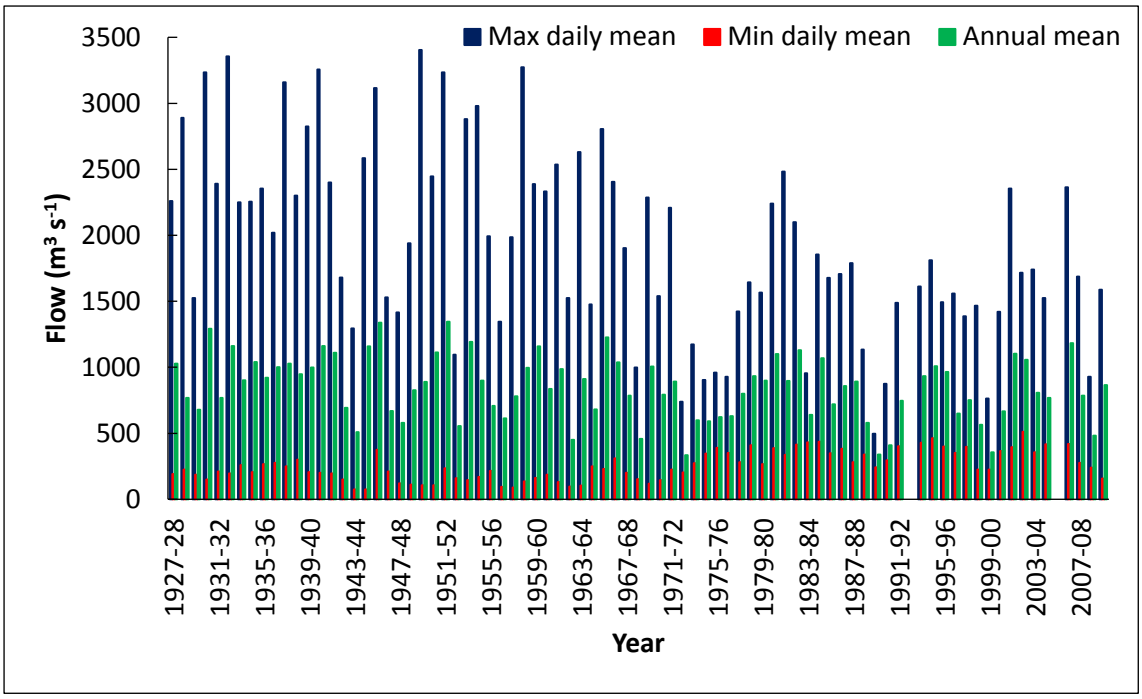

Fig. VII.3: Negro River flow measurements for the period 1997-2010.

To perform the simulation, the required variables to be defined correspond to fluid currents and equipment performance, as indicated in Table VII.1. Changes in the amount of salts both in river and seawater were considered, to establish the variability that can be accepted for this technology.

Table VII.1: Defined variables for PRO simulation.

Current or equipment	Variable	Value	Ref.
Feed solution (FS)	Pressure (bar)	0.02	
	Temperature (°C)	10	
	Composition (% NaCl w/w)	0 to 0.20 for DS 3.50	
Draw solution (DS)	Pressure (bar)	0.0121	
	Temperature (°C)	10	
	Flow (kg/day)	Double of FS	[223]
	Composition (% NaCl w/w)	3.35 to 3.50 for FS 0	[219]
Draw solution going to pressure exchanger (DS to PE)	Pressure (bar)	0.2	[79]

Draw solution going out of pressure exchanger (DS out PE)	Pressure (bar)	12	[79, 91]
Feed solution going to membrane module (FS to M)	Pressure (bar)	0.07	[79]
Diluted draw solution going out of membrane module (DDS)	Composition (% NaCl w/w)	Obtained by mass balance	
Diluted draw solution going to hydroturbine (DDS to T)	Flow (kg/day)	Equal to permeate (responsible for power generation)	
Pumps	Increase of pressure (bar)	DDS Pump: 0.63	
	Efficiency (pump efficiency multiplied by motor efficiency)	0.90 × 0.88 = 0.792	[79]
Pressure exchanger	Efficiency	0.95	[221]
Membrane module	Permeate	$J_w = -A(\Delta P - \Delta\pi)$ (VII.1)	[74, 75]
	A: water permeability coefficient (m s^{-1} kPa^{-1})	1.87×10^{-9}	[74]
Hydroturbine	Efficiency (turbine efficiency multiplied by generator efficiency)	0.92 × 0.98 = 0.90	[79]

The FS flux was also a defined variable. To determine the actual flow to use in the simulation two different scenarios were considered. For the first case, the lowest minimum daily mean flow (75 m^3/s) was considered, in order to avoid variable water flows that would restrict the analysis. For the second one, the average annual mean flow (847 m^3/s) was considered, to obtain more power and to be consistent with literature.[224] In both cases, but more relevantly in the second one, only 10% of these river flows were considered to enter the PRO plant,[84, 225] due to environmental reasons (the river flow after the extraction should not be considerable modified) and economic reasons (such as the power required to move the pumps, the installation equipment, and the turbine capacity). In both cases, the mass flow of the DS was set to double that of the FS.[223] According to the different fluxes employed, a total membrane area

of 5.5×10^5 m^2 and 6×10^6 m^2 were respectively used in the first and in the second cases, as shown in Table VII.2., and in agreement with previous predicted values for a targeted power output of 5 W/m^2.[220]

Table VII.2: Defined FS flow and membrane area for PRO simulation.

Current or equipment	Variable	Value	
		Case 1	Case 2
Feed solution (FS)	Flow (kg/day)	6.48×10^8	7.32×10^9
Membrane module	Membrane area (m^2)	5.5×10^5	6×10^6

The driving force in PRO is the difference in osmotic pressures between the FS and the DS. Dissolved compounds determine the osmotic pressure, so NaCl concentration in the DS and in the FS was varied to evaluate the operation range in terms of the driving force.

The output variables of interest were the power consumed by the pumps and the power obtained from the hydroturbine. In this way, the net power production could be calculated as the difference between them.

VII.3. RESULTS AND DISCUSSION

We investigated the feasibility of obtaining power considering different concentrations of both draw and feed solutions. The most common scenario is to assume salt concentration in rivers to be zero and in seawater to be 3.50% w/w, but these values can vary in real systems introducing less efficiency in the process.

The power obtained from the turbine and the net power (subtracting the consumption by the three pumps) were calculated for FS salt (NaCl) concentration varying between 0 and 0.20% w/w when DS concentration was fixed at 3.50% w/w. The same analysis was performed for FS concentration fixed at 0% w/w and DS salt (NaCl) concentration varying between 3.35 and 3.50% w/w. The extended results are shown in Appendix A.

Osmotic power generated in the membrane module is transformed into extractable power in the hydroturbine and the generator. The two values were not the same since a combined efficiency of 0.90 was applied to the turbine and generator.

As difference in osmotic pressure between FS and DS diminished, permeate flux and consequently obtained power also diminished. Only positive net power results were taken as valid, since the pumping power consumption cannot overcome the power obtained from the hydroturbine.

For the values studied in this work, the variations in salinity of both flows and thus in osmotic pressures resulted very short, taking into account the need to obtain power. As shown in Fig. VII.4, FS salt concentration could be up to 0.15% w/w in case 1 and only up to 0.084% w/w in case 2. The DS salt concentration should be greater than 3.36% w/w in case 1 and greater than 3.42% w/w in case 2, as shown in Fig. VII.5.

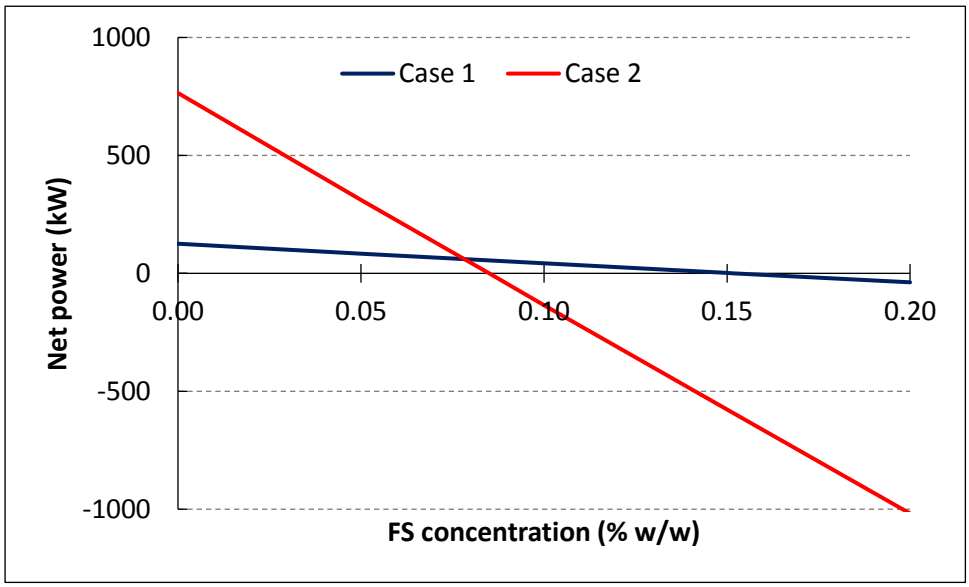

Fig. VII.4: Net power obtained when varying FS concentration for the two scenarios analyzed. Case 1: 10% of the lowest minimum daily flow. Case 2: 10% of the average annual mean flow.

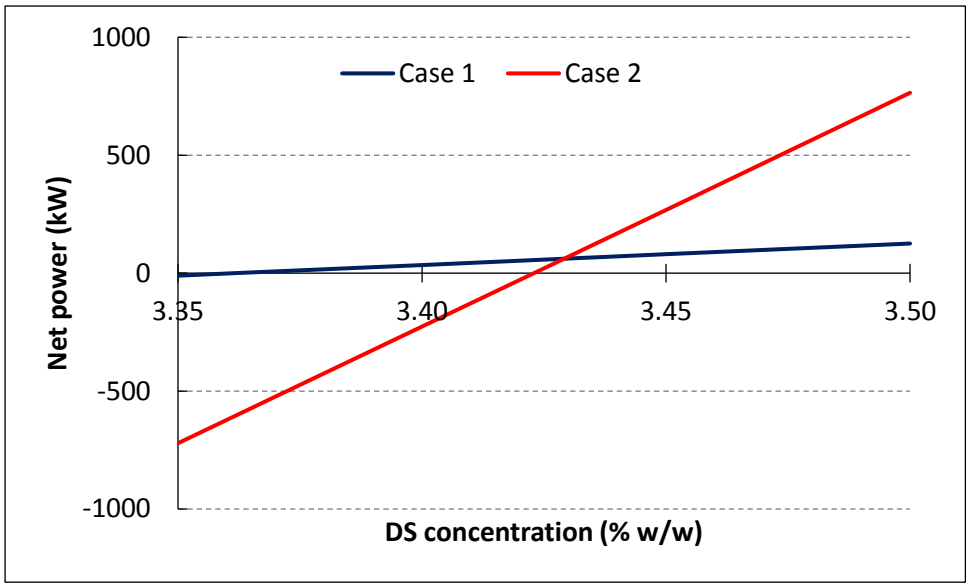

Fig. VII.5: Net power obtained when varying DS concentration for the two scenarios analyzed. Case 1: 10% of the lowest minimum daily flow. Case 2: 10% of the average annual mean flow.

Net power for the maximum difference in osmotic pressures of DS and FS was 125.6 kW in the first case and 764.7 kW in the second, corresponding to 0.22 and 0.13 W/m^2 of membrane respectively. These values are too low and far from an economic implementation, which requires improvements to reach at least the predicted 4 - 6 W/m^2 for commercial membranes.[80, 91, 226]

VII.4. CONCLUSIONS

Simulating PRO process with UniSim is a useful tool to assess the feasibility of this technology.

Energy generation, under the current scenario and theoretical membrane efficiencies, is possible for the Negro River case. Furthermore, improvements to the predicting capacities of the model can be incorporated by a better description of the membrane process. Permeate across the membrane was obtained with Eq. VII.1, but more complex models are available, that take into account internal and external polarization as well as diffusion of salts in the opposite direction to the water flow. Moreover, to avoid this drawback permeate data obtained in a pilot plant can be utilized as it will be a more realistic representation of the process. In real conditions, diffusion of salts and concentration polarization cause the osmotic pressure difference across the membrane to be lower than the bulk osmotic pressure difference, and therefore, the obtained water flux and power are lower than the calculated values.

The efficiency of the hydroturbine was adopted from traditional values proposed in the literature.[79] However, this important parameter can be modified, because it defined the relationship between the obtained power in the hydroturbine and the power obtained thanks to the osmosis.

Additionally, the development of new and better membranes for PRO may result in significant improvements in the flux obtained and therefore, a decrease in the required membrane area, affecting the economics of the process.

Chapter VIII

CONCLUSIONS

VIII.1. Main results

From the work described in the preceding chapters, the most important conclusions are listed below.

Enhanced retention of bacteria by TiO_2 nanoparticles in saturated porous media

- Hydrophilic P25 TiO_2 was effectively retained by the saturated quartz sand due to a combination of particle aggregation that clogged the pores and electrostatic attraction that led to attachment. This attachment was highly increased by raising the ionic strength of the matrix.
- Bacterial (*Pseudomonas aeruginosa*) retention in the saturated quartz porous bed was very poor, since electrical repulsion originated unfavorable conditions for deposition. However, when TiO_2 was present, the bacteria were completely retained. Many factors can be mentioned as the cause of this behavior: heteroaggregation, straining, and ripening effects.
- TiO_2 could be used for retaining bacteria in a well delimited subsurface area.

Virus removal by iron oxide ceramic membranes

- The mechanism that governs the removal of bacteriophages (P22) using ceramic membranes was electrostatic in nature. DLVO analysis of the attachment was useful at predicting it to be effective up to a pH of 6.5.
- Iron oxide ceramic membranes could be applied for the removal of viruses from water, under well controlled chemistry of the medium.

Study of interactions in ultrafiltration for virus removal

- Ultrafiltration showed that partial removal of bacteriophages (PP7) was achieved, and the process was affected by the aqueous matrix. The presence of divalent cations reduced the effectiveness as opposed to monovalent cations and species with amphoteric behavior such as bicarbonate.
- DLVO and X-DLVO modeling proved to effectively predict PP7-PP7 and PP7-membrane interactions energies; highlighting the relevance of electrostatic interactions in virus-membrane ultrafiltration.
- Ultrafiltration membranes can be used as a treatment to remove small viruses, with special care of the salts and species dissolved in the aqueous matrix.

Simulating pressure retarded osmosis (PRO) in the Negro River mouth

- Simulating PRO is useful as a first approach to the process.
- Improvements to the model can be incorporated by a better description of the membrane process and taking into account internal and external polarization as well as diffusion of salts in the opposite direction to the water flow. Moreover, data and results obtained at pilot plant scale would be more reliable.
- Energy generation using PRO, under the current scenario and theoretical membrane efficiencies, is possible but further refinement should be done.

VIII.2. Future work

After having finished the experimental and research work, some complementary projects derived from the present thesis can be performed in the near future, in order to reach a further understanding of the addressed problems and to develop new and useful treatment methods for better water quality.

Transport and fate of viruses in saturated porous media and the effect of TiO_2 nanoparticles needs to be further investigated, as the chemical, physical and biological behavior of these much smaller microorganisms differs greatly from that of bacteria.

In ultrafiltration for virus removal, since the process is in part due to electrostatic nature, membranes with surfaces specially modified can be evaluated and tested, to reach further LRV.

Performing the evaluation of pressure retarded osmosis process at laboratory scale would be of great benefit, provided the necessary equipment and membrane materials are available for the research.

These ideas can constitute new challenges for the quest of more conclusive answers as well as different options concerning the increasing need of safe water and energy.

Appendix A

FURTHER DATA USED IN THE PRO SIMULATION AND EXTENDED RESULTS

Table A.1: Flow measurements for the period 1997-2010.

	Flow (m^3/s)		
Year	Maximum daily mean	Minimum daily mean	Annual mean
1927-28	2,260	190	1,027
1928-29	2,890	225	767
1929-30	1,525	185	679
1930-31	3,235	150	1,292
1931-32	2,390	210	768
1932-33	3,355	195	1,161
1933-34	2,250	260	902
1934-35	2,255	205	1,039
1935-36	2,355	265	922
1936-37	2,020	275	1,001
1937-38	3,160	250	1,028
1938-39	2,300	300	948
1939-40	2,825	205	998
1940-41	3,255	200	1,161
1941-42	2,400	195	1,110
1942-43	1,680	150	692
1943-44	1,295	75	509
1944-45	2,585	75	1,159
1945-46	3,115	375	1,338
1946-47	1,530	210	668
1947-48	1,415	120	580
1948-49	1,940	110	827
1949-50	3,405	105	889
1950-51	2,445	105	1,113
1951-52	3,235	235	1,346

1952-53	1,095	160	554
1953-54	2,880	145	1,193
1954-55	2,980	170	900
1955-56	1,992	215	708
1956-57	1,345	95	614
1957-58	1,986	90	781
1958-59	3,273	136	997
1959-60	2,388	162	1,158
1960-61	2,332	187	837
1961-62	2,536	130	986
1962-63	1,525	97	450
1963-64	2,630	104	911
1964-65	1,475	249	680
1965-66	2,806	230	1,226
1966-67	2,406	310	1,038
1967-68	1,902	200	786
1968-69	998	152	457
1969-70	2,286	117	1,005
1970-71	1,539	145	792
1971-72	2,208	225	892
1972-73	738	204	335
1973-74	1,172	274	598
1974-75	905	345	592
1975-76	960	389	622
1976-77	929	352	631
1977-78	1,423	280	799
1978-79	1,643	410	933
1979-80	1,566	266	899
1980-81	2,241	387	1,100
1981-82	2,482	337	897
1982-83	2,099	413	1,129
1983-84	954	430	639
1984-85	1,854	435	1,068
1985-86	1,677	348	720

1986-87	1,706	382	858
1987-88	1,788	281	891
1988-89	1,133	338	580
1989-90	497	241	339
1990-91	875	296	408
1991-92	1,489	402	745
1992-93			
1993-94	1,612	429	933
1994-95	1,810	462	1,008
1995-96	1,493	399	965
1996-97	1,558	351	650
1997-98	1,386	398	752
1998-99	1,467	226	564
1999-00	763	224	356
2000-01	1,420	366	667
2001-02	2,354	395	1,103
2002-03	1,715	512	1,057
2003-04	1,741	357	806
2004-05	1,524	417	768
2005-06			
2006-07	2,364	418	1,183
2007-08	1,687	276	784
2008-09	928	240	483
2009-10	1,587	158	866
Mean	1,941	255	**847**
Maximum	3,405	512	1,346
Minimum	497	**75**	335

Data obtained from Secretaría de Obras Públicas. Subsecretaría de Recursos Hídricos.[222]

Table A.2: Obtained power and permeate when varying concentration of FS.

Case 1 (10% of the lowest minimum daily flow)					
FS (kg/day)	6.48×10^{8}				
FS (% NaCl w/w)	**0**	**0.05**	**0.10**	**0.15**	**0.20**
DS (kg/day)	1.30×10^{9}				
DS (% NaCl w/w)	3.50				
Permeate (kg/day)	1.39×10^{8}	1.36×10^{8}	1.32×10^{8}	1.29×10^{8}	1.25×10^{8}
DDS (kg/day)	1.44×10^{9}	1.43×10^{9}	1.43×10^{9}	1.42×10^{9}	1.42×10^{9}
DDS (% NaCl w/w)	3.16	3.17	3.19	3.20	3.21
$\Delta\pi$ (kPa)	2,758	2,719	2,680	2,642	2,604
Osmotic power (kW)	1,877	1,830	1,785	1,740	1,695
Turbine power (kW)	1,689	1,647	1,606	1,566	1,525
Net power (kW)	**125.6**	**83.94**	**43.03**	**2.416**	**-38.04**
Case 2 (10% of the average annual mean flow)					
FS (kg/day)	7.32×10^{9}				
FS (% NaCl w/w)	**0**	**0.05**	**0.10**	**0.15**	**0.20**
DS (kg/day)	1.46×10^{10}				
DS (% NaCl w/w)	3.50				
Permeate (kg/day)	1.39×10^{8}	1.36×10^{8}	1.32×10^{8}	1.29×10^{8}	1.25×10^{8}
DDS (kg/day)	1.44×10^{9}	1.43×10^{9}	1.43×10^{9}	1.42×10^{9}	1.42×10^{9}
DDS (% NaCl w/w)	3.16	3.17	3.19	3.20	3.21
$\Delta\pi$ (kPa)	2,758	2,719	2,680	2,642	2,604
Osmotic power (kW)	20,460	19,950	19,460	18,960	18,470
Turbine power (kW)	18,410	17,960	17,510	17,070	16,630
Net power (kW)	**764.7**	**311.1**	**-134.8**	**-577.5**	**-1,018**

Table A.3: Obtained power and permeate when varying concentration of DS.

Case 1 (10% of the lowest minimum daily flow)				
FS (kg/day)	6.48×10^{8}			
FS (% NaCl w/w)	0			
DS (kg/day)	1.30×10^{9}			
DS (% NaCl w/w)	**3.50**	**3.45**	**3.40**	**3.35**
Permeate (kg/day)	1.39×10^{8}	1.35×10^{8}	1.32×10^{8}	1.28×10^{8}
DDS (kg/day)	1.44×10^{9}	1.43×10^{9}	1.43×10^{9}	1.42×10^{9}
DDS (% NaCl w/w)	3.16	3.12	3.09	3.05
$\Delta\pi$ (kPa)	2,758	2,715	2,673	2,632
Osmotic power (kW)	1,877	1,826	1,776	1,726
Turbine power (kW)	1,689	1,644	1,598	1,553
Net power (kW)	**125.6**	**80.02**	**34.59**	**-10.73**
Case 2 (10% of the average annual mean flow)				
FS (kg/day)	7.32×10^{9}			
FS (% NaCl w/w)	0			
DS (kg/day)	1.46×10^{10}			
DS (% NaCl w/w)	**3.50**	**3.45**	**3.40**	**3.35**
Permeate (kg/day)	1.39×10^{8}	1.35×10^{8}	1.32×10^{8}	1.28×10^{8}
DDS (kg/day)	1.44×10^{9}	1.43×10^{9}	1.43×10^{9}	1.42×10^{9}
DDS (% NaCl w/w)	3.16	3.12	3.09	3.05
$\Delta\pi$ (kPa)	2,758	2,715	2,673	2,632
Osmotic power (kW)	20,460	19,910	19,360	18,810
Turbine power (kW)	18,410	17,920	17,420	16,930
Net power (kW)	**764.7**	**268.3**	**-226.9**	**-721**

REFERENCES

1. Elimelech, M.; Gregory, J.; Jia, X.; Williams, R. A.; Gregory, J.; Jia, X.; Williams, R. A., Particle, Deposition & Aggregation. Butterworth-Heinemann: Woburn, 1995.

2. Klaine, S. J.; Alvarez, P. J. J.; Batley, G. E.; Fernandes, T. F.; Handy, R. D.; Lyon, D. Y.; Mahendra, S.; McLaughlin, M. J.; Lead, J. R., Nanomaterials in the environment: Behavior, fate, bioavailability, and effects. *Environ. Toxicol. Chem.* 2008, *27*, (9), 1825-1851.

3. Standard terminology relating to nanotechnology. American Society for Testing and Materials: West Conshohocken, PA, USA, 2006.

4. Lead, J. R.; K.J., W., Environmental Colloids: Current Knowledge and Future Developments. In Environmental Colloids: Behaviour, Structure and Characterization, John Wiley: Chichester, UK, 2006.

5. Ray, P. C.; Yu, H.; Fu, P. P., Toxicity and environmental risks of nanomaterials: Challenges and future needs. *J. Environ. Sci. Health C Environ. Carcinog. Ecotoxicol. Rev.* 2009, *27*, (1), 1-35.

6. Terminology for nanomaterials. British Standards Institution: London, UK, 2007.

7. The appropriateness of the risk assessment methodology in accordance with the Technical Guidance Documents for new and existing substances for assessing the risks of nanomaterials. Scientific Committee on Emerging and Newly Identified Health Risks. European Commission: Brussels, Belgium, 2007.

8. Vance, M. E.; Kuiken, T.; Vejerano, E. P.; McGinnis, S. P.; Hochella Jr., M. F.; Rejeski, D.; Hull, M. S., Nanotechnology in the real world: Redeveloping the nanomaterial consumer products inventory. *Beilstein J. Nanotechnol.* 2015, *6*, 1769-1780.

9. Markowska-Szczupak, A.; Ulfig, K.; Morawski, A. W., The application of titanium dioxide for deactivation of bioparticulates: An overview. *Catal. Today* 2011, *169*, (1), 249-257.

10. O'Brien, N.; Cummins, E., Recent developments in nanotechnology and risk assessment strategies for addressing public and environmental health concerns. *Hum. Ecol. Risk Assess.* 2008, *14*, (3), 568-592.

11. Stone, V.; Nowack, B.; Baun, A.; van den Brink, N.; Kammer, F.; Dusinska, M.; Handy, R.; Hankin, S.; Hassellov, M.; Joner, E.; Fernandes, T. F., Nanomaterials for environmental studies: classification, reference material issues, and strategies for physico-chemical characterisation. *Sci. Total Environ.* 2010, *408*, (7), 1745-54.

12. Mohanraj, V. J.; Chen, Y., Nanoparticles - A Review. *Trop. J. Pharm. Res.* 2006, *5*, (1), 561-573.

13. Oberdörster, G.; Oberdörster, E.; Oberdörster, J., Nanotoxicology: An Emerging Discipline Evolving from Studies of Ultrafine Particles. *Environ. Health Perspect.* 2005, *113*, (7), 823-839.

14. Yokel, R. A.; MacPhail, R. C., Engineered nanomaterials: exposures, hazards, and risk prevention. *J. Occup. Med. Toxicol.* 2011, *6*, 7-7.

15. Robichaud, C. O.; Uyar, A. E.; Darby, M. R.; Zucker, L. G.; Wiesner, M. R., Estimates of upper bounds and trends in nano-TiO_2 production as a basis for exposure assessment. *Environ. Sci. Technol.* 2009, *43*, (12), 4227-4233.

16. Biswas, P.; Wu, C. Y., Nanoparticles and the environment. *J. Air Waste Manage. Assoc.* 2005, *55*, (6), 708-746.

17. Bottero, J.-Y.; Auffan, M.; Borschnek, D.; Chaurand, P.; Labille, J.; Levard, C.; Masion, A.; Tella, M.; Rose, J.; Wiesner, M. R., Nanotechnology, global development in the frame of environmental risk forecasting. A necessity of interdisciplinary researches. *C. R. Geosci.* 2015, *347*, (1), 35-42.

18. Hotze, E. M.; Phenrat, T.; Lowry, G. V., Nanoparticle Aggregation: Challenges to Understanding Transport and Reactivity in the Environment. *J. Environ. Qual.* 2010, *39*, 1909-1924.

19. Aschberger, K.; Micheletti, C.; Sokull-Klüttgen, B.; Christensen, F. M., Analysis of currently available data for characterising the risk of engineered nanomaterials to the environment and human health - Lessons learned from four case studies. *Environ. Int.* 2011, *37*, (6), 1143-1156.

20. Kahru, A.; Dubourguier, H.-C., From ecotoxicology to nanoecotoxicology. *Toxicology* 2010, *269*, (2–3), 105-119.

21. Tufenkji, N., Modeling microbial transport in porous media: Traditional approaches and recent developments. *Adv. Water Resour.* 2007, *30*, (6–7), 1455-1469.

22. Rijnaarts, H. H. M.; Norde, W.; Bouwer, E. J.; Lyklema, J.; Zehnder, A. J. B., Bacterial deposition in porous media related to the clean bed collision efficiency and to substratum blocking by attached cells. *Environ. Sci. Technol.* 1996, *30*, (10), 2869-2876.

23. Schinner, T.; Letzner, A.; Liedtke, S.; Castro, F. D.; Eydelnant, I. A.; Tufenkji, N., Transport of selected bacterial pathogens in agricultural soil and quartz sand. *Water Res.* 2010, *44*, (4), 1182-1192.

24. Redman, J. A.; Walker, S. L.; Elimelech, M., Bacterial adhesion and transport in porous media: Role of the secondary energy minimum. *Environ. Sci. Technol.* 2004, *38*, (6), 1777-1785.

25. Schwegmann, H.; Ruppert, J.; Frimmel, F. H., Influence of the pH-value on the photocatalytic disinfection of bacteria with TiO_2 - Explanation by DLVO and XDLVO theory. *Water Res.* 2013, *47*, (4), 1503-1511.

26. Gales, A. C.; Jones, R. N.; Turnidge, J.; Rennie, R.; Ramphal, R., Characterization of *Pseudomonas aeruginosa* isolates: occurrence rates, antimicrobial susceptibility patterns, and molecular typing in the global SENTRY Antimicrobial Surveillance Program, 1997-1999. *Clin. Infect. Dis.* 2001, *32 Suppl 2*, S146-55.

27. Nap, Rikkert J.; Božič, Anže L.; Szleifer, I.; Podgornik, R., The role of solution conditions in the bacteriophage PP7 capsid charge regulation. *Biophys. J.* 2014, *107*, (8), 1970-1979.

28. Theng, B. K. G., Viruses and Bacteriophages. 2012.

29. Chaudhry, R. M.; Holloway, R. W.; Cath, T. Y.; Nelson, K. L., Impact of virus surface characteristics on removal mechanisms within membrane bioreactors. *Water Res.* 2015, *84*, 144-152.

30. Adams, M. H., Bacteriophages. Interscience Publishers Ltd.: London, UK, 1959.

31. Chrysikopoulos, C. V.; Syngouna, V. I., Attachment of bacteriophages MS2 and ΦX174 onto kaolinite and montmorillonite: Extended-DLVO interactions. *Colloids Surf., B* 2012, *92*, (0), 74-83.

32. Syngouna, V. I.; Chrysikopoulos, C. V., Cotransport of clay colloids and viruses in water saturated porous media. *Colloids Surf., A* 2013, *416*, (0), 56-65.

33. Syngouna, V. I.; Chrysikopoulos, C. V., Cotransport of clay colloids and viruses through water-saturated vertically oriented columns packed with glass beads: Gravity effects. *Sci. Total Environ.* 2016, *545–546*, 210-218.

34. ElHadidy, A. M.; Peldszus, S.; Van Dyke, M. I., An evaluation of virus removal mechanisms by ultrafiltration membranes using MS2 and ϕX174 bacteriophage. *Sep. Purif. Technol.* 2013, *120*, (0), 215-223.

35. Olsthoorn, R. C. L.; Garde, G.; Dayhuff, T.; Atkins, J. F.; Van Duin, J., Nucleotide sequence of a single-stranded RNA phage from *Pseudomonas aeruginosa*: Kinship to coliphages and conservation of regulatory RNA structures. *Virology* 1995, *206*, (1), 611-625.

36. King, A. M. Q.; Adams, M. J.; Carstens, E. B.; Lefkowitz, E. J., Virus Taxonomy: Classification and Nomenclature of Viruses: Ninth Report of the International Committee on Taxonomy of Viruses. Academic Press: London, UK, 2012.

37. Dhaese, P.; Lenaerts, A.; Gielen, J.; Van Montagu, M., Complete amino acid sequence of the coat protein of the *Pseudomonas aeruginosa* RNA bacteriophage PP7. *Biochem. Bioph. Res. Co.* 1980, *94*, (4), 1394-1400.

38. Bradley, D. E., The structure and infective process of a *Pseudomonas Aeruginosa* bacteriophage containing ribonucleic acid. *Microbiology* 1966, *45*, (1), 83-96.

39. Stumm, W.; Morgan, J. J., Aquatic Chemistry: Chemical Equilibria and Rates in Natural Waters. 3rd ed.; John Wiley: New York, 1996.

40. Arellano Díaz, J.; Guzmán Pantoja, J. E., Ingeniería Ambiental. 1st ed.; Alfaomega Grupo Editor S.A. de C.V.: Mexico, D.F., Mexico, 2011.

41. Masters, G. M.; Ela, W. P., Introducción a la Ingeniería Medioambiental. 3rd ed.; Pearson Educación S.A.: Madrid, Spain, 2008.

42. Bitton, G., Wastewater Microbiology. 3rd ed.; John Wiley & Sons, Inc.: Hoboke, NJ, USA, 2005.

43. Cicerone, D., Curso: Modelización de la Dispersión de Contaminantes en Suelo, Agua y Aire.Instituto de Investigación e Ingeniería Ambiental, Universidad Nacional de San Martín: Buenos Aires, Argentina, 2008.

44. Messina, F.; Marchisio, D. L.; Sethi, R., An extended and total flux normalized correlation equation for predicting single-collector efficiency. *J. Colloid Interf. Sci.* 2015, *446*, (0), 185-193.

45. Yao, K.-M.; Habibian, M. T.; O'Melia, C. R., Water and waste water filtration. Concepts and applications. *Environ. Sci. Technol.* 1971, *5*, (11), 1105-1112.

46. Tufenkji, N.; Elimelech, M., Correlation equation for predicting single-collector efficiency in physicochemical filtration in saturated porous media. *Environ. Sci. Technol.* 2003, *38*, (2), 529-536.

47. Rajagopalan, R.; Tien, C., Trajectory analysis of deep-bed filtration with the sphere-in-cell porous media model. *AIChE J.* 1976, *22*, (3), 523-533.

48. Rajagopalan, R.; Tien, C.; Pfeffer, R.; Tardos, G., Letters to the editor. *AIChE J.* 1982, *28*, 871-872.

49. Petosa, A. R.; Jaisi, D. P.; Quevedo, I. R.; Elimelech, M.; Tufenkji, N., Aggregation and deposition of engineered nanomaterials in aquatic environments: Role of physicochemical interactions. *Environ. Sci. Technol.* 2010, *44*, (17), 6532-6549.

50. Vasiliadou, I. A.; Chrysikopoulos, C. V., Cotransport of *Pseudomonas putida* and kaolinite particles through water-saturated columns packed with glass beads. *Water Resour. Res.* 2011, *47*, (2).

51. Tan, Y.; Gannon, J. T.; Baveye, P.; Alexander, M., Transport of bacteria in an aquifer sand: Experiments and model simulations. *Water Resour. Res.* 1994, *30*, (12), 3243-3252.

52. Stevik, T. K.; Aa, K.; Ausland, G.; Hanssen, J. F., Retention and removal of pathogenic bacteria in wastewater percolating through porous media: A review. *Water Res.* 2004, *38*, (6), 1355-1367.

53. Hendry, M. J.; Lawrence, J. R.; Maloszewski, P., Effects of velocity on the transport of two bacteria through saturated sand. *Ground Water* 1999, *37*, (1), 103-112.

54. Camesano, T. A.; Unice, K. M.; Logan, B. E., Blocking and ripening of colloids in porous media and their implications for bacterial transport. *Colloids Surf., A* 1999, *160*, (3), 291-307.

55. Camesano, T. A.; Logan, B. E., Influence of fluid velocity and cell concentration on the transport of motile and nonmotile bacteria in porous media. *Environ. Sci. Technol.* 1998, *32*, (11), 1699-1708.

56. Becker, M. W.; Collins, S. A.; Metge, D. W.; Harvey, R. W.; Shapiro, A. M., Effect of cell physicochemical characteristics and motility on bacterial transport in groundwater. *J. Contam. Hydrol.* 2004, *69*, (3-4), 195-213.

57. Camper, A. K.; Hayes, J. T.; Sturman, P. J.; Jones, W. L.; Cunningham, A. B., Effects of motility and adsorption rate coefficient on transport of bacteria through saturated porous media. *Appl. Environ. Microbiol.* 1993, *59*, (10), 3455-3462.

58. Bolster, C. H.; Haznedaroglu, B. Z.; Walker, S. L., Diversity in cell properties and transport behavior among 12 different environmental *Escherichia coli* isolates. *J. Environ. Qual.* 2009, *38*, (2), 465-72.

59. Simoni, S. F.; Harms, H.; Bosma, T. N. P.; Zehnder, A. J. B., Population heterogeneity affects transport of bacteria through sand columns at low flow rates. *Environ. Sci. Technol.* 1998, *32*, (14), 2100-2105.

60. Gannon, J. T.; Manilal, V. B.; Alexander, M., Relationship between cell surface properties and transport of bacteria through soil. *Appl. Environ. Microbiol.* 1991, *57*, (1), 190-3.

61. Powelson, D. K.; Mills, A. L., Transport of *Escherichia coli* in sand columns with constant and changing water contents. *J. Environ. Qual.* 2001, *30*, (1), 238-45.

62. Kim, S.-B.; Park, S.-J.; Lee, C.-G.; Choi, N.-C.; Kim, D.-J., Bacteria transport through goethite-coated sand: Effects of solution pH and coated sand content. *Colloids Surf., B* 2008, *63*, (2), 236-242.

63. Choi, N.-C.; Kim, D.-J.; Kim, S.-B., Quantification of bacterial mass recovery as a function of pore-water velocity and ionic strength. *Res. Microbiol.* 2007, *158*, (1), 70-78.

64. Jewett, D. G.; Hilbert, T. A.; Logan, B. E.; Arnold, R. G.; Bales, R. C., Bacterial transport in laboratory columns and filters: Influence of ionic strength and pH on collision efficiency. *Water Res.* 1995, *29*, (7), 1673-1680.

65. Cotruvo, J. A.; Vogt, C. D., Rationale for Water Quality Standards and Goals. In Water Quality and Treatment: A Handbook of Community Water Supplies, 4th ed.; Pontius, F. W., Ed. McGraw Hill: New York, USA, 1990.

66. Reinert, P. E.; Hroncich, J. A., Source Water Quality Management Processes. In Water Quality and Treatment: A Handbook of Community Water Supplies, 4th ed.; Pontius, F. W., Ed. McGraw Hill: New York, USA, 1990.

67. Hamann, C. L. J.; McEwen, J. B.; Myers, A. G., Guide to Selection of Water Treatment Processes. In Water Quality and Treatment: A Handbook of Community Water Supplies, 4th ed.; Pontius, F. W., Ed. McGraw Hill: New York, USA, 1990.

68. Mulder, M., Basic Principles of Membrane Technology. 2nd ed.; Springer Netherlands: Dordrecht, The Netherlands, 1996.

69. Habert, A. C.; Borges, C. P.; Nobrega, R., Processos de Separação por Membranas. 1st ed.; E-papers Serviços Editoriais Ltda.: Rio de Janeiro, Brasil, 2006.

70. Jacangelo, J. C.; Patania Brown, N. L.; Madec, A.; Schwab, K.; Huffman, D.; Amy, G.; Mysore, C.; Leparc, J.; Prescott, A., Micro and Ultrafiltration Performance Specifications Based on Microbial Removal. AwwaRF: 2007; p 208.

71. Jacangelo, J. G.; Adham, S. S.; J.M., L., Mechanism of Cryptosporidium, Giardia, and MS2 virus removal by MF and UF. *J. Am. Water Works Ass.* 1995, *87*, 107-121.

72. Fiksdal, L.; Leiknes, T., The effect of coagulation with MF/UF membrane filtration for the removal of virus in drinking water. *J. Membr. Sci.* 2006, *279*, (1–2), 364-371.

73. Kreissel, K.; Bosl, M.; Lipp, P.; Franzreb, M.; Hambsch, B., Study on the removal efficiency of UF membranes using bacteriophages in bench-scale and semi-technical scale. *Water Sci. Technol.* 2012, *66*, (6), 1195-202.

74. Achilli, A.; Cath, T. Y.; Childress, A. E., Power generation with pressure retarded osmosis: An experimental and theoretical investigation. *J. Membr. Sci.* 2009, *343*, (1-2), 42-52.

75. Chou, S.; Wang, R.; Shi, L.; She, Q.; Tang, C.; Fane, A. G., Thin-film composite hollow fiber membranes for pressure retarded osmosis (PRO) process with high power density. *J. Membr. Sci.* 2012, *389*, 25-33.

76. Wiesner, M. R.; Chellam, S., Peer reviewed: The promise of membrane technology. *Environ. Sci. Technol.* 1999, *33*, (17), 360A-366A.

77. Sharqawy, M. H.; Zubair, S. M.; Lienhard, J. H., Second law analysis of reverse osmosis desalination plants: An alternative design using pressure retarded osmosis. *Energy* 2011, *36*, (11), 6617-6626.

78. Tsui, E. M.; Fidalgo de Cortalezzi, M. M.; Wiesner, M. R., Proton conductivity of an iron oxide membrane derived from ferroxane nanoparticles. *J. Membr. Sci.* 2007, *306*, (1-2), 8-15.

79. Loeb, S., Large-scale power production by pressure-retarded osmosis, using river water and sea water passing through spiral modules. *Desalination* 2002, *143*, (2), 115-122.

80. Gerstandt, K.; Peinemann, K. V.; Skilhagen, S. E.; Thorsen, T.; Holt, T., Membrane processes in energy supply for an osmotic power plant. *Desalination* 2008, *224*, (1-3), 64-70.

81. Alvarez-Silva, O.; Osorio, A.; Ortega, S.; Agudelo-Restrepo, P., Estimation of the electric power potential using pressure retarded osmosis in the Leon River's mouth: A first step for the harnessing of saline gradients in Colombia. In OCEANS, 2011 IEEE - Spain, 2011; pp 1-7.

82. Cath, T.; Childress, A.; Elimelech, M., Forward osmosis: Principles, applications, and recent developments. *J. Membr. Sci.* 2006, *281*, (1-2), 70-87.

83. Loeb, S., Osmotic power plants. *Science* 1975, *189*, (4203), 654-655.

84. Helfer, F.; Lemckert, C.; Anissimov, Y. G., Osmotic power with Pressure Retarded Osmosis: Theory, performance and trends - A review. *J. Membr. Sci.* 2014, *453*, 337-358.

85. McGinnis, R. L.; Elimelech, M., Energy requirements of ammonia–carbon dioxide forward osmosis desalination. *Desalination* 2007, *207*, (1-3), 370-382.

86. Yip, N. Y.; Elimelech, M., Performance limiting effects in power generation from salinity gradients by pressure retarded osmosis. *Environ. Sci. Technol.* 2011, *45*, (23), 10273-82.

87. She, Q.; Jin, X.; Tang, C. Y., Osmotic power production from salinity gradient resource by pressure retarded osmosis: Effects of operating conditions and reverse solute diffusion. *J. Membr. Sci.* 2012, *401-402*, 262-273.

88. Post, J. W.; Veerman, J.; Hamelers, H. V. M.; Euverink, G. J. W.; Metz, S. J.; Nymeijer, K.; Buisman, C. J. N., Salinity-gradient power: Evaluation of pressure-retarded osmosis and reverse electrodialysis. *J. Membr. Sci.* 2007, *288*, (1-2), 218-230.

89. Tan, C. H.; Ng, H. Y., Revised external and internal concentration polarization models to improve flux prediction in forward osmosis process. *Desalination* 2013, *309*, 125-140.

90. Kim, Y. C.; Elimelech, M., Potential of osmotic power generation by pressure retarded osmosis using seawater as feed solution: Analysis and experiments. *J. Membr. Sci.* 2013, *429*, 330-337.

91. Skilhagen, S. E.; Dugstad, J. E.; Aaberg, R. J., Osmotic power - Power production based on the osmotic pressure difference between waters with varying salt gradients. *Desalination* 2008, *220*, (1-3), 476-482.

92. Zhao, S.; Zou, L.; Tang, C. Y.; Mulcahy, D., Recent developments in forward osmosis: Opportunities and challenges. *J. Membr. Sci.* 2012, *396*, 1-21.

93. Chung, T.-S.; Zhang, S.; Wang, K. Y.; Su, J.; Ling, M. M., Forward osmosis processes: Yesterday, today and tomorrow. *Desalination* 2012, *287*, 78-81.

94. Achilli, A.; Childress, A. E., Pressure retarded osmosis: From the vision of Sidney Loeb to the first prototype installation - Review. *Desalination* 2010, *261*, (3), 205-211.

95. Boo, C.; Lee, S.; Elimelech, M.; Meng, Z.; Hong, S., Colloidal fouling in forward osmosis: Role of reverse salt diffusion. *J. Membr. Sci.* 2012, *390-391*, 277-284.

96. van der Zwan, S.; Pothof, I. W. M.; Blankert, B.; Bara, J. I., Feasibility of osmotic power from a hydrodynamic analysis at module and plant scale. *J. Membr. Sci.* 2012, *389*, 324-333.

97. Sivertsen, E.; Holt, T.; Thelin, W.; Brekke, G., Pressure retarded osmosis efficiency for different hollow fibre membrane module flow configurations. *Desalination* 2013, *312*, 107-123.

98. Su, J.; Chung, T.-S.; Helmer, B. J.; de Wit, J. S., Enhanced double-skinned FO membranes with inner dense layer for wastewater treatment and macromolecule recycle using Sucrose as draw solute. *J. Membr. Sci.* 2012, *396*, 92-100.

99. Sabbatini, P.; Yrazu, F.; Rossi, F.; Thern, G.; Marajofsky, A.; Fidalgo de Cortalezzi, M. M., Fabrication and characterization of iron oxide ceramic membranes for arsenic removal. *Water Res.* 2010, *44*, (19), 5702-5712.

100. Grabow, W. O. K., Bacteriophages: Update on application as models for viruses in water. *Water SA* 2001, *27*, (2), 251-268.

101. Aranha-Creado, H.; Oshima, K.; Jafari, S.; Howard, G., Jr.; Brandwein, H., Virus retention by a hydrophilic triple-layer PVDF microporous membrane filter. *PDA J. Pharm. Sci. Technol.* 1997, *51*, (3), 119-24.

102. Aranha-Creado, H.; Peterson, J.; Huang, P. Y., Clearance of murine leukaemia virus from monoclonal antibody solution by a hydrophilic PVDF microporous membrane filter. *Biologicals* 1998, *26*, (2), 167-72.

103. Dennehy, J. J., Bacteriophages as model organisms for virus emergence research. *Trends Microbiol.* 2009, *17*, (10), 450-457.

104. Havelaar, A. H.; van Olphen, M.; Drost, Y. C., F-specific RNA bacteriophages are adequate model organisms for enteric viruses in fresh water. *Appl. Environ. Microbiol.* 1993, *59*, (9), 2956-2962.

105. Henry, M.; Debarbieux, L., Tools from viruses: Bacteriophage successes and beyond. *Virology* 2012, *434*, (2), 151-161.

106. Kott, Y.; Roze, N.; Sperber, S.; Betzer, N., Bacteriophages as viral pollution indicators. *Water Res.* 1974, *8*, (3), 165-171.

107. Lytle, C. D.; Budacz, A. P.; Keville, E.; Miller, S. A.; Prodouz, K. N., Differential inactivation of surrogate viruses with merocyanine 540. *Photochem. Photobiol.* 1991, *54*, (3), 489-93.

108. Lytle, C. D.; Truscott, W.; Budacz, A. P.; Venegas, L.; Routson, L. B.; Cyr, W. H., Important factors for testing barrier materials with surrogate viruses. *Appl. Environ. Microbiol.* 1991, *57*, (9), 2549-2554.

109. Rajal, V. B.; McSwain, B. S.; Thompson, D. E.; Leutenegger, C. M.; Kildare, B. J.; Wuertz, S., Validation of hollow fiber ultrafiltration and real-time PCR using bacteriophage PP7 as surrogate for the quantification of viruses from water samples. *Water Res.* 2007, *41*, (7), 1411-1422.

110. Shen, C.; Phanikumar, M. S.; Fong, T. T.; Aslam, I.; McElmurry, S. P.; Molloy, S. L.; Rose, J. B., Evaluating bacteriophage P22 as a tracer in a complex surface water system: The Grand River, Michigan. *Environ. Sci. Technol.* 2008, *42*, (7), 2426-2431.

111. Stetler, R. E., Coliphages as indicators of enteroviruses. *Appl. Environ. Microbiol.* 1984, *48*, (3), 668-670.

112. Aranha-Creado, H.; Brandwein, H., Application of bacteriophages as surrogates for mammalian viruses: A case for use in filter validation based on precedents and current practices in medical and environmental virology. *PDA J. Pharm. Sci. Technol.* 1999, *53*, (2), 75-82.

113. Havelaar, A. H.; Butler, M.; Farrah, S. R.; Jofre, J.; Marques, E.; A., K.; Martins, M. T.; Ohgaki, S.; Sobsey, M. D.; Zaiss, U., Bacteriophages as model viruses in water quality control. *Water Res.* 1991, *25*, (5), 529-545.

114. Poma, H. R.; Gutiérrez Cacciabue, D.; Garcé, B.; Gonzo, E. E.; Rajal, V. B., Towards a rational strategy for monitoring of microbiological quality of ambient waters. *Sci. Total Environ.* 2012, *433*, (0), 98-109.

115. Oshima, K. H.; Evans-Strickfaden, T. T.; Highsmith, A. K.; Ades, E. W., The use of a microporous polyvinylidene fluoride (PVDF) membrane filter to separate contaminating viral particles from biologically important proteins. *Biologicals* 1996, *24*, (2), 137-145.

116. Oshima, K. H.; Evans-Strickfaden, T. T.; Highsmith, A. K.; Ades, E. W., The removal of phages T1 and PP7, and poliovirus from fluids with hollow-fiber ultrafilters with molecular weight cut-offs of 50,000, 13,000, and 6000. *Can. J. Microbiol.* 1995, *41*, (4-5), 316-22.

117. DiLeo, A. J.; Vacante, D. A.; Deane, E. F., Size exclusion removal of model mammalian viruses using a unique membrane system, Part I: Membrane qualification. *Biologicals* 1993, *21*, (3), 275-86.

118. VanRegenmortel, M.; Fauquet, C.; Bishop, D.; Carstens, E.; Estes, M.; Lemon, S., Virus Taxonomy: Seventh Report of the International Committee on Taxonomy of Viruses. Academic Press: San Diego, California, USA, 2000.

119. Morales-Morales, H. A.; Vidal, G.; Olszewski, J.; Rock, C. M.; Dasgupta, D.; Oshima, K. H.; Smith, G. B., Optimization of a reusable hollow-fiber ultrafilter for simultaneous concentration of enteric bacteria, protozoa, and viruses from water. *Appl. Environ. Microbiol.* 2003, *69*, (7), 4098-102.

120. Malvern, Zetasizer Nano Series User Manual. Malvern Instruments Ltd.: Worcestershire, UK, 2007.

121. Corbett, J. C. W.; McNeil-Watson, F.; Jack, R. O.; Howarth, M., Measuring surface zeta potential using phase analysis light scattering in a simple dip cell arrangement. *Colloids Surf., A* 2012, *396*, (0), 169-176.

122. Malvern, Measuring surface zeta potential using the surface zeta potential cell. Malvern Instruments Ltd.: Worcestershire, UK, 2014.

123. Grinstein, J.; Iñón, F., Curso: Introducción a la Espectrofotometría Ultravioleta - Visible (UV - Visible).Jenck S.A.: Buenos Aires, Argentina, 2014.

124. Bizzi, C. A.; Flores, E. M. M.; Barin, J. S.; Garcia, E. E.; Nóbrega, J. A., Understanding the process of microwave-assisted digestion combining diluted nitric acid and oxygen as auxiliary reagent. *Microchem. J.* 2011, *99*, (2), 193-196.

125. Vinent, V., Seminario: Reduciendo los Tiempos de Digestión, Secado y Calcinación: Química Asistida por Microondas.Jenck S.A.: Buenos Aires, Argentina, 2014.

126. El-Sheikh, A. H.; Sweileh, J. A., A rapid and simple microwave-assisted digestion procedure for spectrophotometric determination of titanium dioxide photocatalyst on activated carbon. *Talanta* 2007, *71*, (5), 1867-1872.

127. Rajal, V. B., Curso: PCR en Tiempo Real.Facultad de Ingeniería, Universidad Nacional de Salta: Salta, Argentina, 2013.

128. Gregory, J., Interaction of unequal double layers at constant charge. *J. Colloid Interf. Sci.* 1975, *51*, (1), 44-51.

129. Hogg, R.; Healy, T. W.; Fuerstenau, D. W., Mutual coagulation of colloidal dispersions. *J. Chem. Soc. Faraday Trans.* 1966, *62*, (0), 1638-1651.

130. Devereux, O. F.; De Bruyn, P. L., Interaction of Plane-Parallel Double Layers. M.I.T. Press: Cambridge, Mass., 1963.

131. Gregory, J., Approximate expressions for retarded van der Waals interaction. *J. Colloid Interf. Sci.* 1981, *83*, (1), 138-145.

132. Molina-Bolívar, J. A.; Ortega-Vinuesa, J. L., How proteins stabilize colloidal particles by means of hydration forces. *Langmuir* 1999, *15*, (8), 2644-2653.

133. Ohshima, H., Electrokinetic phenomena in a concentrated suspension of soft particles. *Colloids Surf., A* 2001, *195*, (1–3), 129-134.

134. Duval, J. F. L.; Gaboriaud, F., Progress in electrohydrodynamics of soft microbial particle interphases. *Curr. Opin. Colloid. Interface Sci.* 2010, *15*, (3), 184-195.

135. Duval, J. F. L.; Ohshima, H., Electrophoresis of diffuse soft particles. *Langmuir* 2006, *22*, (8), 3533-3546.

136. Tripathi, S.; Champagne, D.; Tufenkji, N., Transport behavior of selected nanoparticles with different surface coatings in granular porous media coated with *Pseudomonas aeruginosa* biofilm. *Environ. Sci. Technol.* 2012, *46*, (13), 6942-6949.

137. Ruckenstein, E.; Prieve, D. C., Adsorption and desorption of particles and their chromatographic separation. *AIChE J.* 1976, *22*, (2), 276-283.

138. Smith Jr, J. E.; Perdek, J. M., Assessment and management of watershed microbial contaminants. *Crit. Rev. Environ. Sci. Tecnol.* 2004, *34*, (2), 109-139.

139. Fidalgo de Cortalezzi, M. M.; Gallardo, M. V.; Yrazu, F.; Gentile, G. J.; Opezzo, O.; Pizarro, R.; Poma, H. R.; Rajal, V. B., Virus removal by iron oxide ceramic membranes. *J. Environ. Chem. Eng.* 2014, *2*, (3), 1831-1840.

140. WHO, Preventing diarrhoea through better water, sanitation and hygiene. Exposures and impacts in low- and middle-income countries; Geneva, Switzerland, 2014.

141. Ryan, J. N.; Elimelech, M., Colloid mobilization and transport in groundwater. *Colloids Surf., A* 1996, *107*, 1-56.

142. McCarthy, J. F.; Zachara, J. M., Subsurface transport of contaminants. Mobile colloids in the subsurface environment may alter the transport of contaminants. *Environ. Sci. Technol.* 1989, *23*, (5), 496-502.

143. Harvey, R. W.; Garabedian, S. P., Use of colloid filtration theory in modeling movement of bacteria through a contaminated sandy aquifer. *Environ. Sci. Technol.* 1991, *25*, (1), 178-185.

144. Tufenkji, N.; Ryan, J. N.; Elimelech, M., The promise of bank filtration. *Environ. Sci. Technol.* 2002, *36*, (21), 422A-428A.

145. Steffan, R. J.; Sperry, K. L.; Walsh, M. T.; Vainberg, S.; Condee, C. W., Field-scale evaluation of in situ bioaugmentation for remediation of chlorinated solvents in groundwater. *Environ. Sci. Technol.* 1999, *33*, (16), 2771-2781.

146. Boncagni, N. T.; Otaegui, J. M.; Warner, E.; Curran, T.; Ren, J.; Fidalgo de Cortalezzi, M. M., Exchange of TiO_2 nanoparticles between streams and streambeds. *Environ. Sci. Technol.* 2009, *43*, (20), 7699-7705.

147. Xiao, Y.; Wiesner, M. R., Transport and retention of selected engineered nanoparticles by porous media in the presence of a biofilm. *Environ. Sci. Technol.* 2013, *47*, (5), 2246-2253.

148. Indris, S.; Amade, R.; Heitjans, P.; Finger, M.; Haeger, A.; Hesse, D.; Grünert, W.; Börger, A.; Becker, K. D., Preparation by high-energy milling, characterization, and catalytic properties of nanocrystalline TiO_2. *J. Phys. Chem. B* 2005, *109*, (49), 23274-23278.

149. Murdock, R. C.; Braydich-Stolle, L.; Schrand, A. M.; Schlager, J. J.; Hussain, S. M., Characterization of nanomaterial dispersion in solution prior to in vitro exposure using dynamic light scattering technique. *Toxicol. Sci.* 2008, *101*, (2), 239-253.

150. Chen, X.; Mao, S. S., Titanium dioxide nanomaterials: Synthesis, properties, modifications and applications. *Chem. Rev.* 2007, *107*, (7), 2891-2959.

151. Jucker, B. A.; Harms, H.; Hug, S. J.; Zehnder, A. J. B., Adsorption of bacterial surface polysaccharides on mineral oxides is mediated by hydrogen bonds. *Colloids Surf., B* 1997, *9*, (6), 331-343.

152. Chowdhury, I.; Cwiertny, D. M.; Walker, S. L., Combined factors influencing the aggregation and deposition of nano-TiO_2 in the presence of humic acid and bacteria. *Environ. Sci. Technol.* 2012, *46*, (13), 6968-6976.

153. Horst, A. M.; Neal, A. C.; Mielke, R. E.; Sislian, P. R.; Suh, W. H.; Mädler, L.; Stucky, G. D.; Holden, P. A., Dispersion of TiO_2 nanoparticle agglomerates by *Pseudomonas aeruginosa*. *Appl. Environ. Microbiol.* 2010, *76*, (21), 7292-7298.

154. Verwey, E. J. W.; Overbeek, J. T. G., Theory of the stability of lyophobic colloids. *J. Colloid Sci.* 1955, *10*, (2), 224-225.

155. Derjaguin, B.; Landau, L., Theory of the stability of strongly charged lyophobic sols and of the adhesion of strongly charged particles in solutions of electrolytes. *Acta Physicochim. URSS* 1941, *14*, 733-762.

156. Romanello, M. B.; Fidalgo de Cortalezzi, M. M., An experimental study on the aggregation of TiO_2 nanoparticles under environmentally relevant conditions. *Water Res.* 2013, *47*, (12), 3887-3898.

157. Packman, A. I.; Brooks, N. H.; Morgan, J. J., Kaolinite exchange between a stream and streambed: Laboratory experiments and validation of a colloid transport model. *Water Resour. Res.* 2000, *36*, (8), 2363-2372.

158. Ren, J.; Packman, A. I., Effects of background water composition on stream-subsurface exchange of submicron colloids. *J. Environ. Eng.* 2002, *128*, (7), 624-634.

159. Ren, J.; Packman, A. I.; Welty, C., Correlation of colloid collision efficiency with hydraulic conductivity of silica sands. *Water Resour. Res.* 2000, *36*, (9), 2493-2500.

160. Chowdhury, I.; Hong, Y.; Honda, R. J.; Walker, S. L., Mechanisms of TiO_2 nanoparticle transport in porous media: Role of solution chemistry, nanoparticle concentration, and flowrate. *J. Colloid Interf. Sci.* 2011, *360*, (2), 548-555.

161. Çetin, E. T.; Töreci, K.; Anğ, Ö., Encapsulated *Pseudomonas aeruginosa* (*Pseudomonas aeruginosa mucosus*) strains. *J. Bacteriol.* 1965, *89*, (5), 1432-1433.

162. Mandzy, N.; Grulke, E.; Druffel, T., Breakage of TiO_2 agglomerates in electrostatically stabilized aqueous dispersions. *Powder Technol.* 2005, *160*, (2), 121-126.

163. Thio, B. J. R.; Zhou, D.; Keller, A. A., Influence of natural organic matter on the aggregation and deposition of titanium dioxide nanoparticles. *J. Hazard. Mater.* 2011, *189*, (1–2), 556-563.

164. Ben-Moshe, T.; Dror, I.; Berkowitz, B., Transport of metal oxide nanoparticles in saturated porous media. *Chemosphere* 2010, *81*, (3), 387-393.

165. Kosmulski, M., The pH-dependent surface charging and the points of zero charge. *J. Colloid Interf. Sci.* 2002, *253*, (1), 77-87.

166. Johnson, P. R.; Elimelech, M., Dynamics of colloid deposition in porous media: Blocking based on random sequential adsorption. *Langmuir* 1995, *11*, (3), 801-812.

167. Johnson, P. R.; Sun, N.; Elimelech, M., Colloid transport in geochemically heterogeneous porous media: Modeling and measurements. *Environ. Sci. Technol.* 1996, *30*, (11), 3284-3293.

168. Jucker, B. A.; Harms, H.; Zehnder, A. J. B., Polymer interactions between five gram-negative bacteria and glass investigated using LPS micelles and vesicles as model systems. *Colloids Surf., B* 1998, *11*, (1–2), 33-45.

169. Jiang, X.; Wang, X.; Tong, M.; Kim, H., Initial transport and retention behaviors of ZnO nanoparticles in quartz sand porous media coated with *Escherichia coli* biofilm. *Environ. Pollut.* 2013, *174*, (0), 38-49.

170. Mitzel, M. R.; Tufenkji, N., Transport of industrial PVP-stabilized silver nanoparticles in saturated quartz sand coated with *Pseudomonas aeruginosa* PAO1 biofilm of variable age. *Environ. Sci. Technol.* 2014, *48*, (5), 2715-23.

171. Foppen, J. W.; Lutterodt, G.; Röling, W. F. M.; Uhlenbrook, S., Towards understanding inter-strain attachment variations of *Escherichia coli* during transport in saturated quartz sand. *Water Res.* 2010, *44*, (4), 1202-1212.

172. Jaisi, D. P.; Saleh, N. B.; Blake, R. E.; Elimelech, M., Transport of single-walled carbon nanotubes in porous media: Filtration mechanisms and reversibility. *Environ. Sci. Technol.* 2008, *42*, (22), 8317-8323.

173. Borchardt, M. A.; Spencer, S. K.; Kieke, B. A.; Lambertini, E.; Loge, F. J., Viruses in nondisinfected drinking water from municipal wells and community incidence of acute gastrointestinal illness. *Environ. Health Persp.* 2012, *120*, (9), 1272-1279.

174. Farrah, S. R.; Gerba, C. P.; Wallis, C.; Melnick, J. L., Concentration of viruses from large volumes of tap water using pleated membrane filters. *Appl. Environ. Microbiol.* 1976, *31*, (2), 221-226.

175. Chang, L. T.; Farrah, S. R.; Bitton, G., Positively charged filters for virus recovery from wastewater treatment plant effluents. *Appl. Environ. Microbiol.* 1981, *42*, (5), 921-924.

176. Gerba, C. P.; Lance, J. C., Poliovirus removal from primary and secondary sewage effluent by soil filtration. *Appl. Environ. Microbiol.* 1978, *36*, (2), 247-51.

177. Rose, J.; Cortalezzi-Fidalgo, M. M.; Moustier, S.; Magnetto, C.; Jones, C. D.; Barron, A. R.; Wiesner, M. R.; Bottero, J.-Y., Synthesis and characterization of carboxylate-FeOOH nanoparticles (ferroxanes) and ferroxane-derived ceramics. *Chem. Mat.* 2002, *14*, (2), 621-628.

178. Cortalezzi, M. M.; Rose, J.; Wells, G. F.; Bottero, J.-Y.; Barron, A. R.; Wiesner, M. R., Ceramic membranes derived from ferroxane nanoparticles: A new route for the fabrication of iron oxide ultrafiltration membranes. *J. Membr. Sci.* 2003, *227*, (1–2), 207-217.

179. Christian, P. D.; Richards, A. R.; Williams, T., Differential adsorption of occluded and nonoccluded insect-pathogenic viruses to soil-forming minerals. *Appl. Environ. Microbiol.* 2006, *72*, (7), 4648-52.

180. Wang, S.; Ang, H. M.; Tadé, M. O., Novel applications of red mud as coagulant, adsorbent and catalyst for environmentally benign processes. *Chemosphere* 2008, *72*, (11), 1621-1635.

181. Flynn, R.; Taylor, R.; Kulabako, R.; Miret-Gaspa, M., Haematite in lateritic soils aids groundwater disinfection. *Water Air Soil Pollut.* 2011, *223*, (5), 2405-2416.

182. Wang, Y.; Li, Y.; Fortner, J. D.; Hughes, J. B.; Abriola, L. M.; Pennell, K. D., Transport and retention of nanoscale C60 aggregates in water-saturated porous media. *Environ. Sci. Technol.* 2008, *42*, (10), 3588-3594.

183. Meschke, J. S.; Sobsey, M. D., Comparative adsorption of Norwalk virus, poliovirus 1 and F+ RNA coliphage MS2 to soils suspended in treated wastewater. *Water Sci. Technol.* 1998, *38*, (12), 187-189.

184. Gerba, C. P.; Smith, E. M.; Melnick, J. L., Development of a quantitative method for detecting enteroviruses in estuarine sediments. *Appl. Environ. Microbiol.* 1977, *34*, (2), 158-163.

185. Fernandez, M. D.; Torres, C.; Poma, H. R.; Riviello-Lopez, G.; Martinez, L. C.; Cisterna, D. M.; Rajal, V. B.; Nates, S. V.; Mbayed, V. A., Environmental surveillance of norovirus in Argentina revealed distinct viral diversity patterns, seasonality and spatio-temporal diffusion processes. *Sci. Total Environ.* 2012, *437*, 262-9.

186. Bradley, I.; Straub, A.; Maraccini, P.; Markazi, S.; Nguyen, T. H., Iron oxide amended biosand filters for virus removal. *Water Res.* 2011, *45*, (15), 4501-4510.

187. Park, J.-A.; Kim, J.-H.; Kang, J.-K.; Son, J.-W.; Yi, I.-G.; Kim, S.-B., Flow-through experiments for bacteriophage MS2 removal by iron oxide-impregnated fiberglass. *Desalin. Water Treat.* 2015, *54*, (8), 2314-2323.

188. Pecson, B. M.; Decrey, L.; Kohn, T., Photoinactivation of virus on iron-oxide coated sand: Enhancing inactivation in sunlit waters. *Water Res.* 2012, *46*, (6), 1763-70.

189. Gutierrez, L.; Li, X.; Wang, J.; Nangmenyi, G.; Economy, J.; Kuhlenschmidt, T. B.; Kuhlenschmidt, M. S.; Nguyen, T. H., Adsorption of rotavirus and bacteriophage MS2 using glass fiber coated with hematite nanoparticles. *Water Res.* 2009, *43*, (20), 5198-208.

190. Nangmenyi, G.; Li, X.; Mehrabi, S.; Mintz, E.; Economy, J., Silver-modified iron oxide nanoparticle impregnated fiberglass for disinfection of bacteria and viruses in water. *Mater. Lett.* 2011, *65*, (8), 1191-1193.

191. Michen, B.; Fritsch, J.; Aneziris, C.; Graule, T., Improved virus removal in ceramic depth filters modified with MgO. *Environ. Sci. Technol.* 2013, *47*, (3), 1526-1533.

192. Brown, J.; Sobsey, M. D., Ceramic media amended with metal oxide for the capture of viruses in drinking water. *Environ. Technol.* 2009, *30*, (4), 379-91.

193. Farrah, S. R.; Preston, D. R., Adsorption of viruses by diatomaceous earth coated with metallic oxides and metallic peroxides. *Water Sci. Technol.* 1991, *24*, (2), 235-240.

194. Chrysikopoulos, C. V.; Aravantinou, A. F., Virus attachment onto quartz sand: Role of grain size and temperature. *J. Environ. Chem. Eng.* 2014, *2*, (2), 796-801.

195. Casjens, S., Molecular organization of the bacteriophage P22 coat protein shell. *J. Mol. Biol.* 1979, *131*, (1), 1-19.

196. Chang, J.; Weigele, P.; King, J.; Chiu, W.; Jiang, W., Cryo-EM asymmetric reconstruction of bacteriophage P22 reveals organization of its DNA packaging and infecting machinery. *Structure* 2006, *14*, (6), 1073-1082.

197. Earnshaw, W.; Casjens, S.; Harrison, S. C., Assembly of the head of bacteriophage P22: X-ray diffraction from heads, proheads and related structures. *J. Mol. Biol.* 1976, *104*, (2), 387-410.

198. Masago, Y.; Shibata, T.; Rose, J. B., Bacteriophage P22 and Staphylococcus aureus attenuation on nonporous fomites as determined by plate assay and quantitative PCR. *Appl. Environ. Microbiol.* 2008, *74*, (18), 5838-40.

199. Hamaker, H. C., The London-van der Waals attraction between spherical particles. *Physica* 1937, *4*, (10), 1058-1072.

200. Leite, F. L.; Bueno, C. C.; Da Róz, A. L.; Ziemath, E. C.; Oliveira, O. N., Theoretical models for surface forces and adhesion and their measurement using atomic force microscopy. *Int. J. Mol. Sci.* 2012, *13*, (10), 12773-12856.

201. Gilbert, B.; Lu, G.; Kim, C. S., Stable cluster formation in aqueous suspensions of iron oxyhydroxide nanoparticles. *J. Colloid Interf. Sci.* 2007, *313*, (1), 152-159.

202. Tokunaga, T. K., Physicochemical controls on adsorbed water film thickness in unsaturated geological media. *Water Resour. Res.* 2011, *47*, (8).

203. Cornell, R. M.; Schwertmann, U., The Iron Oxides: Structure, Properties, Reactions, Occurrences and Uses. 2nd ed.; Wiley-VCH Verlag GmbH & Co. KGaA: Weinheim, 2004.

204. Girones, R.; Ferrús, M. A.; Alonso, J. L.; Rodriguez-Manzano, J.; Calgua, B.; de Abreu Corrêa, A.; Hundesa, A.; Carratala, A.; Bofill-Mas, S., Molecular detection of pathogens in water - The pros and cons of molecular techniques. *Water Res.* 2010, *44*, (15), 4325-4339.

205. Sabatino, C. M.; Maier, S., Differential inactivation of three bacteriophages by acid and alkaline pH used in the membrane adsorption-elution method of virus recovery. *Can. J. Microbiol.* 1980, *26*, (12), 1403-7.

206. Amin, M. K.; Day, M. J., Influence of pH value on viability and transduction frequency of *Pseudomonas aeruginosa phage* F116. *Lett. Appl. Microbiol.* 1988, *6*, (4), 93-96.

207. Willett, I. R.; Chartres, C. J.; Nguyen, T. T., Migration of phosphate into aggregated particles of ferrihydrite. *J. Soil Sci.* 1988, *39*, (2), 275-282.

208. Fuller, C. C.; Davis, J. A.; Waychunas, G. A., Surface chemistry of ferrihydrite: Part 2. Kinetics of arsenate adsorption and coprecipitation. *Geochim. Cosmochim. Acta* 1993, *57*, (10), 2271-2282.

209. Park, J. A.; Kim, S. B.; Lee, C. G.; Lee, S. H.; Choi, J. W., Adsorption of bacteriophage MS2 to magnetic iron oxide nanoparticles in aqueous solutions. *J. Environ. Sci. Health A Tox. Hazard. Subst. Environ. Eng.* 2014, *49*, (10), 1116-24.

210. Healy, T. W.; Homola, A.; James, R. O.; Hunter, R. J., Coagulation of amphoteric latex colloids: reversibility and specific ion effects. *Farad. Discuss.* 1978, *65*, (0), 156-163.

211. Melnick, J. L.; Gerba, C. P.; Berg, G., The ecology of enteroviruses in natural waters. *Crit. Rev. Env. Cont.* 1980, *10*, (1), 65-93.

212. Huang, H.; Young, T. A.; Schwab, K. J.; Jacangelo, J. G., Mechanisms of virus removal from secondary wastewater effluent by low pressure membrane filtration. *J. Membr. Sci.* 2012, *409–410*, (0), 1-8.

213. Kang, S.; Hoek, E. M. V.; Choi, H.; Shin, H., Effect of membrane surface properties during the fast evaluation of cell attachment. *Separ. Sci. Technol.* 2006, *41*, (7), 1475-1487.

214. Rumnieks, J.; Tars, K., Diversity of pili-specific bacteriophages: genome sequence of IncM plasmid-dependent RNA phage M. *BMC Microbiol.* 2012, *12*, (1), 1-8.

215. Langlet, J.; Gaboriaud, F.; Duval, J. F. L.; Gantzer, C., Aggregation and surface properties of F-specific RNA phages: Implication for membrane filtration processes. *Water Res.* 2008, *42*, (10–11), 2769-2777.

216. Furiga, A.; Pierre, G.; Glories, M.; Aimar, P.; Roques, C.; Causserand, C.; Berge, M., Effects of ionic strength on bacteriophage MS2: Behavior and their implications for the assessment of virus retention by ultrafiltration membranes. *Appl. Environ. Microbiol.* 2011, *77*, (1), 229-236.

217. Nascimento, M. A.; Magri, M. E.; Schissi, C. D.; Barardi, C. R., Recombinant adenovirus as a model to evaluate the efficiency of free chlorine disinfection in filtered water samples. *Virol. J.* 2015, *12*, (1), 30.

218. Kielland, J., Effective diameters of unhydrated and hydrated ions. *J. Am. Chem. Soc.* 1937, *59*, 1675-1678.

219. Millero, F. J.; Feistel, R.; Wright, D. G.; McDougall, T. J., The composition of standard seawater and the definition of the reference-composition salinity scale. *Deep-Sea Res. Pt .* 2008, *55*, (1), 50-72.

220. Sivertsen, E.; Holt, T.; Thelin, W.; Brekke, G., Modelling mass transport in hollow fibre membranes used for pressure retarded osmosis. *J. Membr. Sci.* 2012, *417-418*, 69-79.

221. Stover, R. L., Seawater reverse osmosis with isobaric energy recovery devices. *Desalination* 2007, *203*, (1–3), 168-175.

222. Red Hidrológica Nacional - Publicaciones Hidrometeorológicas 2010. 1st ed.; Secretaría de Obras Públicas. Subsecretaría de Recursos Hídricos: Buenos Aires, Argentina, 2011.

223. Thorsen, T.; Holt, T., The potential for power production from salinity gradients by pressure retarded osmosis. *J. Membr. Sci.* 2009, *335*, (1-2), 103-110.

224. Wick, G. L., Power from salinity gradients. *Energy* 1978, *3*, (1), 95-100.

225. Stenzel, P.; Wagner, H.-J., Osmotic power plants: Potential analysis and site criteria. In 3rd International Conference on Ocean Energy, Bilbao, Spain, 2010.

226. Aaberg, R. J., Osmotic power: A new and powerful renewable energy source? *Refocus* 2003, *4*, (6), 48-50.